Catalysis with Dispersed Cation-Exchanged Polyoxometalates

by

Trenton J. Wilke

A dissertation submitted in partial fulfillment
of the requirements for the degree of
Doctor of Philosophy
(Chemical Engineering)
in the University of Michigan
2018

Doctoral Committee:

Adjunct Professor Mark A. Barteau, Co-Chair
Professor Levi T. Thompson, Co-Chair
Professor Bart Bartlett
Professor Suljo Linic

Trenton J. Wilke

tjwilke@umich.edu

ORCID iD: 0000-0001-9444-7820

Acknowledgements

I would like to thank my advisor, Professor Mark Barteau, for the opportunity to join his research group and for his mentorship and guidance throughout this journey. I could not ask for a better advisor; supportive, available, brilliant, and a critical eye would begin a list longer than I have vocabulary to construct. I cannot adequately portray his knowledge and wit which I found invaluable time and time again. The challenge and opportunity of setting up the lab from scratch is something that I will cherish and benefit from throughout my career. I would also like to acknowledge Professor Barteau and the University of Michigan Energy Institute for providing funding throughout my PhD.

Thank you to Professor Levi Thompson, for serving as an unofficial co-advisor since my early days in the Barteau lab and as a co-chair on my dissertation committee. The support and experience I gained through your mentorship, the mentorship of your students, and by honing my presentation skills through Thompson group meetings was essential to my success as a PhD student. I also want to gratefully acknowledge your generosity for allowing me to use equipment in your lab throughout my PhD, including the equipment necessary for many of the characterization techniques discussed in this work, including BET, NH_3 TPD, TGA, the catalyst press, and the like.

I would like to thank Professor Suljo Linic for his critical eye during my committee meetings and for his generosity in allowing me access to crucial equipment, as all of the spectroscopic data presented in this work were obtained using equipment in the Linic lab.

Many thanks also to Professor Bart Bartlett for serving as the cognate on my dissertation committee and for providing valuable feedback and advice in all of my committee meetings.

For helping me getting started in the new lab, I would like to thank Dr. Calvin Boerigter, Dr. Tim Van Cleve, and especially Dr. Brian Wyvratt, who was my finest resource for anything catalysis related, troubleshooting, and critical feedback. As I have grown as a researcher, I hope I was able to step into their shoes to mentor the next generation of researchers as they did for me.

For helpful discussions, friendships, and fruitful (and not-so-fruitful) collaborations, I would like to thank Dr. Umar Aslam and Steven Chavez. Umar and Steven were crucial in helping me set up and evaluate spectroscopic experiments that were essential for my success on this project. I also truly enjoyed Umar and Steven's trips to the Phoenix lab to attempt some truly exciting experiments, whether they worked or not!

I would like to thank all the members of the Thompson group - for friendships and aid in this project. In particular, I would like to thank Sarah Paleg, Wei-Chung Wen, Dr. Abdoulaye "Abdul" Djire, Dr. Jennifer Jocz, Zixuan Wang, and Dr. Tapiwa Mushove for being, each in their own way, a great colleague, a contributor to this work, and for making the Phoenix building a better place to work.

For being great mentors and friends, I would like to thank Dr. Trent Silbaugh and Dr. Shawn Eady. Trent made the office a fun, welcoming place to work, was a great role model, and was one of my closest friends during my time at Michigan. I cannot thank him enough for his guidance. Shawn was truly a pleasure to work with and wonderful person. Everyone in the lab benefited from Shawn's willingness to help!

For being great friends and co-workers, I would like to thank Xiaowen Zhao and Elizabeth Wilson. These last few months, especially, have been such a joy, and I will truly miss you both!

For letting me win at Fantasy Football all the time (and for being great friends), I would like to thank Dr. Dave Hietala, Mason Smith, Brett Hill, Cornelius "CC" Cilliers, Vikesh Chandrashekar, Dr. Sumit Bhatnagar, and Nishanth "Bob" Bobba Bharadwaj. I will miss football Sundays, the floats down the river, and the blessing of living near to such close friends.

I would like to thank my family for being my foundation through this journey. Thank you to my mother, Theresa, for keeping me grounded during difficult times and to my dad, Arlyn, for teaching me dedication, work ethic, and the importance of taking pride in the quality of your work. I would also like to send my love to my siblings Joni, Eric, Ethan, and Lauren, and their families. I am proud to be part of such a unique and awesome bunch of goofballs. I would like to acknowledge Snapchat for letting me feel close to those closest to me while I am far away, especially to be able to see my nieces and nephews grow up before my eyes. I love you all.

For always being there for me, for your contributions to this project and this dissertation, and for so much more, thank you to my wonderful girlfriend Sarah Carl. I was blessed to be able to work near my best friend, and I will miss our daily lunches, walks, and having someone so dear to me as a colleague. We have grown so much together, I love you and I look forward to the many more happy and fruitful years ahead of us!

Table of Contents

List of Tables

List of Figures

Abstract

Heterogeneous catalysts are complex materials that present challenges in understanding their physical and chemical properties as well as improving their performance in chemical processes. The pursuit of catalysts with well-defined active sites that are stable under practical reaction conditions may lead to the improved fundamental understanding of catalyst function at the molecular level and enable the development of catalysts tailored for a specific reaction. Polyoxometalates (POMs) supported on a high surface area support are model transition-metal oxide catalysts possessing well-defined, isolated, and tunable catalytic sites that are active for both selective oxidation and acid catalysis. POM acid and redox properties may be systematically varied by the replacement of a portion of POM protons with other cations, such as copper or sodium.

The model catalyst system phosphomolybdic acid ($H_3PMo_{12}O_{40}$) supported on fumed silica was used to evaluate the effects of cation exchange on POM properties and reactivity, for both oxidation and acid-catalyzed reactions. The as-prepared catalysts were characterized by a variety of techniques to confirm that the POMs were intact and well-dispersed on the silica surface and to quantify changes in POM reducibility and acid properties with cation addition. The interaction of POMs and the cations was evident by the variation of many POM properties with the incremental addition of counter-cations.

The effect of cation addition on the POM catalytic activity was evaluated using parallel pathways of methanol dehydration to dimethyl ether and oxidation to formaldehyde and its derivatives as probe reactions. The catalytic activity of POMs for both the dehydration and oxidation of methanol decreased dramatically as cations (Na, Mg, Cu, or Al) replaced protons. The measured oxidation and dehydration rates over Na, Mg, and Cu exchanged POMs were remarkably similar, and the differences in the cation charge had little impact. Al-exchanged POMs tended to have a higher quantity of acid sites and higher TOF at comparable extents of cation exchange compared to the other cations. The perturbation of POM acid sites, via the introduction of counter-cations, was determined to be responsible for the decrease in the rates for both dehydration and oxidation of methanol. Although cation exchange was demonstrated to alter the POM reducibility, this had no observable effect on the oxidation activity of the cation-exchanged catalysts. Rather, the quantity of acid sites per POM was the primary reactivity descriptor for both the dehydration and oxidation of methanol over POMs, perhaps due to the presence of a proton-mediated intermediate in both the methanol dehydration and oxidation pathways over POMs.

While cation addition does not result in the production of a more active catalyst, there are many exciting applications for a model catalyst with a well-defined and tunable structure. For example, activity coefficients were developed to describe the non-ideal behavior of POM acid sites with cation addition. The acid sites of a heterogeneous catalyst were described using activity coefficients for the first time, providing a framework for the treatment of ionic environments in heterogeneous systems using the rigorous thermodynamic formalisms usually applied to solutions.

This work demonstrates the merits of investigating catalysts that retain a well-defined structure under practical reaction conditions to elucidate the underlying mechanisms behind their catalytic functions and to evaluate the effects of the composition and structure of the catalyst active sites on the function of the catalyst.

Chapter 1: Introduction

1.1 A model transition metal-oxide catalyst

Heterogenous catalysts are complex materials that present challenges in understanding their physical and chemical properties, as well as improving their performance in chemical processes. There are many different approaches to improve our understanding of catalysis, from DFT calculations of proposed actives structures,[1] to kinetic and calorimetric measurements,[2] and the application of a variety of in-situ[3] and in-operando[4] techniques to evaluate the catalyst under reaction conditions. Another approach that has gained interest recently is the pursuit of catalysts with well-defined active sites that are stable under practical reaction conditions.[5] The use of catalysts with well-defined active sites may lead to the improved fundamental understanding of catalyst function at the molecular level and enable the development of catalysts tailored to a specific reaction, in pursuit of the goal of a 100% selective catalyst. Examples of catalysts with well-defined active sites include the following materials dispersed on a high surface area support: nanoparticles of well-defined size,[6] atomically dispersed metals,[7] or organo-metallic complexes immobilized[8] on the support surface. The approach we have adopted is supporting polyoxometalates on a high surface areas support, to obtain a transition-metal oxide catalyst with well-defined and isolated catalytic sites that are active for both selective oxidation and acid catalysis.

1.2 Polyoxometalates (POMs)

1.2.1 The Keggin structure

Polyoxometalates (POMs) constitute a class of metal-oxide clusters consisting of transition metal-oxygen octahedra linked together through shared oxygen atoms.[9,10] POMs possessing the Keggin structure (see Figure 1-1) are the most catalytically relevant[10] and are the only POM species discussed in this work. POMs with the Keggin structure ($XM_{12}O_{40}^{8-x}$) act as oxidation and acid catalysts, and by varying the heteroatom (X= P^{5+}, Si^{4+}, As^{5+}, etc.) and framework metal atoms (M = Mo^{6+}, W^{6+} or V^{5+}), one may vary the acid and redox properties systematically while maintaining the same framework structure.[10–12] Counter-cations (H^+, Na^+, Cs^+, Ca^+, Cu^+…) balance charge and may also impact the POM acid[13–15] and redox properties.[13,14,16–19]

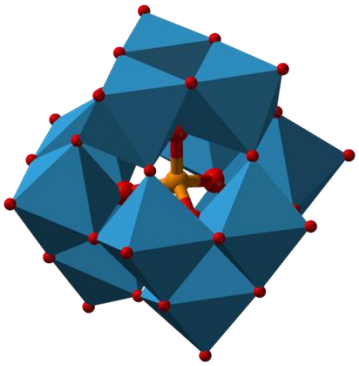

Figure 1-1: An example of a POM with the Keggin structure. The heteroatom, transition metal octahedra, and oxygens are color coded with the formula below the structure.

1.2.2 Secondary structure

POM structure can be classified into the primary structure, the polyanion (e.g., $PMo_{12}O_{40}^{3-}$), the secondary structure defined as the 3D arrangement of the polyanions, counter-cations, waters of

hydration, and other molecules,[11] and the tertiary structure which is defined as the higher order arrangement of POMs. All POMs used in this work have the composition of $PMo_{12}O_{40}^{3-}$, as the effects of varying the POM heteroatom and framework metal atoms on POM properties and catalytic behavior are well documented.[10,16,20] Thus the primary structure is held constant throughout this work.

What is varied significantly over the course of this work is the POM secondary structure. In particular the counter-cation is varied, from the POM as-received from the manufacturer possessing Brønsted acidic protons (H^+) as the cations, to POMs with various quantities of protons exchanged for other cations, such as with sodium: $Na_xH_{3-x}PMo_{12}O_{40}$ where x = 0 – 3. Other changes to the POM secondary structure examined in this work include variations in the waters of hydration and alterations of the interactions of POMs with nearby structures, such as other POMs or a high surface area support.

The nature of the secondary structure can greatly influence POM properties and is highly variable depending on the counter-cation and the environmental conditions.[9–11,21] Thus changes in the POM properties and catalytic activity in this work may often be interpreted through the lens of changes in the POM secondary structure.

1.2.3 Tertiary structure

The tertiary structure is the higher-order arrangement of POMs.[11] The tertiary structure may include the particle size, pore structure, composition gradients, etc. of POM agglomerates or

crystallites. Some of the considerations involving the tertiary structure are discussed below for bulk POM crystallites.

1.2.3.1 Bulk-POMs

In this work, "bulk POMs" refers to POM crystallites consisting of POMs, their cations, waters of hydration (up to 30 H_2O per POM), and other molecules (e.g., methanol); generally possessing a low surface area (~ 1 – 10 m^2/g) and capable of pseudo-liquid behavior under reaction conditions.[10,11,21] Briefly, the pseudo-liquid behavior describes the ability of polar molecules to rapidly diffuse in the interstitial regions between POMs, with diffusivities approaching that of a liquid under certain conditions.[11] In some cases, the catalytic activity of bulk POMs is proportional to catalyst mass, rather than the surface area, as reactants can access active sites throughout the catalyst bulk.[21] The behavior of bulk POMs is sensitive to the composition of the POM, and especially sensitive to the cation identity.[11,21] For example, POMs exchanged with "type A" cations such as H^+, Na^+, Mg^{2+}, Al^{3+}, and Cu^{2+} behave as described above; possessing low surface area, pseudo-liquid behavior, many waters of hydration at ambient conditions, and having a high solubility in polar solvents.[11] In contrast, large cations, classified as "type B", such as K^+, Cs^+, and NH_4^+ exhibit starkly different behavior. POMs exchanged with type B cations are insoluble, possess high surface area (100 – 200 m^2/g), retain few waters of hydration, and are not capable of pseudo-liquid catalysis.[10,11,21]

While bulk POMs have been investigated as heterogeneous catalysts extensively and have even found industrial applications,[11,22–24] for the purposes of this work the complicated nature of the tertiary structure for bulk POMs is undesirable for the preparation of a model catalyst.

1.2.4 Supported POMs

Dispersing POMs on a high surface area support is the preferred method to prepare a model transition metal-oxide catalyst using POMs. Dispersing POMs on the support surface allows for the preparation of a catalyst with a known quantity of dispersed and isolated sites of identical composition and structure. Common POM supports include silica, activated carbon, and POMs exchanged with type B cations (e.g., $Cs_3PMo_{12}O_{40}$, etc.).[11,21,23,25,26] The most commonly used support is silica,[10,11] which is used as the support in this work. Basic supports, such as Al_2O_3 and MgO, are generally incompatible with POMs and may lead to POM decomposition.[10,11] At low loadings POMs may interact strongly with the supports while POMs generally retain the properties of the bulk POM at high loadings.[11] The interactions between POMs and the support may lead to a decrease of the POM acidity or the decomposition of the POM.[10,11] Thus there may be an optimum POM loading for well-defined, well-dispersed catalysts. Loadings that are too high will result in agglomeration; at low loadings POMs may interact strongly with the support and potentially decompose.

1.3 Cation-exchanged POMs as model metal-oxide catalysts

POMs of the Keggin-type supported on a high surface area support (Figure 1-2) can be viewed as model transition metal oxide catalysts that permit tuning of the composition and therefore the catalytic properties of the POM,[16,25] all while maintaining a constant structure.

The properties of POMs may be tuned by varying the heteroatom, framework metal atom, and the counter-cation.[10–12,16] Generally, the catalytic activity of POMs for acid-catalyzed and selective oxidation pathways track the acid and redox properties of the POM, respectively.[16,20]

Reactivity trends with varying POM composition have been established for POMs with varying heteroatom and framework metal atoms.[10–12,16,25,27] It has been previously demonstrated that counter-cations may influence POM reducibility,[16–18] however the link between the counter-cation, POM reducibility, and oxidation activity is yet to be established.

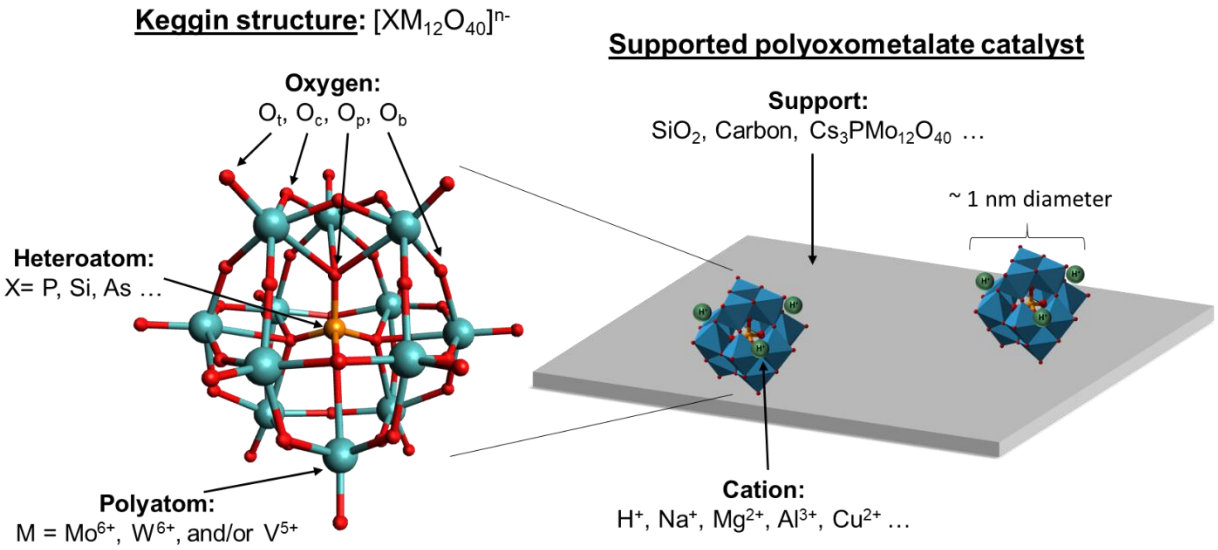

Figure 1-2: POMs dispersed on a high surface area support. Examples of Keggin-type POM constituent atoms have been included for the heteroatom, polyatom, cation and the heterogenous support.

The addition of counter-cations, as well as supporting POMs on silica, tends to render POMs less acidic[10,11,15,20,28,29] than the unsupported bulk POM without cation-exchange, $H_3PMo_{12}O_{40}$. A decrease in the POM acidity is expected to lead to decreased catalytic activity for acid-catalyzed pathways.[20,29,30]

While correlations may be lacking between changes in the POM redox properties induced by cation-exchange and oxidation catalytic activity, cation-exchanged POMs have been studied

extensively;[11,13,21,23,31] some illustrative examples are summarized here. Cations such a K^+, Cs^+, and NH_4^+ have been studied extensively as they modify POM textural characteristics.[11] Others have investigated the addition of small quantities of cations such as Fe, Cu, Pd, Pt, Ag etc. that may influence POM redox properties[16,32] , re-oxidation,[33] reduction,[33] or acid[34,35] properties, or assist the formation of oxygen vacancies[36,37] or lead to other synergies[22,23,38–40], while still maintaining a population of acid sites. Detailed studies in which counter-cation populations have been systematically varied, however, are largely lacking.

The model catalyst employed in this work was intended to explore the systematic variation of counter-cation type and quantity to evaluate the effect of cations on POM properties and reactivity, for both oxidation and acid-catalyzed reactions. By controlling the identity and quantity of the counter-cations one may, in principle, vary the population of acid sites and the POM reducibility *independently* for these model catalysts. This model system of cation-exchanged POMs supported on silica presents an opportunity to develop relationships between the catalytic activity and the POM acid and redox properties for a catalyst with well-defined, isolated, and tunable active sites.

1.3.1 Evaluation of a model catalyst

The first step after the synthesis of a target well-defined catalyst is to ascertain if the desired material was in fact synthesized. The cation-exchanged catalysts must be confirmed to possess intact POMs that are well-dispersed and interacting with the counter-cations. In addition, the catalysts should retain their structure and composition under practical reaction conditions.

Finally, the effect of counter-cation addition on catalyst acid and redox properties should be evaluated for comparison with the catalytic properties of the catalyst.

Common techniques for characterizing POM structure include Fourier transform infrared spectroscopy (FTIR),[21,41–44] Raman spectroscopy,[21,45] and nuclear magnetic resonance spectroscopy (NMR).[21,25] The dispersion characteristics may be evaluated using X-ray diffraction (XRD)[46] or transmission electron microscopy (TEM).[25] Correlations between the identity of the counter-cation and POM reducibility may be established using ultraviolet-visible spectroscopy (UV-Vis),[17,19] electrochemical reduction,[18] scanning tunneling spectroscopy,[16,19] and thermochemical reduction with H_2.[13] The acidity of POM catalysts is commonly measured using ammonia temperature programmed desorption (NH_3 TPD),[47] titrations under reaction conditions,[48] FTIR of adsorbed pyridine,[49] or ammonia adsorption calorimetry.[29]

In addition to the evaluation of the catalyst structure and properties, the catalytic activity of the cation-exchanged POMs must also be quantified, as discussed below.

1.4 Methanol oxidation and dehydration over supported POMs

Methanol was chosen as the primary probe reactant for this catalyst system as parallel pathways (see Equation 1-1) for methanol dehydration to dimethyl ether ($(CH_3)_2O$, DME) and oxidative dehydrogenation (oxidation) to formaldehyde (HCHO) probe the acid and redox sites properties of the POMs, respectively.[25,26] Formaldehyde may react further with additional equivalents of methanol to form methyl formate ($HCOOCH_3$, MF) and dimethoxymethane ($(CH_3O)_2CH_2$, DMM). Over-oxidation of methanol to CO_x is typically not observed at mild oxidation

conditions.[25] Mild reaction conditions were adapted from the literature[25] to promote POM stability, as POMs have been observed to partially decompose under harsh reaction conditions.[45,50–53] Turnover frequencies (TOFs) are defined for the dehydration and oxidation pathways in order to describe POM reactivities on a per site basis.

Equation 1-1: The primary reaction pathways for methanol dehydration to dimethyl ether and methanol oxidative dehydrogenation to formaldehyde.

Dehydration: $2\ CH_3OH \rightarrow (CH_3)_2O + H_2O$

Oxidative dehydrogenation: $CH_3OH + ½\ O_2 \rightarrow HCHO + H_2O$

A significant barrier to the utilization of counter-cation exchange to create tunable, selective, and active catalysts is that acidity often plays an important role in the selective oxidation pathway of many reactants over POMs.[24–26] For methanol oxidative dehydrogenation to formaldehyde and dehydration to dimethyl ether (Equation 1-1), the primary focus of the current work, it has been reported that acid sites may activate methanol,[25,26] and that the POM redox properties (typically varied by the inclusion of various quantities of V, Mo, and W in the POM framework) determine the selectivity between parallel oxidation and dehydration pathways.[26,45,54] Thus we might expect a tradeoff between selectivity and activity with supported cation-exchanged POMs, as cation-exchange may improve POM reducibility in some cases[16] but also decrease the quantity of acid sites necessary to activate reactants.

Other probe reactions investigated include the conversion of the C2 compounds: ethanol, ethylene, and acetaldehyde. Ethanol is converted to products along analogous pathways as methanol,[28,55] involving the dehydration and oxidation of ethanol to diethyl ether and

acetaldehyde, respectively. The POMs investigated in this work were not able to activate and convert ethylene to a potential oxidation product, acetaldehyde.[56] Nor could POMs convert acetaldehyde[57] to acetic acid under the mild conditions employed in this study (T ≤ 200˚C).

1.5 Activity Coefficients

The concepts of activity coefficients and thermodynamic activity are briefly introduced here. These concepts are applied later to describe non-idealities that arise in the cation-exchanged POM system, in particular between POM protons and other cations.

The thermodynamic activity (depicted by the lowercase letter 'a'), not to be confused with catalytic activity discussed in other parts of this work, represents the effective concentration of a species in a non-ideal solution. The thermodynamic activity is related to the chemical potential of a real solution through Equation 1-2.[58]

Equation 1-2: Thermodynamic activity and chemical potential

$$a = e^{\frac{\mu - \mu_o}{RT}}$$

where a is the thermodynamic activity, μ is the chemical potential, μ_o is the standard state chemical potential, R is the gas constant, and T is absolute temperature.

For systems that exhibit non-ideal behavior, the reaction rates and equilibrium constants can be defined using the thermodynamic activity of the system components,[59] rather than their concentrations. Under ideal conditions the thermodynamic activity of a given species is equal to

the actual concentration of that species. Activity coefficients (γ) are used to relate the thermodynamic activity of a species to its concentration as shown in Equation 1-3 below.

Equation 1-3: Relation between thermodynamic activity, activity coefficients, and concentration

$$a_i = \gamma_i \cdot \frac{c_i}{c^o}$$

where, for component *i*, a_i is the thermodynamic activity, γ_i is the activity coefficient, c_i is the concentration of *i*, and c^o is the standard concentration. By convention a_i and γ_i are unitless and typically the standard state is chosen to set both quantities equal to 1 for a pure substance.

Debye-Hückel theory describes the deviation from ideality of dilute solutions of electrolytes. In this model, each ion is surrounded by an ion cloud of equal but opposite charge. This accounts for the electrostatic interactions expected for aqueous anions and cations, where an ion is expected to be surrounded by multilayers of water and oppositely charged ions, even in dilute solutions.[59,60] The Debye-Hückel limiting law,[59] which may be used to calculate activity coefficients in a dilute solution, is presented in Equation 1-4 below.

Equation 1-4: Debye-Hückel limiting law

$$\ln(\gamma) = -A|z_+ z_-| \frac{\sqrt{I}}{1 + B\text{å}\sqrt{I}}$$

where A and B are constants that depend on the temperature and dielectric constant (ε) of the solvent, z_+ and z_- are the ion charges, å is the effective ion size, and I is the ionic strength of the solution, defined in Equation 1-5 below:

Equation 1-5: Ionic Strength

$$I = \frac{1}{2}\sum_{i}^{n} m_i z_i^2$$

where I is the ionic strength of the system, m_i is the concentration of component *i* in molality (mol/kg), and z_i is the ion charge. The summation is over all electrolyte components, both anions and cations.

Extensions of Debye-Hückel theory are discussed later and applied to the ionic systems investigated in this work, but at this point let it suffice that in its most basic form, Debye-Hückel theory relates the activity of component *i* to simple parameters of the system such as the charge of the ion, the ionic strength of the solution, and the dielectric constant of the solvent. The similarities between the model catalyst system described in this work and an aqueous electrolyte solution that may be described using Debye-Hückel theory are also explored further and the activity coefficients for solid acid catalysts are described for the first time.

1.6 Motivation

Opportunity exists for the development of a truly tunable metal-oxide catalyst with well-defined sites. The bifunctional POM catalyst, active for both oxidation and acid catalysis, is expected to retain the same structure at ambient conditions and under practical reaction conditions, in this work $T \leq 200^{\circ}C$. This consistent structure over a wide range of conditions is exciting as it allows

us to bridge the gap between surface science studies of well-defined surfaces and catalyst studies at industrial conditions.[16]

Cation-exchanged POMs have been investigated extensively for the ability of the POM to impact the secondary and tertiary structure of bulk POMs and for a number of other synergistic effects.[11,13,21,23,31] However there have been few studies where counter-cations were systematically varied, under mild conditions, and where POMs are confirmed to remain intact. Thus, the role of the counter-cation in the oxidation and dehydration activity of the POM catalysts is not always clear. For example, a link between counter-cation, redox properties, and oxidation activity is suspected[16] but not conclusively demonstrated, due to the limited range of cation-exchange explored and the harsh conditions used in previous studies. Additionally the relationship between oxidation activity and acidity is often empirical,[24,26] and while mechanistic studies have suggested a possible proton-mediated intermediate for methanol oxidation,[25] conclusive experimental evidence is still wanting.

An opportunity exists to extend the concepts of activity coefficients for concentrated aqueous solutions to describe the non-ideal thermodynamics of ionic species on a catalyst surface. As demonstrated in this work, the exchange of other cations for protons gives rise to non-linear changes in catalyst acidity. Concepts derived from Debye-Hückel theory are explored in this work to describe non-ideal behavior of supported ionic species such as cation-exchanged POMs.

1.7 Research Goals

Cation-exchanged POMs supported on silica were examined as model transition-metal oxide catalysts with well-defined, isolated, and tunable active sites. The obtained material included the presence of POMs well-dispersed on the silica support with an intimate interaction of cations and POMs, which is essential in order to tune the POM properties. A variety of characterization techniques were used to confirm that the desired material was synthesized and to evaluate the effect of cation addition on POM acid and redox properties.

The identity of the counter-cations and the quantity of cation per POM was systematically varied to determine the relationship between the counter-cation and the POM catalytic activity for methanol dehydration and oxidation. This included an investigation of the role of acidity in the oxidation pathway of methanol, previously proposed by others,[25,26] and establishing a link between the counter-cation, POM acidity, and the catalytic activity of POMs both for methanol dehydration and oxidation. Additionally, the role of POM reducibility was examined for the methanol oxidation pathway, including the potential impact of changes in POM redox properties induced by cation-exchange.

Finally, activity coefficients for solid acid catalysts were explored for the first time. The variation of the activity coefficients of the POM protons with cation addition was used to explain the observed behavior for cation-exchanged POMs. POMs were modeled as an electrolyte solution via the application of Harned's rule, which may be derived from Debye-Hückel theory.

1.8 Chapter Summaries

1.8.1 Chapter 2: Preparation and Characterization of Dispersed POM Catalysts

Chapter 2 contains an overview of the methods and considerations that went into the preparation and characterization of cation-exchanged supported POMs. First the literature precedents for the preparation and characterization of supported POMs are reviewed along with a detailed account of the preparation and characterization methods used in this work. Supported cation-exchanged POMs were synthesized with Na^{+}, Mg^{2+}, Al^{3+}, or Cu^{2+} as the counter-cation in various quantities including 0, 0.5, 1, 2 & 3 cations per POM. The characterization results for the cation-exchanged supported POMs are presented, including the confirmation of dispersed and intact POMs by XRD and FTIR, respectively. Additionally, UV-Vis were used to track POM reducibility with cation-exchange and a variety of techniques are used to characterize POM acid sites with cation-exchange. In particular, the strength and quantity of POM Brønsted acid sites were measured using NH_3 TPD and 2,6-di-*tert*-butylpyridine (DTBP) titration under reaction conditions, respectively. Overall, Chapter 2 details the synthesis and characterization of a model transition metal-oxide catalyst system with isolated, tunable, and well-characterized active sites.

1.8.2 Chapter 3: Dehydration and Oxidation of Alcohols with Supported Polyoxometalates: Effect of Cation-Exchange and Acidity

Chapter 3 explores the behavior of POMs exchanged with Na^{+} for the probe reaction of methanol dehydration and oxidation. First the expected reaction pathways for methanol conversion over POMs are detailed. Additionally, the possible role of acidity in the methanol oxidation pathway over POMs was introduced along with the reaction conditions and apparatus used in this work. With respect to the methanol reactivity results, the results for varying POM loading on silica are

first introduced. It is shown that the dehydration and oxidation TOFs do not vary strongly between catalysts with different POM coverages. In contrast, methanol dehydration and oxidation TOFs decrease rapidly with the addition of sodium as the POM counter-cation. This decrease in TOF with sodium addition is attributed to the essential role of acidity in activating methanol for both dehydration and oxidation reaction pathways, possibly due to a decrease in POM acid strength with sodium addition. Identical trends of decreasing TOF with sodium addition were also observed when ethanol dehydration and oxidation was used as the probe reaction.

1.8.3 Chapter 4: Dehydration and Oxidation of Methanol with Supported Polyoxometalates: Effect of Cation Identity and Reducibility

Chapter 4 follows the investigation of the effect of the identity of the POM cation on the reactivity of the POMs for methanol dehydration and oxidation. The cation-exchanged POMs investigated contain cations, either Na^{+}, Mg^{2+}, Al^{3+}, or Cu^{2+}, in quantities varying from 0 – 3 cations per POMs. The oxidation and dehydration TOFs again decreased with cation addition. The trends for the decreasing dehydration and oxidation TOFs with cation addition could be described by a single parameter, the quantity of acid sites per POM. The POM reducibility was influenced by the identity of the cation but these changes in POM redox properties were not catalytically relevant, possibly due to the strong influence of POM acid properties on methanol reactivity. The critical role of acidity in the oxidation pathway of methanol suggests the oxidation of methanol may proceed via C-H activation of a protonated methanol intermediate. Thus, the opportunity to use cation exchange to improve POM activity and selectivity for

selective oxidation catalysis is quite limited by the adverse impact of cation exchange on POM acid properties.

1.8.4 Chapter 5: Activity Coefficients for Solid Acid Catalysts

Chapter 5 includes the development and application of activity coefficients to heterogeneous catalysts that exhibit non-ideal behavior. A case is made for the treatment of POMs as a hydrated electrolyte solution and justification is provided for the applicability of Debye-Hückel theory to describe the thermodynamics of hydrated POM clusters with cation exchange. Harned's rule, which may be derived from Debye-Hückel theory, is introduced and shown to describe activity coefficients for aqueous acid-salt mixtures. Harned's rule was used to calculate activity coefficients for cation-exchanged supported POMs and the calculated activity coefficients tracked the dehydration TOF of cation-exchanged POMs remarkably well. Turnover frequencies for the dehydration and oxidation of methanol were also redefined using the thermodynamic activity of POM protons, rather than the concentration of POM protons as was used elsewhere in this work. The methods used in this chapter suggest a framework for the development of activity coefficients for other solid acid catalysts that exhibit non-ideal behavior with changes in the quantity or identity of ionic species.

1.8.5 Chapter 6: Conclusions and Recommended Future Directions

Chapter 6 summarizes the overall conclusions from this work as well as recommended future directions. Highlights include the confirmation that intact POMs were dispersed on silica and were interacting intimately with the cations, that perturbing POM Brønsted acid sites decreases rates, and ultimately that the opportunities to create an active and selective oxidation catalyst

using cation-exchange are quite limited due to the role of acidity in the oxidation pathway. Additionally, activity coefficients were defined for supported POMs that were able to account for non-linear behavior observed for POMs with cation exchange. Potential new directions include extensions of the current work via in-situ XRD to elucidate POM dispersion under reaction conditions, kinetics to reveal the mechanisms behind POM deactivation with cation addition, and the use of ammonia adsorption calorimetry as a more rigorous measure of POM acid strength. In addition, density function theory is discussed as a powerful tool to provide insight into the conversion of methanol over cation-exchanged POM model catalysts.

Chapter 2: Preparation and Characterization of Dispersed POM Catalysts

2.1 Introduction

This chapter discusses the procedures used to prepare metal-oxide catalysts with well-defined and tunable active sites, utilizing cation-exchanged polyoxometalates supported on fumed silica as the model system. The tools and techniques used to characterize the catalysts are also discussed, as confirming that the desired material was indeed the material synthesized is crucial for evaluating catalyst performance and the effects of catalyst composition.

2.1.1 Precedents for preparation of well-dispersed POM catalysts

POMs dispersed on a high surface area support (SiO_2, carbon black, $Cs_3PMo_{12}O_{40}$, etc.) have been investigated extensively for use in both acid and selective oxidation catalysis.[11,21,23,25,26] Achieving a good dispersion of POMs is essential to the model catalyst system envisioned in this work, for purposes of simplicity in evaluating the effects of POM composition on reactivity. If all POMs are dispersed on a high surface area support then all POMs are accessible to reactants, and therefore the number of active sites is the number of POMs in the system. Of course, another important requirement is that all POMs remain intact, both after synthesis and under reaction conditions.

Suitable high surface area supports for preparing dispersed POM catalysts include silica, activated carbon[11] and insoluble POM salts such as $Cs_3PMo_{12}O_{40}$.[23] Silica is the most commonly used support for POMs,[10,11] and was chosen as the support for this work. The choice of silica as

the POM support is typical because it is generally inert toward POMs, at least at moderate to high loadings.[10] At low loadings POM may interact strongly with surface silanols, otherwise they generally retain their structure and properties.[11] In the context of this work, the relatively inert nature of the silica towards the POMs means that POM-support interactions should not mask the influence of POM composition on POM properties and catalytic behavior. Further motivating the choice of silica as the POM support, literature precedents and detailed kinetics[25,61] are widely available for methanol conversion over POMs of various compositions supported on silica.[25,26,54,62]

A great variety of procedures have been explored in the literature for the preparation of silica-supported POMs.[10,25,30,54,61–64] Procedures in this work were adapted from those published by the Iglesia group[25,30] that were found to optimize the catalyst dispersion, POM structural integrity, and catalyst shelf-life, as well as ease of synthesis. Variables considered in the synthesis of silica supported POMs include type of silica, silica treatment conditions, POM preparation conditions, incipient wetness impregnation procedures, drying and calcination conditions, and finally catalyst storage conditions.

2.1.2 Common techniques for supported POM characterization

The primary POM characteristics that were investigated in this work include the POM dispersion, reducibility, and integrity of the Keggin structure, as well as the number and strength of POM acid sites.

An intact POM structure is defined in this work as a POM possessing the Keggin structure characteristic of POMs such as $H_3PMo_{12}O_{40}$, without significant defects, such as the formation of a lacunary POM ($HPMo_{11}O_{39}^{7-}$).[21] The presence of intact POMs can be verified by Fourier transform infrared spectroscopy (FTIR), where POMs are expected to exhibit four bands corresponding to the four types of oxygens present in Keggin-type POMs,[21,41–44] as discussed in detail later. Other techniques that have been utilized to confirm that POMs are intact and retain the Keggin structure include Raman spectroscopy[21,45] and nuclear magnetic resonance spectroscopy (NMR).[21,25]

The POM dispersion was investigated using X-ray diffraction (XRD). The presence of well-dispersed POMs is indicated either by the absence of diffraction features, as isolated POMs (1.2 nm in diameter) are too small to exhibit diffractions. Small disordered POM clusters, on the order of several nanometers in diameter, exhibit a single broad diffraction at low angles (~ 8˚).[46] Larger POM clusters or crystallites exhibit diffraction patterns characteristic of bulk POMs.[46] POM dispersion has also been investigated using transmission electron microscopy (TEM) for catalysts prepared in a similar manner to this work.[25]

The reducibility of POMs was investigated using ultraviolet-visible spectroscopy (UV-Vis) to determine the adsorption edge energy, which correlates very well with the POM reducibility.[17] A variety of techniques have previously been used to correlate changes in POM composition to changes in POM reducibility, including UV-Vis,[17,19] electrochemical reduction,[18] scanning tunneling spectroscopy,[16,19] and thermochemical reduction with H_2.[13] While the trends in POM reducibility with cation exchange are fairly well established with bulk POMs,[13,16–18] data for

cation-exchanged POMs supported on silica were not available. Thus, the UV-Vis edge energy was measured to confirm the expected trends in reducibility with cation-exchange for silica supported POMs.

The quantity and strength of POM acid sites were also investigated. The quantity of POM acid sites was primarily measured using titration of POM Brønsted acid sites with 2,6-di-*tert*-butylpyridine (DTBP) under reaction conditions, as pioneered by Iglesia.[48] POM acid site quantity was also probed with chemisorption of 1-butene and methanol, using a gravimetric chemisorption apparatus. The strength of POM acid sites was determined using ammonia temperature programmed desorption (NH_3 TPD). Other techniques that have been explored in the literature to investigate POM acid strength and/or quantity include Hammett indicators,[15] NH_3 adsorption calorimetry,[28,29] and pyridine absorption with FTIR.[49]

2.2 Experimental

2.2.1 Catalyst Preparation

Supported POM samples were prepared similarly to those reported previously in the literature.[25] The silica support was prepared by washing several grams of silica (Cab-O-Sil M5, 189 m^2/g, 1.5 ml/g wet point) with 500 mL of ultrapure water, followed by drying at 110˚C, crushing and sieving to less than 25 mesh, and finally calcining at 300˚C overnight. Aqueous solutions for use in incipient wetness impregnation that contained the appropriate quantity of POM (phosphomolybdic acid hydrate, Nippon Inorganic Color and Chemical Co.) and cation (sodium carbonate monohydrate, 99.5%, Fisher; magnesium carbonate hydroxide hydrate, 99%, Sigma-Aldrich; aluminum nitrate nonahydrate, 99.997% trace metals basis, Sigma-Aldrich; copper(II)

carbonate basic, reagent grade, Sigma-Aldrich) were prepared, using nitric acid addition when required to keep solutions sufficiently acidic to prevent POM decomposition[9] or to decompose insoluble carbonates. The POM-cation solutions were added several drops at a time, with intermittent mixing using a vortex mixer, to vials containing ~0.5g of the previously prepared silica. After incipient wetness impregnation was complete, the samples were placed in closed vials and stored in a drawer for 24 hours before drying in vacuum at 50˚C for 24 hours. Catalyst samples were stored in a drawer at ambient conditions until use. The effect of storage conditions is discussed in detail later.

Several series of cation-exchanged supported POM catalysts were prepared with varying POM surface coverages and a wide range of cation to POM ratios. For the first series, the POM loading was varied from 0.04 to 1.35 POM/nm^2 (2.2 - 44 wt% POM, 4.5 - 150% of a monolayer, defining monolayer coverage as 0.88 POM/nm^2, corresponding to a POM van der Waals radius of 1.2 nm for consistency with previous studies[25]). These catalysts are denoted HPMo Y, where Y is the loading in POM/nm^2. Values of Y range from 0.04 to 1.35 POM/nm^2, and the most common loading used in this work is Y = 0.2 POM/nm^2. The rest of the catalyst series involve cation-exchange with either Na^+, Mg^{2+}, Al^{3+}, or Cu^{2+} at one of two POM loadings, either 0.2 POM/nm^2 (10.3 wt % POM) or 0.7 POM/nm^2 (28.6 wt % POM). Cations (Na, Mg, Al, or Cu) were added in quantities between 0 and 6 cations per POM. Catalysts are denoted as CxPMo Y, where C is the identity of the cation (Na, Mg, Al, or Cu), x is the nominal number of cations per POM, and Y is the POM loading, either 0.2 or 0.7 POM/nm^2. For example, Al_2PMo 0.2 was prepared using two equivalents of Al per POM (2 units of $Al(NO_3)_3 \cdot 9H_2O$ per 1 unit of

$H_3PMo_{12}O_{40}$) at the appropriate concentrations to yield a catalyst with a POM loading of 0.2 POM/nm^2, and an aluminum loading of 0.4 Al/nm^2.

2.2.2 Catalyst Characterization

Attenuated Total Reflectance-Fourier Transform Infrared (ATR-FTIR) spectra of as-prepared catalyst samples at ambient conditions were obtained using a Nicolet iS50 spectrometer from Thermo Scientific, with a built-in diamond window and a DTGS detector. UV-Vis spectra were obtained using a ThermoFisher Scientific Evolution 300 spectrophotometer equipped with a Harrick Praying Mantis diffuse reflectance accessory and a Harrick High Temperature Reaction Chamber. Catalysts samples, held in the reaction chamber, were kept at 200°C in flowing air for 30 minutes prior to and during UV-Vis measurements. The UV-Vis adsorption edge energy was calculated by applying the Kubelka-Munk function with MgO as the reference.[25] The XRD diffraction patterns of the as-prepared catalysts were recorded using a Rigaku Miniflex 600 with a Cu-Kα radiation source with a D/teX Ultra silicon strip detector.

2.2.3 Titration with DTBP

The quantity of Brønsted acid sites was determined by titration with 2,6-di-*tert*-butylpyridine (DTBP) under reaction conditions. In a system similar to that used in steady state activity testing, catalyst samples (typically 40 mg) were loaded into a ¼" quartz tube that was placed in a resistively heated furnace (Mellen Microtherm) with a thermocouple placed at the top of the catalyst bed. Argon (99.99%, Purity Plus) and O_2 (99.99%, Purity Plus) were supplied using mass flow controllers (GF80/GF40, Brooks), while the liquid reagents contained in syringes (HSW Soft-Ject) were pumped using individual syringe pumps (New Era Pump Systems NE-

300) and evaporated in a homebuilt manifold in flowing Argon. The liquid reagents used were water (Ultrapure, Millipore Milli-Q), methanol (99.99%, Fisher) or ethanol (99.5%, Acros Organics), and 2,6-di-*tert*-butylpyridine (97%, Sigma-Aldrich) dissolved in methanol or ethanol.

The catalysts were pretreated in 30 sccm total flow of 2.7 kPa H_2O, 20 kPa O_2, balance Argon, at the reaction temperature (200°C for methanol, 160°C for ethanol) for 30 minutes. The feed was then switched to a reactant mixture containing 2.7 kPa H_2O, 4kPa of either CH_3OH or C_2H_5OH, 20 kPa O_2, balance Argon, 30 sccm total flow, and the catalyst was allowed to reach steady state for four hours. At this point the titration was started by switching the alcohol feed from a syringe containing alcohol only to one containing DTBP dissolved in methanol or ethanol, resulting in an identical reaction mixture except with the addition of 2 Pa DTBP in the feed. The concentrations of the reagents fed as liquids (CH_3OH or C_2H_5OH, H_2O, DTBP) and the primary acid catalyzed products, (dimethyl ether (DME) or diethyl ether (DEE) and ethylene (C_2H_4)), were monitored with an on-line mass spectrometer (Hiden HPR-20 R&D). The quantity of acid sites was determined with a linear fit of the dimethyl ether (DME) or diethyl ether (DEE) rates as a function of the quantity of DTBP added per POM.

2.2.4 NH_3 TPD

Ammonia Temperature Programmed Desorption (NH_3 TPD) of supported POM samples was conducted using a Micromeritics AutoChem II 2920 chemisorption instrument equipment with a mass spectrometer (Balzers ThermoStar) according to procedures outlined by Song and coworkers.[47] Catalyst samples (typically 30 mg on a POM basis) were loaded into the instrument quartz sample tube and pretreated in 20 sccm He at 200˚C for 2 hours. The sample was then

cooled to room temperature before the He flow was reduced to 5 sccm and ammonia was pulsed in using a 0.5 mL loop until the sample was saturated, typically around 6 pulses. The ammonia exposure was monitored using a thermal conductivity detector (TCD). The sample was then heated to 100˚C in 5 sccm He for 1 hour to desorb weakly bound ammonia. Finally, the catalyst was cooled to ambient temperature, then ramped at 5˚C/min to 600˚C in 10 sccm He to desorb strongly bound ammonia and oxidized ammonia products (N_2, N_2O, trace NO). The masses recorded with the mass spectrometer were: 4, 14, 16, 17, 18, 28, 30, 32, 44, and 46 in order to measure He, nitrogen, NH_3, H_2O, N_2, NO, O_2, N_2O, and NO_2, respectively.

2.2.5 Gravimetric Chemisorption

The quantity of POM acid sites was probed using gravimetric chemisorption. A thermogravimetric analysis (TGA) system (TA Instruments Q50), equipped with a microbalance, a glass-lined evolved gas analysis (EGA) furnace, and a custom gas supply manifold was used for the gravimetric chemisorption measurements. The manifold was used to provide pretreatment gases (dry air or He), adsorbent gases (500ppm CH_3OH in He or 1% 1-butene in N_2), and an inert purge gas (He). The methanol in He was supplied using bubblers in an evaporator-saturator setup in a refrigerated bath. The total gas flow rate for all stages of the experiment was 100 sccm. A typical experiment involved loading the catalyst (20 mg) into the platinum pan of the TGA microbalance and pretreating in either dry air at 200˚C for methanol chemisorption or in He at 60˚C for 1-butene chemisorption. Catalysts were ramped to the pretreatment temperature at 10˚C/min and held at the pretreatment temperature for 30 minutes.

For methanol chemisorption, after pretreating the catalyst at 200˚C in dry air for 30 minutes, the catalyst was cooled to 100˚C in flowing air. After the sample weight had stabilized, the gas feed was switched to He for 30 minutes to allow for the mass to stabilize again. Then, by simultaneously switching the two three-way valves on the gas manifold, the gas feed was switched to 500 ppm CH_3OH in He. The mass increase as methanol adsorbed on the catalyst surface was recorded, and the system was allowed to reach saturation for four hours. Then, the gas feed was switched back to He to allow the desorption of weakly bound methanol and water, again four hours were allowed for the sample mass to stabilize. The quantity of acid sites was calculated by assuming a 1:1 reaction between H^+, CH_3OH, and a POM oxygen to form a methoxy ligand ($-OCH_3$) and a water molecule. It was also assumed that the methoxy ligand was stable at 100˚C for an extended period of time[65] and that the water desorbed from the catalyst. Therefore, the quantity of acid sites could be calculated using Equation 2-1,

Equation 2-1: Calculation of H^+/POM for gravimentric chemisorption.

$$\frac{H^+}{POM} = \frac{(m_f - m_i)}{\Delta MW \cdot N_{POM}}$$

where m_f is the sample mass after purging the methanol exposed sample in He for four hours, m_i is the sample mass prior to methanol exposure, ΔMW is the additional mass per ligand (14 g/mol assuming Mo-OCH_3 replaces Mo-OH), and N_{POM} is the number of moles of POM loaded into the TGA sample pan.

For 1-butene chemisorption, the catalyst was first treated in flowing He at 60˚C until the mass was stable, typically 30 minutes. Then, by simultaneously switching the two three-way valves on

the gas manifold, the gas feed was switched to 1% 1-butene in N_2. The increase in mass was recorded as 1-butene adsorbed onto the catalyst surface and the system was allowed to reach saturation for four hours. Then, the gas feed was switched back to He, and the mass decrease was recorded as physisorbed 1-butene was removed, again for four hours. The quantity of acid sites was calculated by assuming a 1:1 reaction between MoO-H^+ and 1-butene to form an alkoxy ligand (Mo-OC_4H_9). The alkoxy formation was assumed to be facile and irreversible at 60˚C.[66–68] The quantity of acid sites could again be calculated using Equation 2-1, where m_f is the sample mass after desorbing weakly bound 1-butene in flowing He for four hours, m_i is the sample mass prior to butene exposure, ΔMW is the additional mass per ligand (56 g/mol assuming Mo-OH + $C_4H_8 \rightarrow$ Mo-OC_4H_9), and N_{POM} is the number of moles of POMs loaded into the TGA sample pan.

2.3 Results

2.3.1 Influence of Catalyst Preparation and Storage Methods

The methods for catalyst synthesis were primarily adapted from methods published by the Iglesia group.[25,30,61] In the initial phase of this project, several different catalyst preparation and storage techniques were investigated, but ultimately it was determined that the Iglesia group had set the standard for synthesis of POMs that were both well-dispersed and stable over long periods at either ambient conditions or under reaction conditions. Generally, their techniques for synthesis and reaction involve mild conditions that keep the POMs hydrated as much as is practical. The following sections discuss the details of the catalyst synthesis and storage to appropriately outline the benefits of the current synthesis methods as compared to previous techniques attempted in this lab.

2.3.1.1 Silica Preparation and Treatment

Fumed silica (Cab-O-Sil M5, 189 m^2/g) was used as the support for the dispersed POM catalysts, as it is well-known to be inert, to promote the dispersion of POMs, and to increase POM thermal stability, as compared to a bulk POM crystallite.[10] Various fumed silica samples with different surface areas were examined (100 – 350 m^2/g); Cab-O-Sil M5 (189 m^2/g) was used as few differences were observed between the various samples and Cab-O-Sil M5 was the only fumed silica readily available for purchase. In order to facilitate the facile synthesis of the supported POM catalysts, the fumed silica as received needed to be densified, as out of the bottle it has a density near 0.03g/mL, making it extremely difficult to handle in a laboratory setting. Initial catalyst synthesis without pre-densifying the catalyst was quite tedious and required physically mixing the powder with a spatula to incorporate the active species into the catalyst particles during incipient wetness impregnation. In contrast, with the pre-densified material, only a vortex mixer was required to incorporate the impregnation solution into the silica, greatly simplifying the procedure and allowing for better reproducibility as well, since all active species and support particles were ensured to remain in the sample vial.

The Iglesia group reported washing the fumed silica with nitric acid[25] as the initial step in catalyst preparation. Notably, the nitric acid wash was deemed unnecessary for a raw material such as fumed silica, due to its high purity.[69] No differences in activity were observed with or without the initial acid wash. However, the washing step was adapted, with water instead of nitric acid, as it was found to be a facile method of densifying the initial fumed silica, compared to other methods, such as pressing with a catalyst press followed by sieving. For the silica wash,

~50g of fumed silica was placed over filter paper in a Buchner flask and funnel and the silica was hydrated with ~ 0.5L of ultrapure water to form a gel. Vacuum was then applied to the flask and used to removed excess water. The resulting gel was dried in a lab oven at 110˚C overnight, then crushed with a mortar and pestle before sieving to less than 25 mesh (< 707 microns). The silica was then calcined at 300˚C in order to remove water, both hydrogen-bonded and weakly interacting, as well as to remove a portion of the surface hydroxyls (≡SiOH groups). The silica support was stored in a desiccator to avoid the re-adsorption of water. The calcination temperature was chosen based on the work of Zhuravlev.[70] The Zhuravlev model states that when heating silica from ambient to 180-200˚C, water is removed from the silica surface without significantly impacting the concentration of surface silanols. Calcining the catalyst at temperatures higher than 200 ˚C results in the dehydroxylation of the silica surface and removal of surface silanols according to Equation 2-2.

Equation 2-2: Condensation reaction of two silanols.

$$2 \equiv SiOH \rightarrow \equiv Si\text{-}O\text{-}Si\equiv + H_2O$$

Silanol concentration decreases from the maximum concentration of 4.6 ≡SiOH per nm^2 to 3.55 and 1.8 ≡SiOH per nm^2 for calcination at 300˚C and 500˚C, respectively.[70]

Initial synthesis procedures for preparing supported POM catalysts were adapted from works[63,64] that outlined methods to prepare POMs highly dispersed on a high surface area support. These procedures typically involved calcining the silica support at temperatures above 500˚C in order to prepare a catalyst support with isolated silanols. However, reducing the calcination temperature to 300˚C resulted in a catalyst with a longer shelf-life and with equal or better

dispersion of POMs. Evidently POMs (or small POM clusters) are readily dispersed and stabilized by interactions with silanol groups,[25,71] likely due to the formation of hydrogen bonding networks between POMs, silanols, and waters of hydration.

2.3.1.2 Incipient wetness impregnation, drying, and calcination

POMs were loaded onto the silica support using incipient wetness impregnation, again following the methods of Iglesia.[25,30,61] Incipient wetness impregnation involves impregnation of the silica with an aqueous solution of POMs that has a solution volume corresponding to the pore volume of the support. The Iglesia procedure is unique in that after impregnation the wet samples were allowed to rest in closed vials for 24 hours prior to drying at 50˚C. The resting step is claimed to promote the distribution of POMs evenly on the silica support.[72] The drying temperature of 50˚C is unique as well, since POM/SiO_2 catalysts are typically dried after impregnation at 100 to 120˚C overnight in the majority of the literature.[54,62] Some researchers also calcined the catalysts after drying, typically at temperatures of 200-300˚C for several hours.[63,73]

Heating POMs to temperatures between 100-200˚C renders the POM almost completely anhydrous.[9] Thus the hydration level of POMs may easily be determined gravimetrically by heating the POMs to 200˚C and assuming that the mass decrease with heating is due to the loss of waters of hydration. Using this method, it was determined the POMs used in this work ($H_3PMo_{12}O_{40}\cdot 31H_2O$, Nippon Inorganic Color and Chemical Co.) retained 4.5 waters of hydration upon heating to 50°C in vacuo. The same POMs retained 1 and 0 H_2O per POM upon heating in air at 120 and 200˚C, respectively, as determined by TGA and via the gravimetric technique described.

It is clear that the procedures adopted by the Iglesia group are intended to keep the POMs in a hydrated state until use in a catalytic reactor or for characterization. Similarly, the mild reaction temperatures (160˚C) and the presence of co-fed water during reactions with methanol (2.7 kPa H_2O, 4 kPa CH_3OH) employed during their studies is consistent with the fact that POMs are more stable in a hydrated environment. Indeed, after adopting these mild drying procedures, catalysts were noted to have a longer shelf life when kept in their hydrated state.

2.3.1.3 Catalyst Storage

As alluded to in the previous section, the storage conditions can have a significant impact on the shelf-life of the as-synthesized POM catalysts, although it should be noted that no differences in activity for methanol dehydration and oxidation were observed for catalysts of different ages. As synthesized, catalysts were typically bright yellow; however, over time they tend to turn pale green and eventually dark blue. These color changes may be associated with the POM reduction, a breakdown of the POM structure to form lacunary POMs, and/or the formation MoO_3 monomers or oligomers. It has been previously noted that $H_4SiMo_{12}O_{40}$ decomposes at room temperature over long periods of time.[9] If POMs are reduced, they may be easily re-oxidized under reaction conditions. Similarly, after decomposition, POMs are known to reconstruct under hydrated conditions at elevated temperatures in the presence of oxygen.[9] Thus it is not surprising that no differences in activity were observed when an old POM sample, now a deep blue, gave similar reactivity results as the fresh catalyst. In spite of the reactivity behavior, it was deemed poor practice to use POM samples that had undergone color change, so catalyst samples were

used in experiments typically within 2-3 weeks of synthesis, prior to the onset of significant color change.

Factors that impact catalyst shelf-life (an "expired" sample is defined as possessing significant color change from the initial catalyst) include temperature, hydration, coverage, and the counter-cation. Storing supported POM catalysts at 4˚C extends the shelf-life,[72] this storage method was confirmed for samples in this study; however, a suitable refrigerator was not available to safely store large quantities of catalyst samples, which being strong oxidizers, are incompatible with organics typically stored in lab refrigerators. As mentioned previously, keeping POMs hydrated is important for POM stability. All samples used in this study were stored in a drawer in closed vials at ambient conditions, to maintain a moderate hydration level, perhaps at or above the 4.5 H_2O per POM that were observed to be present after drying POMs at 50˚C in vacuo. Storing POMs in a desiccator to prevent POM re-hydration significantly decreases the shelf-life. Storing POMs at 100% relative humidity gives the POM a very long shelf life but also may lead to the redistribution of POMs.[72] Additionally, as the material is very hydrated, it may be difficult to know the exact weight percent of active material. Storing catalysts fully hydrated would have required drying a portion of the sample to quantify the POM wt% in parallel with each use in reactions or characterization.

The specific composition of the catalyst also has an impact on its shelf life. At lower loadings (e.g., 0.04 POM/nm^2) the shelf-life is much shorter than at loadings near a monolayer, which is consistent with the tendency of POMs to decompose at very low loadings.[9] Also, the POMs with protons as the cations tended to be the least stable over time, and the addition of cations,

especially large quantities (≥ 3) led to catalysts that turn blue much more slowly. POMs exchanged with cations such as Cs^+ and Ag^+ never turned blue, while the stabilizing effect of Na^+ was minimal compared to other cations.

2.3.2 XRD of Supported POM Catalysts

2.3.2.1 HPMo at various coverages

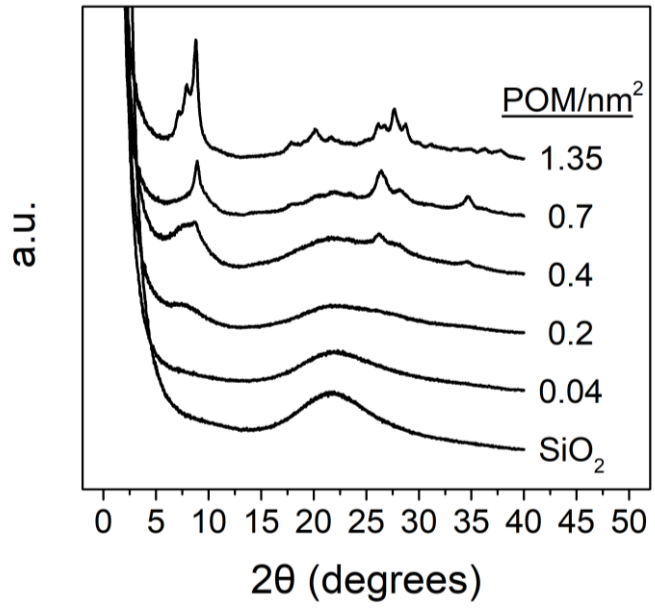

Figure 2-1: XRD for HPMo at various POM loadings: $H_3PMo_{12}O_{40}/SiO_2$ 0.04 to 1.35 POM/nm^2. The bare silica support was included as a reference.

XRD was used to detect the presence of POM clusters and crystallites. Figure 2-1 shows the diffraction patterns for supported HPMo samples at different loadings. At the lowest POM loadings (0.04 POM/nm^2), POMs are well dispersed so only the broad band due to silica at ~ 22˚ is observed. As the loading is increased to 0.2 POM/nm^2 a broad band at 8˚ 2θ appears, corresponding to scattering by small 2D clusters of POMs.[74] Further increasing the POM loading

(0.4-0.7 POM/nm^2) leads to a sharpening of the peaks, a shift of the low angle peak to 9˚, and the appearance of peaks at higher angles (26.5˚, 28˚, 35˚), indicating at these loadings some POM crystallites have formed. Iglesia and coworkers investigated POMs supported on silica at similar loadings using TEM,[25] observing clusters with diameters from 1-3.5 nm (mean: 1.9 nm) for a loading of 0.7 POM/nm^2 and clusters with diameters from 1-2.5 nm for loadings of 0.04 and 0.16 POM/nm^2 (mean: 1.2nm and 1.5 nm respectively). Evidently clusters larger than ~ 2-2.5 nm have enough long range order to yield reflections at higher angles, which is in good agreement with the XRD data.[74] The highest loading of 1.35 POM/nm^2 was above a theoretical monolayer (~ 0.88 POM/nm^2), and not surprisingly exhibited a diffraction pattern consistent with the presence of hydrated bulk POMs.

2.3.2.2 NaPMo at 0.2 POM/nm^2 and 0.7 POM/nm

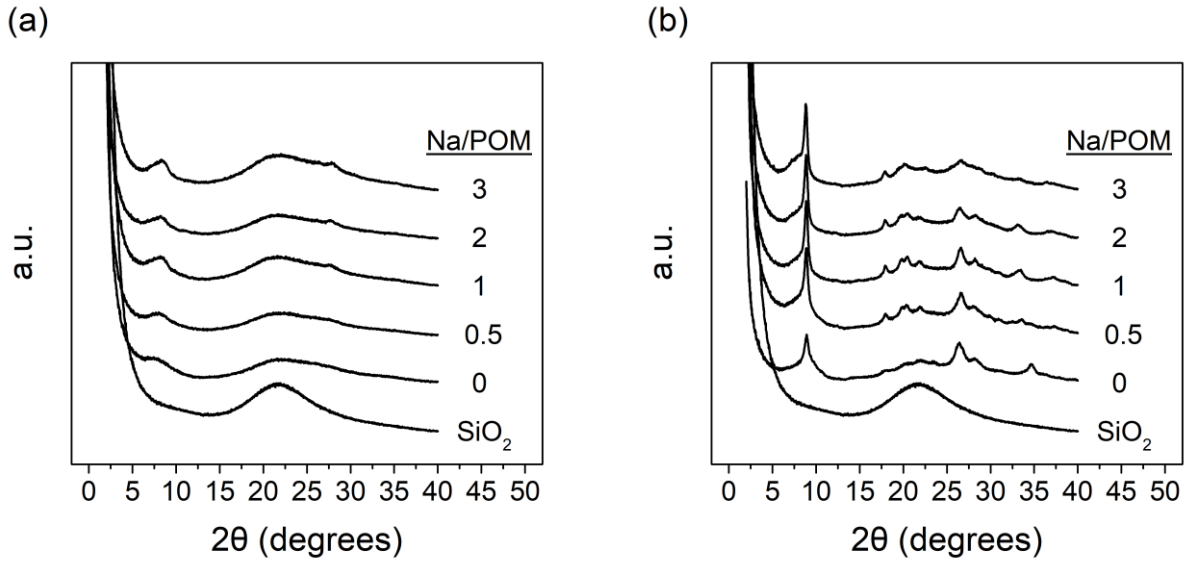

Figure 2-2: XRD for Na_xPMo at a) 0.2 POM/nm^2 and b) 0.7 POM/nm^2; x = 0, 0.5, 1, 2, 3. The bare silica support was included on all plots as a reference.

The XRD patterns for supported POMs exchanged with Na are given in Figure 2-2. At a loading of 0.2 POM/nm^2 (Figure 2-2a), POMs are generally well dispersed for all but the highest levels of cation exchange. In Figure 2-2a, with increasing sodium addition at 0.2 POM/nm^2 the low angle peak grows in intensity and shifts from 8˚ to 8.5˚, while at higher sodium concentrations, a peak at ~ 28˚ is apparent indicative of small amounts of crystallite formation. Both of these observations suggest that for low POM loadings, sodium addition promotes the formation of both 2-D and 3-D POM clusters, possibly due to the smaller size of Na^+ as compared to hydrated protons, e.g., $(H_2O)_2H^+$.

Cation exchange was also investigated at a higher loading of 0.7 POM/nm^2 for sodium-exchanged POMs. The XRD results are given in Figure 2-2b. Bulk POM diffractions are observed at all levels of cation exchange at this loading, although increasing the cation content leads to an increase in intensity of the peak at 9˚ with a weakening of reflections at higher angles. This observation suggests that high extents of sodium exchange favor the formation of smaller or more disordered POM clusters at high POM loadings. It should again be noted that the average cluster size for similarly prepared catalysts at an identical loading (without cation exchange) was ~ 2nm,[25] to point out that at all levels of cation exchange and loading POM clusters only contain a few POMs in diameter and are accessible to reactants.[25]

2.3.2.3 [Mg, Al, Cu]PMo at 0.2 POM/nm^2

The XRD patterns for supported POMs exchanged with Mg and Cu are given in Figure 2-3. For the catalysts exchanged with varying concentrations of Mg^{2+} and Cu^{2+} the POMs retain excellent dispersion, with only the slightest hint of higher order diffractions with excess cation exchange.

For example, with Mg_3PMo 0.2, the low angle peak shifts slightly with the addition of divalent cations, although not monotonically. For MgPMo 0.2, the low angle peak shifts from 8˚ to 9˚ for Mg_1PMo and then decreased to 7.5˚ for $Mg_{1.5}PMo$ and 7˚ for Mg_3PMo. Catalysts exchanged with Cu^{2+} exhibit similar but less pronounced trends with the low angle peak shifting from 8˚ to 8.7˚ for $Cu_{0.5}PMo$ then incrementally decreasing back to 8˚ for Cu_3PMo.

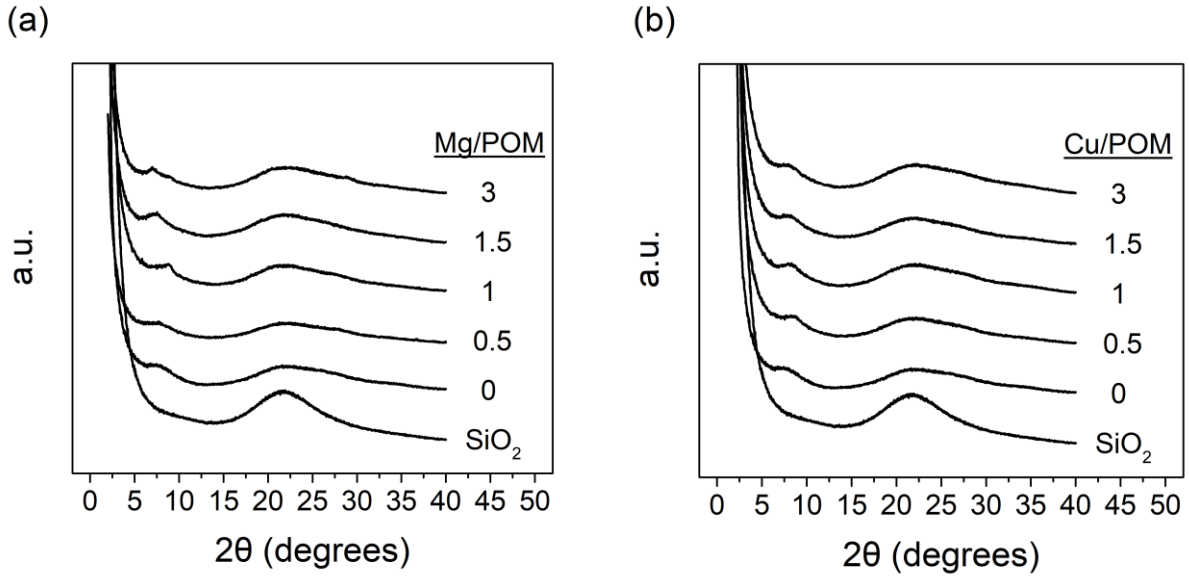

Figure 2-3: XRD for $[Mg,Cu]_xPMo$ at 0.2 POM/nm^2; x = 0, 0.5, 1.5, 2, 3. The bare silica support was included on all plots as a reference.

While it is difficult to describe the exact local structure in the vicinity of the POM that leads to the observed trends, the shifts in the low angle peak are certainly due to changes in inter-POM spacing as Mg^{2+} and Cu^{2+} exchange with $(H_2O)_2H^+$. It should be noted that shifts were observed with each equivalent of cation, from 0.5 to 3 cations per POM, indicating an intimate interaction of the POMs and the added counter-cations.

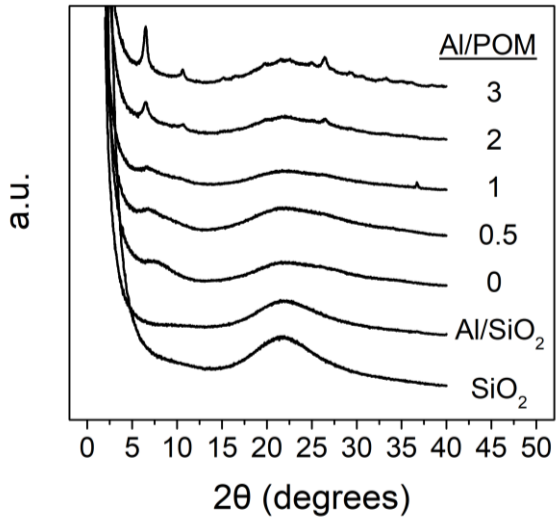

Figure 2-4: XRD for Al_xPMo at 0.2 POM/nm^2; x = 0, 0.5, 1, 2, 3. Also included are Al/SiO_2 at a loading of 0.6 Al/nm^2 and the bare silica support.

The addition of increasing quantities of Al^{3+} (Figure 2-4) resulted in a steady decrease in the location of the low angle peak, from 8˚ for HPMo to 6.5˚ for Al_3PMo, along with the emergence of a significant quantity of bulk POM diffractions for catalysts with excess Al (Al_2PMo and Al_3PMo. Features at 37˚ (for example in Al_1PMo) are due to the aluminum sample holder and may be neglected. The shift in location of the low angle peak is again indicative of the POM-POM spacing changing as Al^{3+} replace hydrated POM protons. The sample denoted as Al/SiO_2, prepared by loading only aluminum nitrate on silica at a loading of 0.6 Al/nm^2, was included to demonstrate that an ordered Si_xAl_yO phase was not observed when Al is loaded on these catalysts.

2.3.2.4 Post-reaction characterization of selected catalysts

In order to ensure that significant changes in POM dispersion did not occur during reactions of supported POMs with methanol, XRD of selected catalysts was collected for catalysts as-synthesized and catalysts post-reaction, as shown in Figure 2-5. Post-reaction catalysts were collected from spent reactor tubes and stored in closed vials for several days at ambient conditions prior to analysis. For the unexchanged catalyst, HPMo, and catalysts with one cation per POM (either Na, Mg, or Cu), no significant changes in diffraction patterns were observed before and after reaction with methanol at 200˚C. It should be noted that these results do not preclude the possibility that POM clusters may aggregate under reaction conditions (typically 2.7 kPa H_2O, 4 kPa CH_3OH, 20 kPa O_2, 200˚C), as no measurements of dispersion were done under reaction conditions.

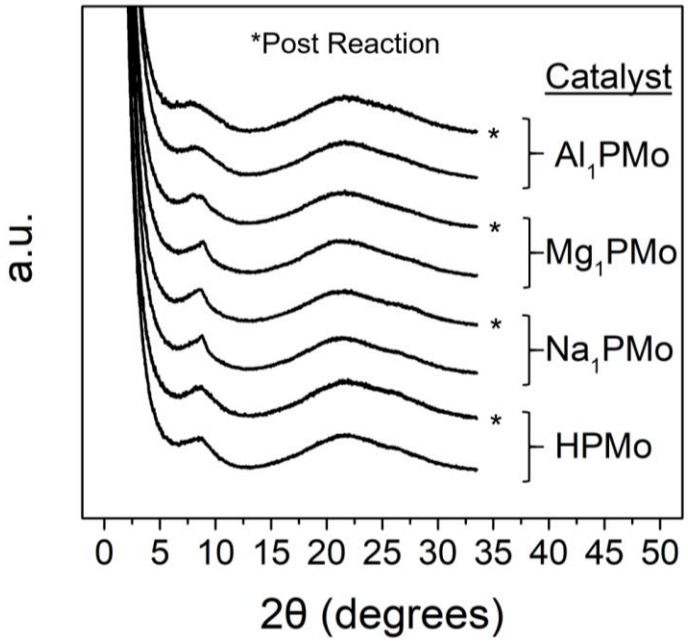

Figure 2-5: XRD of HPMo 0.2 and [Na, Mg, Al]$_1$PMo 0.2 as-synthesized and after reaction with methanol at 200˚C (post-reaction curves indicated with *).

2.3.2.5 XRD of POMs exposed to NH_3

The effect of ammonia exposure on POM dispersion was investigated in order to validate NH_3 TPD as a probe of catalyst activity. If ammonia exposure drastically alters POMs dispersion, NH_3 TPD may not accurately portray the characteristics of the original catalyst. HPMo 0.2 and HPMo 0.7 were pretreated, exposed to NH_3, and purged in flowing He at 100˚C for 1 hour according to the standard procedures for NH_3 TPD used in this work. The catalyst was then removed from the chemisorption apparatus and prepared for XRD similarly to other samples.

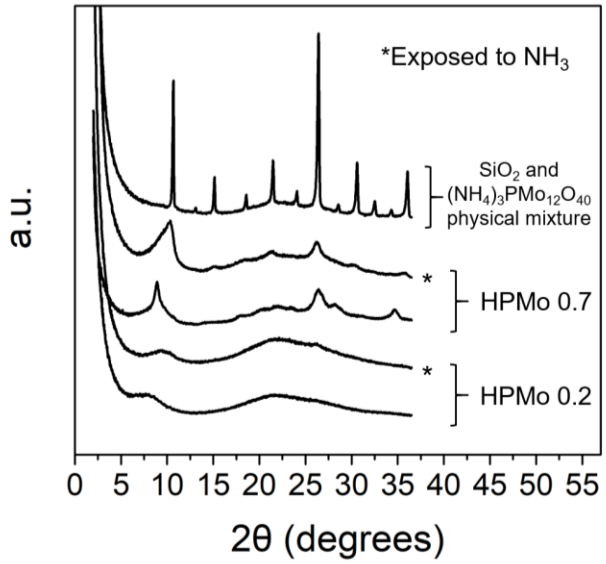

Figure 2-6: XRD for 0.2 and 0.7 POM/nm^2 $H_3PMo_{12}O_{40}/SiO_2$ before and after ammonia exposure (post-reaction curves indicated with *). Bulk $NH_4PMo_{12}O_{40}$ dried at 50˚C in vacuo included as a reference.

Figure 2-6 illustrates diffraction patterns for HPMo 0.2 and HPMo 0.7 before and after NH_3 exposure, with a physical mixture of bulk $(NH_4)_3PMo_{12}O_{40}$ and fumed silica included as a reference. The physical mixture was in the same proportion of POM and SiO_2 as the HPMo 0.7 catalyst on a mass fraction basis. The low angle peak shifted from ~8-9˚ to 10.5˚ for all samples as hydrated protons[1] were replaced by smaller NH_4^+ cations. However, for both HPMo 0.2 that

was originally dispersed and for HPMo 0.7 that exhibited evidence of cluster formation, no additional bulk POM formation due to ammonia exposure was observed. The fact that HPMo 0.7 exposed to NH_3 looks much more similar to the original HPMo 0.7 catalyst than the physical mixture of the same proportions and composition confirms that the POM textural properties are not significantly altered by exposure to ammonia. Similar results were found for partially exchanged catalysts, such as Na_1PMo 0.7, when exposed to ammonia. Based on these results, exposing the catalysts to ammonia can be concluded to not significantly alter the catalysts' textural properties or dispersion.

2.3.3 FTIR of Supported POM Catalysts

ATR-FTIR spectroscopy was used to demonstrated that the supported POM catalysts retain their molecular structure over a wide range of coverages and with cation exchange. The presence of POM vibrations at 1054, 963, 884, and 787 cm^{-1} corresponding to P-O, M=O_t, Mo-O_b-Mo, and Mo-O_c-Mo (O_p, O_t, O_b, and O_c are defined in Figure 2-7), respectively,[41,42] in the following figures confirms that the Keggin structure remains intact at these low loadings.

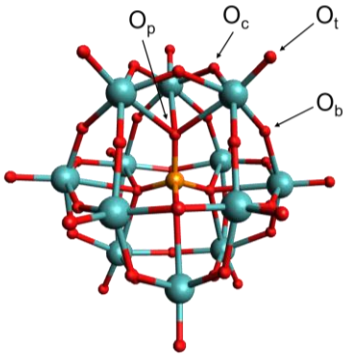

Figure 2-7: Schematic of a polyoxometalate with the Keggin structure, with the four types of oxygen labeled: P-O (O_p), corner (O_c), terminal (O_t), and bridging (O_b).

2.3.3.1 HPMo at various coverages

Spectra for the HPMo 0.04-1.35 (Figure 2-8) series of catalysts are shown, along with the bare silica support as a reference. In Figure 2-8, following the trend for bare silica to a catalyst with 44 wt% POM (1.35 POM/nm^2), the characteristic POM peaks can clearly be seen growing in. POM vibrations at 1054, 963, 884, and 787 cm^{-1} corresponding to P-O, M=O_t, Mo-O_b-Mo, and Mo-O_c-Mo (O_t, O_b, and O_c are defined in Figure 2-8), respectively,[41,42] are clearly distinguishable from the bands for the silica support at 1060, 976, and 805 cm^{-1} at the higher POM loadings.

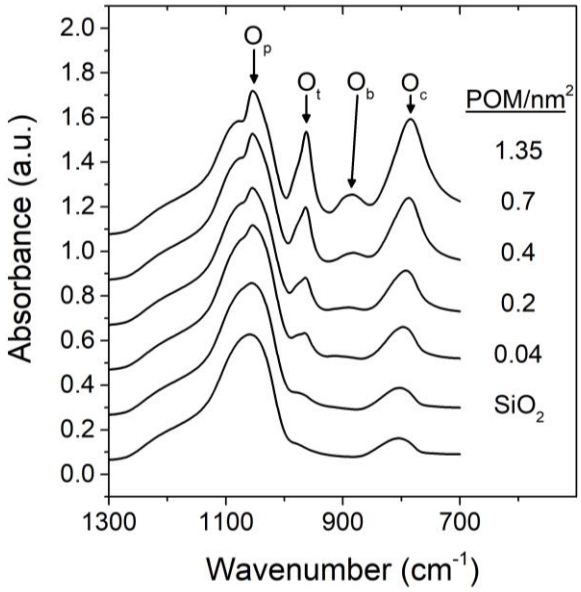

Figure 2-8: ATR-FTIR for $H_3PMo_{12}O_{40}/SiO_2$ 0.04 to 1.35 POM/nm^2. The bare silica support was included on all plots as a reference. O_p, O_t, O_b, and O_c are defined as shown in Figure 2-7.

At low POM loadings (0.04 POM/nm^2), the signals are too weak with respect to silica to definitively confirm the POM structure is intact via FTIR; however, others have used NMR[25,43] and Raman[41,43] spectra for supported POMs at similar loadings to confirm that the Keggin structure remains intact at these low loadings. As reported previously,[42] the Mo-O_c-Mo band is

sensitive to POM loading on silica, as seen with the ~20 cm^{-1} band shift as POM loading varies from 0.04 to 1.35 POM/SiO_2 (Figure 2-9). This band shift has been attributed to the absence of anion-anion interactions at low loadings.[42]

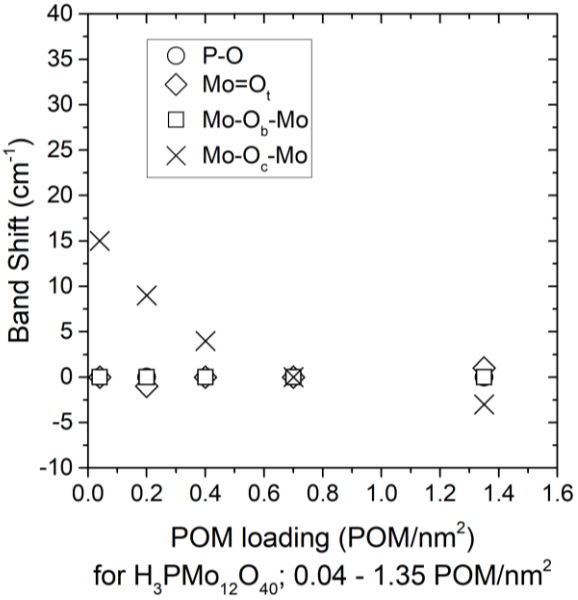

Figure 2-9: Band shifts for varying HPMo loading on silica (0.04 – 1.35 POM/nm^2). Shifts are relative to the band positions measured for HPMo 0.7.

2.3.3.2 NaPMo at 0.2 POM/nm^2 and 0.7 POM/nm^2

ATR-FTIR spectra for the Na_xPMo 0.2 and Na_xPMo 0.7 series of catalysts are shown in Figure 2-10, along with the bare silica support as a reference. All of the characteristic POM bands were observed, indicating that the POM structure is retained with sodium exchange. The band shifts for cation addition at 0.7 POM/nm^2 are illustrated in Figure 2-11. The P-O stretches are typically insensitive to cation substitution[44], as observed here. The decrease in the Mo=O_t stretching frequency and the larger increase in the Mo-O_b-Mo and Mo-O_c-Mo bands have been variously attributed to polarization effects due to replacement of protons with more electropositive sodium

cations[42,44] and/or the loss of water and inter-POM hydrogen bonding networks,[44] or other changes in anion-anion and anion-cation interactions as sodium is added. In any case, these observations indicate that POM electronic properties are sensitive to the identity and population of associated counter-cations.

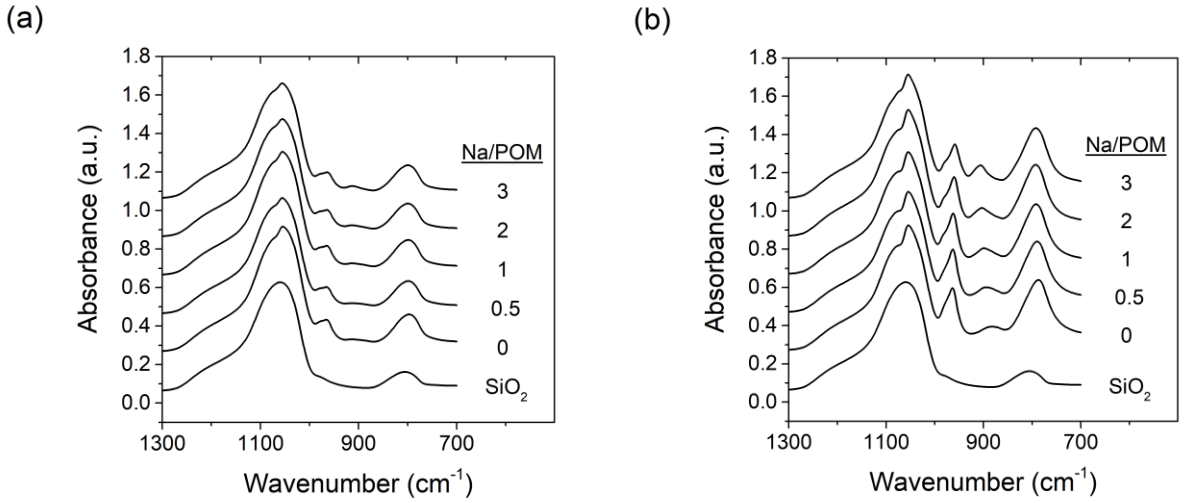

Figure 2-10: ATR-FTIR for $Na_{3-x}H_xPMo_{12}O_{40}/SiO_2$ at **a)** 0.2 POM/nm^2 or **b)** 0.7 POM/nm^2 where x = 0, 0.5, 1, 2, 3. The bare silica support was included on all plots as a reference. O_p, O_t, O_b, and O_c are defined as shown in Figure 2-7.

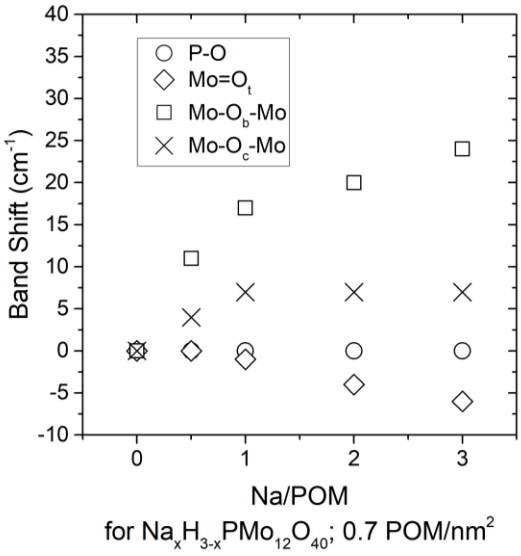

Figure 2-11: Band shifts for sodium addition at 0.7 POM/nm^2. Shifts are relative to the band positions measured for HPMo 0.7.

2.3.3.3 [Mg,Al,Cu]PMo at 0.2 POM/nm^2

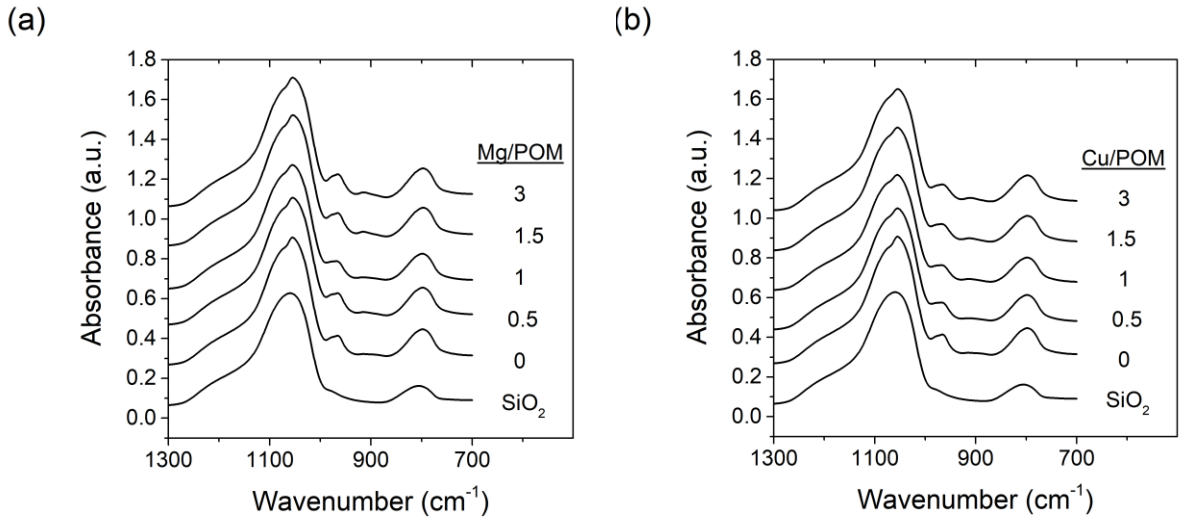

Figure 2-12: ATR-FTIR for **a)** MgPMo and **b)** CuPMo at 0.2 POM/nm^2; x = 0, 0.5, 1.5, 2, 3. The bare silica support is included as a reference. O_p, O_t, O_b, and O_c are defined as shown in Figure 2-7.

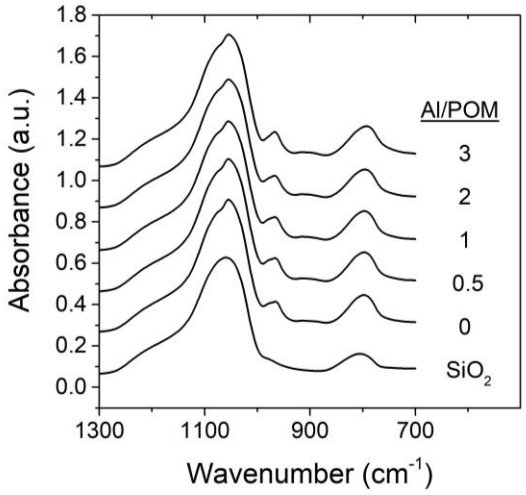

Figure 2-13: ATR-FTIR for Al$_x$PMo at 0.2 POM/nm^2; x = 0, 0.5, 1, 2, 3. The bare silica support is included as a reference. O_p, O_t, O_b, and O_c are defined as shown in Figure 2-7.

The as-prepared catalysts exchanged with Cu and Mg (Figure 2-12) and with Al (Figure 2-13) were analyzed by ATR-FTIR to confirm the presence of intact POMs on the silica surface. No

significant shifts of the characteristic POM bands were observed with the addition of cations at a POM loading of 0.2 POM/nm^2, with the addition of up to three cations per POM, regardless of cation identity. These results demonstrated that POMs are intact as-synthesized with cation exchange, and that shifts in FTIR bands are only weakly dependent on cation identity. Rather, the only significant shifts in FTIR bands were observed with varying POM loading (Figure 2-9) and with cation addition at a high loading (Figure 2-11).

2.3.3.4 Post-reaction characterization of selected catalysts

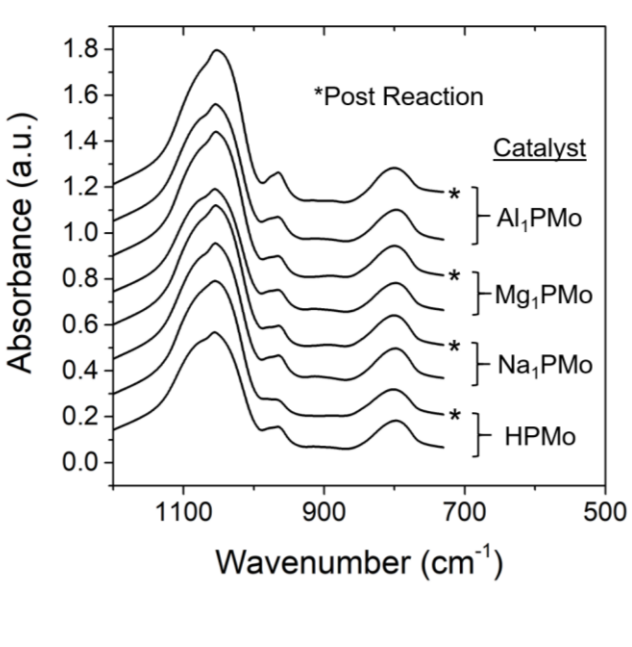

Figure 2-14: ATR-FTIR of HPMo 0.2 and [Na, Mg, Al]$_1$PMo 0.2 as-synthesized and after reaction with methanol at 200˚C (post-reaction curves indicated with *).

Analysis of POM FTIR bands post-reaction (Figure 2-14) generally indicates that all POM bands are retained after reaction, although they may weaken and broaden. In particular, HPMo 0.2 was observed to be significantly reduced post-reaction[25] as indicated by the deep blue color of the used catalyst. Cation-exchanged catalysts tended to be green in color after reaction, or yellow for

fully-exchanged catalysts (ex. Na_3PMo), consistent with the fact that they were much less active for methanol oxidation (as will be shown in the following chapters).

2.3.4 UV-Vis of Supported POM Catalysts

UV-Vis was used to determine the effect of cation addition on redox properties, as shown previously.[17] The UV-Vis adsorption edge energy reflects the ligand-to-metal charge-transfer (LMCT) transition between the POM HOMO (located on the terminal oxygens, generally does not change with POM composition changes) and the POM LUMO (delocalized primarily on the POM Mo, is sensitive to POM composition changes).[17] Thus, the changes in the LUMO energy can be probed to reflect the reducibility of the POM. Altering POM reducibility my impact the rate of selective oxidation of methanol over POMs,[16,45] since the rate-limiting step for this reaction has been suggested to involve simultaneous C-H bond breaking and transfer of the H to the POM, resulting in a reduced Mo center (Mo^{VI} to Mo^{V}) and the formation of a new O-H bond.[25]

2.3.4.1 UV-Vis of [Na, Mg, Al, Cu]PMo 0.2 at 200°C in air

It is essential that the UV-Vis adsorption spectra are collected under well-controlled conditions, as differences in the POM hydration level between experiments lead to shifts in the spectra, and therefore skew the measured edge energies.[75] UV-Vis spectra were recorded in-situ with catalysts at 200˚C in flowing air, since $H_3PMo_{12}O_{40}$ and the catalysts exchanged with Na, Mg, Al, and Cu are expected to be anhydrous at this temperature.[10,75]

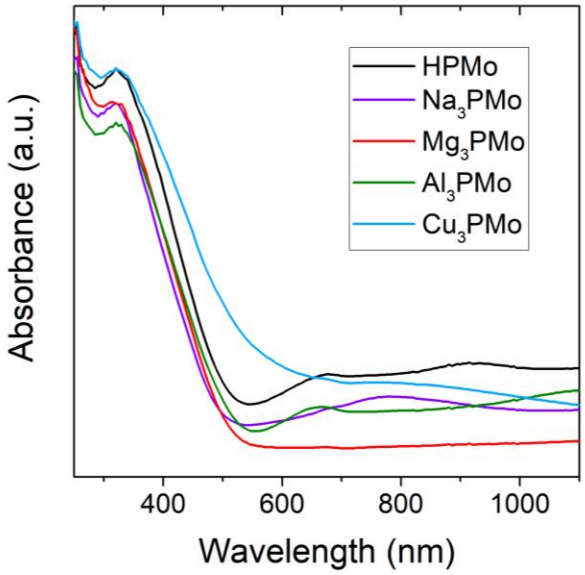

Figure 2-15: UV-Vis absorption spectra for HPMo 0.2 and [Na,Mg,Al,Cu]$_3$PMo 0.2. Spectra were recording in-situ at 200˚C in flowing air using a diffuse reflectance cell.

The UV-Vis absorption spectra for catalysts without cation exchange (HPMo 0.2) and with three cations exchanged per POM ([Na,Mg,Al,Cu]$_3$PMo 0.2) were taken at 200˚C in flowing air; the resulting spectra are presented in Figure 2-15. The background was taken with MgO in the sample chamber under conditions identical to those used for the POM samples.

2.3.4.2 Edge energy calculations and results

Prior to determining the edge energy, the raw reflectance was converted to absorbance by applying the Kubelka – Munk function with MgO as the reference reflector,[25] according to Equation 2-3:

Equation 2-3: Kubelka – Munk function.

$$\boldsymbol{F(R_\infty) = \frac{(1 - R_\infty)^2}{2R_\infty}}$$

where R_∞ is the ratio of the reflectance of the sample to the reflectance of the reference, MgO.

The edge energy was defined as the x-intercept of a linear fit of the near edge region for a plot of $[F(R_\infty)h\nu]^{1/2}$ vs. $h\nu$, where h is Planck's constant and ν is the frequency. An example of the determination of the edge energies for HPMo and $[Na,Mg,Al,Cu]_xPMo$ is shown in Figure 2-16.

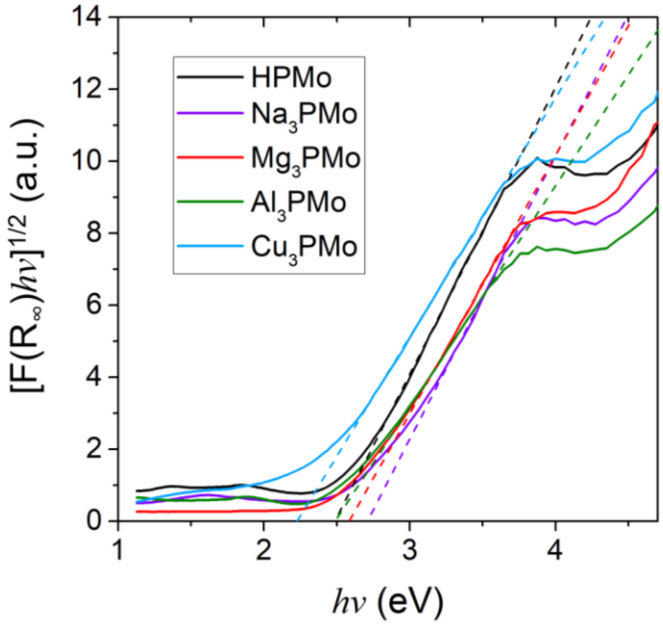

Figure 2-16: Determination of the edge energy of HPMo 0.2 and $[Na,Mg,Al,Cu]_3PMo$ 0.2 by applying the Kubelka Munk function to the reflectance of catalyst samples held at 200˚C in flowing air. MgO was used as the reference reflector.

The UV-Vis adsorption edge energy shifts for cation-exchanged POMs are contained in Table 2-1. It can be seen that the edge energy for Na- and Mg-exchanged catalysts increases by 0.1 – 0.2 eV, indicating these cations render the POMs less reducible. Al exchanged POMs have a subtler effect, decreasing the edge energy by 0 – 0.1 eV, perhaps making the POMs slightly more reducible. Cu appears to have the strongest effect, decreasing the edge energy by up to 0.3 eV, which is expected to render the POMs much more reducible. These results are consistent with the

expected influence of cation exchange on POM reducibility.[13,17,19] For reference, changing the POM from $H_3PMo_{12}O_{40}$ to $H_3PW_{12}O_{40}$ increases the edge energy by 0.7 eV (the W-containing POM is less reducible) and exchanging a few Mo atoms in the framework for V ($H_5PV_2Mo_{10}O_{40}$) decreases the edge energy by 0.3 eV (the V-containing POM is more reducible).[17,45]

	Edge Energy shifts relative to HPMo (eV)			
Cation/POM	Na	Mg	Al	Cu
0	0.00	0.00	0.00	0.00
1	0.16	0.14	-0.08	-0.03
2	0.19	0.14	-0.08	-0.32
3	0.22	0.10	0.00	-0.26

Table 2-1: UV-Vis adsorption edge energy shifts for supported cation exchanged POMs, $[Na,Mg,Al,Cu]_xH_{3-x}PMo_{12}O_{40}/SiO_2$ 0.2 POM/nm^2, where x is 0, 1, 2, or 3. Shifts are relative to $H_3PMo_{12}O_{40}/SiO_2$ at 0.2 POM/nm^2. Spectra were taken after 0.5 hours in flowing air at 200°C in a Harrick high temperature cell.

2.3.5 POM Acid Site Characterization

Several methods of characterizing POM acid sites were explored. The most useful method was the titration of POM Brønsted acid sites with a sterically hindered pyridine during reaction with methanol, as this technique was able to count acid sites under reaction conditions. Gravimetric chemisorption techniques were also explored to count acid sites using adsorbates such as methanol and butene. Temperature programmed desorption (TPD) of adsorbed NH_3 was also used to gain additional information on the strength of POM acid sites, as well as the quantity.

2.3.5.1 DTBP Titration

Brønsted acid sites were quantified using the method of DTBP titration under reaction conditions developed by Iglesia and co-workers.[25,30,48,62,72,76,77] As shown in Figure 2-17, the methanol conversion was allowed to reach steady state for four hours before the start of the titration. The titration was started by switching the feed to a DTBP and MeOH mixture to provide 2 Pa of DTBP in addition to the normal reactants. After an initial spike in pressure when switching between syringe pumps, the acid-catalyzed product, DME, began to decrease linearly with time, and no DTBP broke though the catalyst bed until the catalyst was nearly completely titrated. The simple assumptions that DTBP preferentially, instantaneously, and irreversibly titrates the Brønsted acid sites in a plug flow fashion are consistent with the observed behavior and justify using a linear fit of the DME rate vs. cumulative DTBP/POM to estimate acid site quantity.

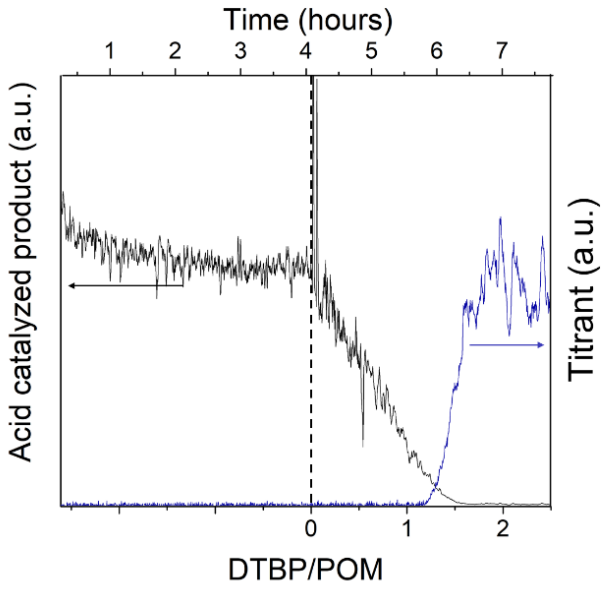

Figure 2-17: Mass spectrometer signal for a titration with DTBP during reaction for $Na_1H_2PMo_{12}O_{40}/SiO_2$ (0.2 POM/nm^2). The acid-catalyzed product, DME (m/q = 46), and the titrant, DTBP, (m/q = 146) were monitored using an online mass spectrometer. The catalyst was allowed to reach steady state for four hours at standard conditions (40 mg catalyst at 200˚C with 30 sccm of 2.7 kPa H_2O, 4 kPa MeOH, 20 kPa O_2, balance Argon) prior to the start of the titration. The vertical dashed line indicates the start of the titration, which was conducted under identical conditions except with 2 Pa DTBP added to the feed.

2.3.5.1.1 HPMo at various coverages

The DTBP titration results for HPMo at various loadings are shown in Figure 2-18. For all loadings, DME production could be fully suppressed and all catalytically active protons were titrated. For coverages from 0.2 to 0.7 POM/nm^2 the average uptake of DTBP is 1.96 ± 0.08 DTBP/POM. As this uptake is one proton less than the stoichiometric value for bulk $H_3PMo_{12}O_{40}$, at 200˚C under reaction conditions the POM may undergo condensation with a surface silanol group[25] to form a POM anchored to the silica surface:

Equation 2-4: Condensation reaction of a POM with a silanol.

$$\equiv Si\text{-}OH + H_3PMo_{12}O_{40} \rightarrow [\equiv SiO]H_2PMo_{12}O_{39} + H_2O$$

POM protons are known to interact strongly with silanols,[20,25,26,71,78,79] and as fumed silicas typically retain hydroxyls at a level of 2-3 OH/nm^2 or higher,[80] there are likely sufficient surface hydroxyls present for this reaction to occur even at monolayer POM coverages.

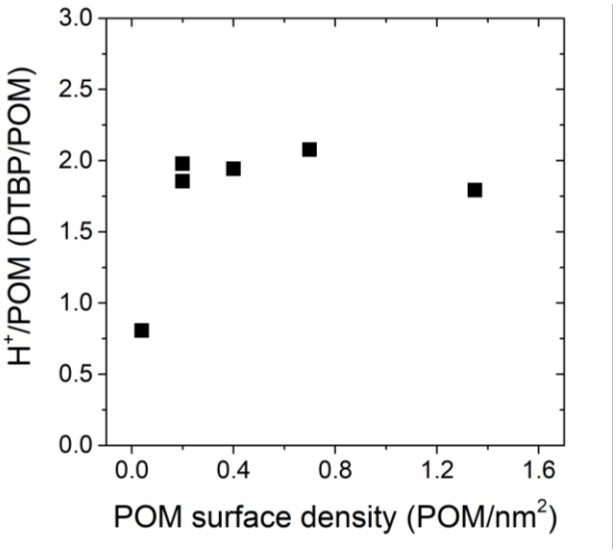

Figure 2-18: DTBP uptake per POM during reaction with methanol for $H_3PMo_{12}O_{40}/SiO_2$ 0.04 to 1.35 POM/nm^2.

At the lowest loading of 0.04 POM/nm^2, the DTBP/POM ratio of 0.8 is significantly reduced, suggesting that isolated POMs interact strongly with the silica support and undergo additional deprotonation.[26] The highest H^+/POM ratio (~2) is observed at a submonolayer POM coverage range above 20-25% of a theoretical monolayer where POMs are well dispersed but not well isolated from each other. This regime is characterized in XRD by the presence of the low angle peaks (8-10˚ 2θ) due to 2D cluster formation with relatively little crystallite formation as evident from higher angle peaks (> 20˚).

2.3.5.1.2 NaPMo at 0.2 and 0.7 POM/nm^2

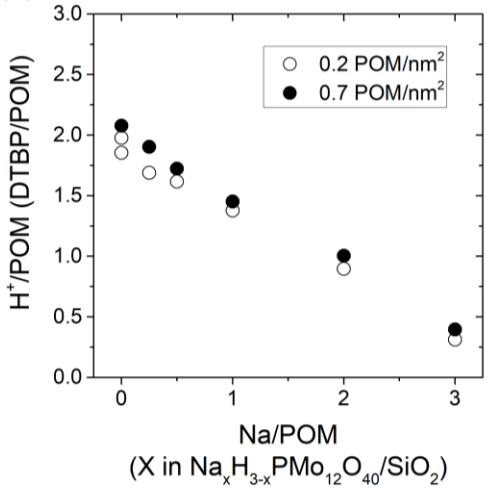

Figure 2-19: DTBP uptake per POM during reaction with methanol for $Na_{3-x}H_xPMo_{12}O_{40}/SiO_2$ at 0.2 POM/nm^2 (open) and 0.7 POM/nm^2 (closed) where x = 0, 0.25, 0.5, 1, 2, 3.

The DTBP titration results for NaPMo at 0.2 and 0.7 POM/nm^2 (Figure 2-19) show the effect of sodium addition on the acid site populations of these materials. Each equivalent of sodium exchanges with approximately 0.5 H^+ in a linear fashion between 0 and 3 Na^+/POM. The catalysts at the higher POM loading have a slightly higher quantity of protons at all levels of exchange. Catalysts with a nominally stoichiometric quantity of sodium still retain 0.3 – 0.4

H^+/POM; however, the addition of a large excess of sodium cations (twice the stoichiometric amount) reduces the acid site concentration to less than 0.1 H^+/POM.

2.3.5.1.3 [Na,Mg,Al,Cu]PMo at 0.2 POM/nm^2

The titration results and corresponding quantity of acid sites per POM for Mg, Al, and Cu are presented in Figure 2-20, along with the results for Na exchange as a comparison. For supported POMs exchanged with Na^+, Mg^{2+}, or Cu^{2+}, the quantity of Brønsted acid sites decreases linearly with cation addition, at an approximate rate of ~0.5 ± 0.1 H^+ removed per addition of one cation. Clearly, stoichiometric exchange based on cation charge was not observed, for either divalent or monovalent cations.

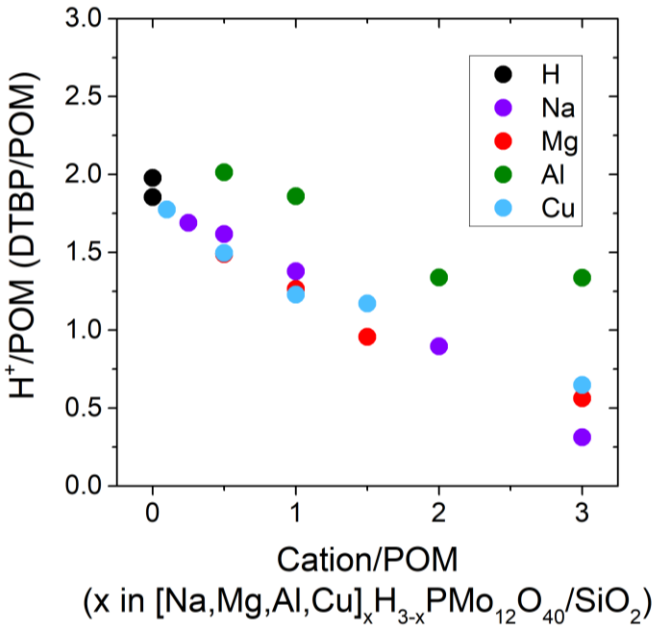

Figure 2-20: DTBP uptake per POM during reaction with methanol for $[Na,Mg,Al,Cu]_xH_{3-x}PMo_{12}O_{40}/SiO_2$ 0.2 POM/nm^2 where x is 0 for H; 0.25, 0.5, 1, 2, or 3 for Na; 0.5, 1, 1.5, or 3 for Mg; 0.5, 1, 2, or 3 for Al; 0.1, 0.5, 1, 1.5, or 3 for Cu.

With the inclusion of Al^{3+} in the supported POM catalysts, the quantity of acid sites remains nearly constant at ~2 H^+/POM for POMs with one or less Al and decreases to ~1.4 H^+/POM for Al_2PMo and Al_3PMo. At all levels of exchange examined here, Al exchanged catalysts retain ~0.5 more H^+/POM than the catalysts exchanged with other cations. This higher level of acidity may be attributed to the generation of Brønsted acid sites via interaction of water with Lewis acidic Al cations[21] (Equation 2-5). Alternatively, the Al may not interact as intimately with the POM anions as the other cations examined, as the formation of bulk POMs and peak shifts with the addition of Al cations in XRD may indicate a different cation-POM interaction.

Equation 2-5: Interaction of Lewis acidic Al cations to generate a Brønsted acid site

$$Al^{3+} + H_2O \rightarrow Al^{3+}(OH)^- + H^+$$

2.3.5.1.4 NaPMo with ethanol

The titration of sodium-exchanged POMs during reaction with ethanol at 160°C gave nearly identical results as those obtained during reaction with methanol at 200°C for identical catalysts. During reaction with ethanol, the unexchanged POM supported on silica, HPMo, retained 1.95 H^+/POM, and cation addition resulted in a decrease of 0.5 H^+ per Na^+. The nominally stoichiometrically exchanged POM, Na_3PMo, retained 0.53 H^+/POM during reactions with ethanol. Based on these results, under the conditions used in this study, the quantity of POM acid sites was not particularly sensitive to the reaction temperature (160°C vs. 200°C), the probe molecule (methanol or ethanol), or the identity of the cation (with the exception of Al^{3+}). The most important factor in determining the quantity of acid sites is the quantity of cations per POM.

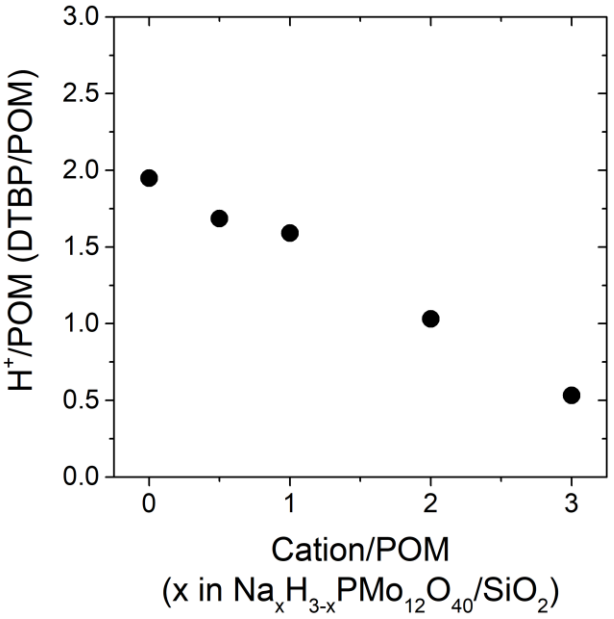

Figure 2-21: DTBP uptake per POM during reaction with ethanol for $Na_{3-x}H_xPMo_{12}O_{40}/SiO_2$ at 0.2 POM/nm^2 where x = 0, 0.5, 1, 2, 3.

2.3.5.2 Gravimetric Chemisorption

The quantity of Brønsted acid sites was also measured gravimetrically using either methanol or 1-butene. The concept of using gravimetric chemisorption was adopted from Kim et al.[66] In that work the amount of butene irreversibly adsorbed on the catalyst at 25˚C was measured using a microbalance to calculate the POM dispersion. This method is effective as non-polar molecules such as alkenes only react with surface acid sites.[9] In contrast, polar molecules such as methanol readily diffuse through the POM bulk crystallites and may interact with both surface and interstitial acid sites.[9]

At mild temperatures, 1-butene is expected to react with surface Brønsted acid sites to form an alkoxide.[66–68] Kim et al. observed alkoxide formation at 25˚C, however, 60˚C was used in this

work in order to minimize the quantity of physisorbed 1-butene, significantly reducing the time requirements of the experiments. Although methanol oxidation may not proceed through a methoxy intermediate at the reaction conditions used in this study,[25] there is evidence that methanol reacts with POMs to form a stable methoxy at lower temperatures.[65] Based on TPD studies of methanol adsorbed on POMs,[65,81] 100˚C was chosen as the chemisorption temperature. At lower temperatures the physical absorption of water and methanol[81] may interfere with the measurements, while at higher temperatures the methoxy ligands may react to form products (~120˚C).[65]

2.3.5.2.1 1-Butene

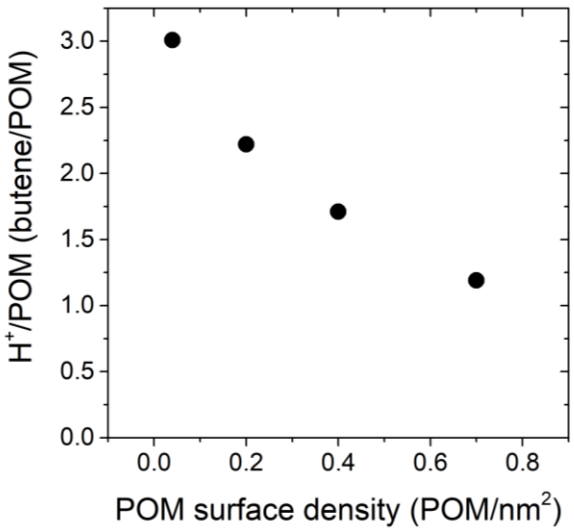

Figure 2-22: Butene uptake at 60˚C for $H_3PMo_{12}O_{40}/SiO_2$ at 0.04, 0.2, 0.4, and 0.7 POM/nm^2.

The 1-butene gravimetric chemisorption results for HPMo 0.02 – 0.7 are given in Figure 2-22. As demonstrated by Kim et al.,[66] 1-butene is an excellent probe molecule for measuring POM dispersion. At 0.04 POM/nm^2, POMs are very well-dispersed, as demonstrated by the stoichiometric uptake of 3 butene/POM. For loading of 0.2 to 0.7 POM/nm^2, the butene uptake

decreases as inter-POM protons are inaccessible to non-polar probe molecules. These results are consistent with TEM of supported POM catalysts prepared in an identical manner,[25] with average cluster diameters of 1.3, 1.5, and 1.9nm for 0.04, 0.16 and 0.7 POM/nm^2, respectively. Thus, the increasing degree of POM-POM interaction with increasing loading renders a portion of protons inaccessible to butene.

The results for butene uptake over POMs exchanged with Na, Mg, and Al are given in Figure 2-23. These results agree quite well with the results obtained with identical catalysts for DTBP titration during reaction with methanol. From a quantity of 2.2 H^+/POM for HPMo 0.2, the quantity of acid sites decreases linearly with cation addition, at an average rate of 0.5 H^+/POM for Na and Mg and 0.3 H^+/POM for Al. With a large excess of cation (Na_6PMo 0.2), the quantity of adsorbed butene decreases to 0.4 H^+/POM.

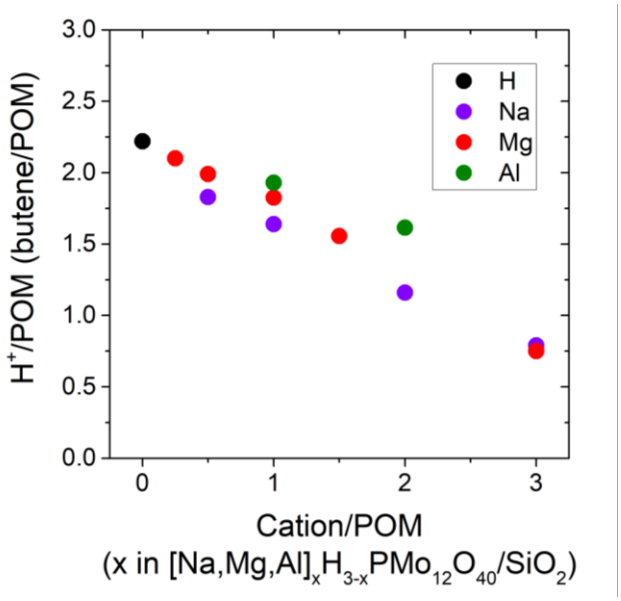

Figure 2-23: Butene uptake at 60˚C for $[Na,Mg,Al]_xH_{3-x}PMo_{12}O_{40}/SiO_2$ 0.2 POM/nm^2 where x is 0 for H; 0.5, 1, 2, or 3 for Na; 0.25, 0.5, 1, 1.5, or 3 for Mg; 1 or 2 for Al.

Ultimately butene chemisorption was abandoned as the results for HPMo 0.04 – 0.7 describe the POM dispersion but not the observed catalytic behavior. Interestingly, butene is able to react with a stoichiometric quantity of POM protons for HPMo 0.04, while other techniques (DTBP titration and NH_3 TPD) suggested a lower quantity of acid sites at low loading, consistent with the literature.[9,10] Perhaps butene may also react with undercoordinated Mo sites (for example, formed during condensation of protons with silanols, see Equation 2-4) as well as Brønsted acid sites. Thus, butene is an excellent probe of dispersion but a poor probe of acidity, at least for analyzing catalysts with varying dispersions and/or undercoordinated Mo sites. With a set of cation-exchanged POMs at a constant loading, the butene results agreed quite well with DTBP titration results, however, as the butene uptakes were not conducted under reaction conditions, the DTBP titrations were deemed to be a more reliable measure of acid site concentrations.

2.3.5.2.2 Methanol

The results for methanol chemisorption were less promising for acid site quantification than for those obtained using 1-butene as the probe molecule. For instance, while negligible uptake of 1-butene was observed on the bare silica support, fumed silica possesses active sites capable of methanol adsorption which are present at a concentration of 0.2 μmol/m^2.[81] The quantity of methoxy formed per POM is included in Figure 2-24 both without taking into account the contributions of the silica (closed symbols) and by subtracting the contribution of silica using the relation in Equation 2-6 (open symbols):

Equation 2-6: Subtraction of the silica contribution to methanol adsorption.

$$\text{Silica contribution} = (1 - \theta) \cdot 0.2 \text{ umol/nm}^2$$

where θ is the fractional POM coverage. It was assumed that POMs block a portion of silica sites in proportion to the POM coverage. For example, according to Equation 2-6, at 50% POM coverage silica contributes 0.1 μmol/nm^2 to methoxy formation. As a comparison, the typical POM loading used in this work of 0.2 POM/nm^2 has a POM surface density of 0.3 μmol/m^2. For HPMo 0.04, 40% of the adsorption could be accounted for by contributions from the silica surface, while the maximum contribution from the silica is 5% for HPMo 0.7.

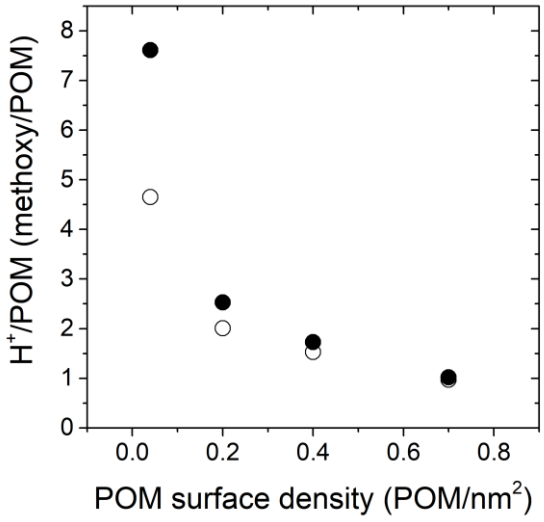

Figure 2-24: Methanol uptake at 100˚C for $H_3PMo_{12}O_{40}/SiO_2$ at 0.04, 0.2, 0.4, and 0.7 POM/nm^2. Closed symbols are original data and open symbols include the subtraction of the silica contribution according to Equation 2-6.

The results in Figure 2-24 for HPMo 0.04 – 0.7 are inconsistent with the expected behavior with methanol chemisorption, as methoxy formation was assumed to be facile at 100˚C [65,81] and independent of coverage, as methanol may readily diffuse in POM crystallites.[9] In contrast, at the lowest loading the quantity of methoxy observed was in excess of the stoichiometric quantity of POM protons, and decreased rapidly with increasing loading. Subtracting the possible

contributions of silica has little impact on the problematic observations with methanol chemisorption described above.

With cation addition, the quantity of methoxy per POM decreases slightly, from 2.6 H^+/POM for HPMo 0.2 to 1.7 H^+/POM for Na_3PMo 0.2. No further decrease in acid sites was observed with the addition of a large excess of cation (Na_6PMo 0.2). Subtracting the potential contribution of silica decreases the quantity of acid sites for all levels of cation exchange by ~ 0.5 H^+/POM, as all cation exchange experiments were conducted at a constant loading of 0.2 POM/nm^2.

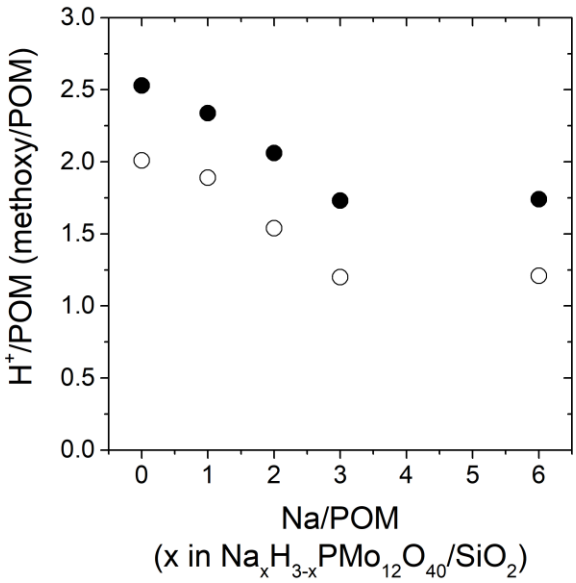

Figure 2-25: Methanol uptake at 100˚C for $Na_xH_{3-x}PMo_{12}O_{40}/SiO_2$ 0.2 POM/nm^2 where x is 0, 1, 2, 3, or 6. Closed symbols are original data and open symbols include the subtraction of the silica contribution according to Equation 2-6.

2.3.5.3 Ammonia Temperature Programmed Desorption

Ammonia Temperature Programmed Desorption (NH_3 TPD) was carried out to provide a descriptor for the acid strength of the supported POM catalysts, in particular to characterize the

impact of cation exchange. Figure 2-26 illustrates NH_3 TPD spectra for HPMo 0.7 POM/nm^2. The primary desorption products were NH_3, H_2O, and oxidized ammonia products N_2 and trace N_2O. The oxidation of NH_3 to N_2 and NO_x has been observed by others.[82,83] Here we assume that the temperature at which products appear reflects the binding strength of NH_3 to the catalyst for peaks below 450°C. Furthermore, based on studies of the decomposition of bulk $NH_4PMo_{12}O_{40}$,[82] we assume that desorption events at ~500°C coincide with complete POM thermal decomposition and are not reflective of ammonia binding to the catalyst.

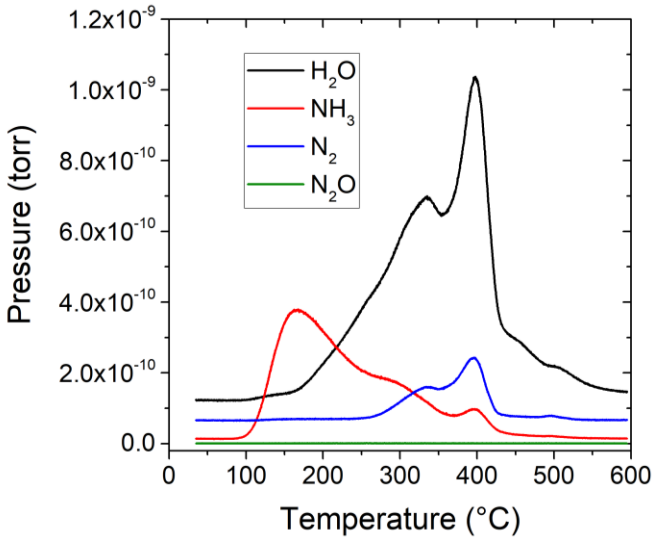

Figure 2-26: Uncorrected mass spectrometer signals for NH_3 TPD from $H_3PMo_{12}O_{40}/SiO_2$, 0.7 POM/nm^2. H_2O, NH_3, N_2, and N_2O were monitored using m/e = 18, 16, 28, and 46 respectively.

The majority of NH_3 was weakly bound to supported POM catalysts and desorbed between 100 and 300˚C. No ammonia uptake was observed for the silica support. The amount typically desorbed in this range was ~ 3 NH_3/POM for the NaPMo 0.7 series. Near 300˚C or above, shoulders on the ammonia desorption peak were observed, along with the evolution of water and an ammonia oxidation product, N_2. These high temperature peaks appeared at the same temperature, suggesting that they result from the same species, protonated ammonia (NH_4^+). The

net reactions corresponding to these desorption peaks are represented by Equation 2-7 and Equation 2-8 below, where the oxygen is supplied by the POM:

Equation 2-7: Desorption of ammonia from an ammonium cation

$$NH_4^+ \rightarrow NH_3 + H^+$$

Equation 2-8: Oxidation of an ammonium cation

$$NH_4^+ + 2\ O^*\ (\text{from POM}) \rightarrow 0.5\ N_2 + 2\ H_2O\ (+\ \text{reduced POM})$$

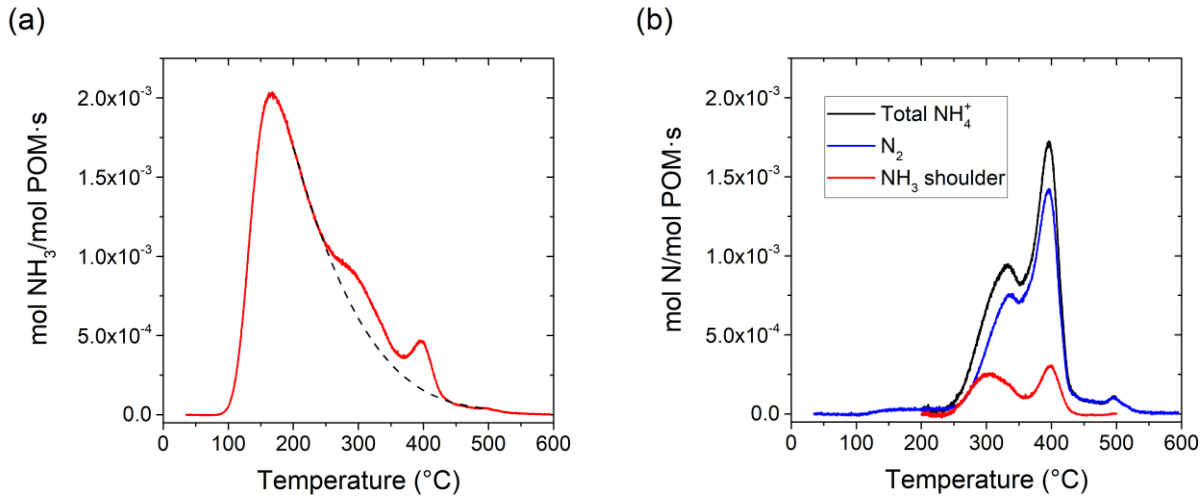

Figure 2-27: a) Fitting of NH_3 desorption shoulders for HPMo 0.7 **b)** NH_3 shoulders, N_2, and total protonated ammonia for HPMo 0.7.

The high temperature NH_3 shoulders were subtracted from the large, loosely bound NH_3 desorption peak using a cubic fit as shown in Figure 2-27a. The relative contributions of NH_3 and N_2 to the total quantity of NH_4^+ is shown in Figure 2-27b for HPMo 0.7. The quantity of NH_4^+/POM determined in this manner agrees reasonably well with the results obtained from

titration with DTBP under reaction conditions: 1.87 NH_4^+/POM as compared to 2.08 DTBP/POM, for HPMo 0.7.

2.3.5.3.1 HPMo 0.04 – 1.35 POM/nm^2

Figure 2-28 shows that, at low loadings (0.04 – 0.4 POM/nm^2), the quantity of NH_4^+/POM measured from NH_3 TPD significantly underestimates the quantity of H^+ determined by DTBP titration. At these low loadings, protons may be trapped by silanol groups to form $SiOH_2^+$ species.[43,79] Therefore, NH_3 TPD is most suited to characterize supported POMs at high (near-monolayer) coverages.

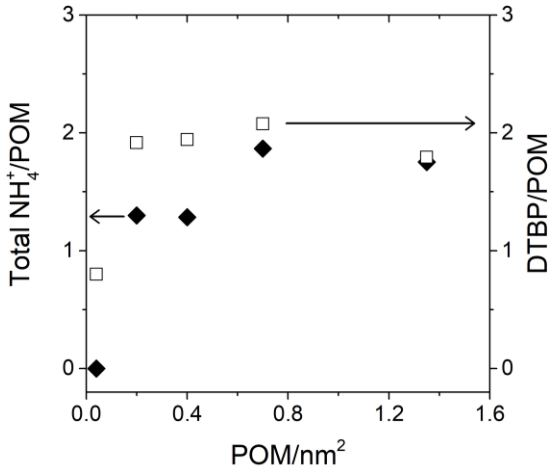

Figure 2-28: Total NH_4^+/POM and DTBP/POM amounts determined for HPMo 0.04 – 1.35.

2.3.5.3.2 NaPMo 0.7

The quantity of ammonium cations measured for NaPMo 0.7 tracks the quantity of acid sites as determined by DTBP titration remarkably well, as shown in Figure 2-29. The quantitative

agreement for H^+/POM between DTBP titration and NH_3 TPD suggests that the NH_3 desorption behavior may be a good probe of the catalytically active Brønsted acid sites, as discussed below.

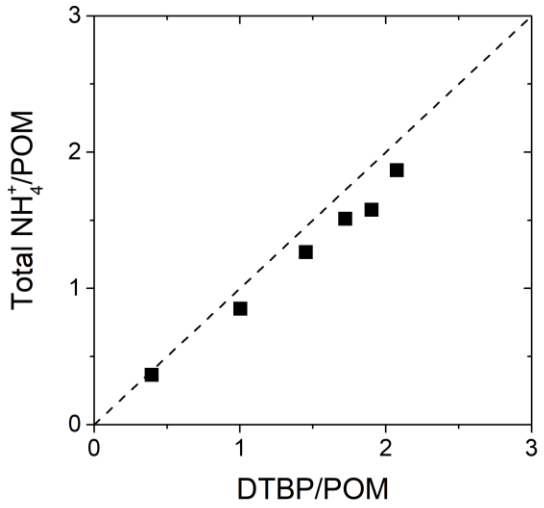

Figure 2-29: Correlation of total NH_4^+/POM from NH_3 and N_2 desorption with DTBP uptake for the Na_xPMo 0.7 series of catalysts. Dashed line indicates 1:1 NH_4^+:DTBP.

The desorption profiles of nitrogen-containing products from NH_4^+ for the Na_xPMo 0.7 series of catalysts are shown in Figure 2-30a for 0 – 1 Na/POM and Figure 2-30b for 1 – 3 Na/POM. The quantity of the ammonium species as well as the maximum temperature of desorption decreased with sodium addition. The decreasing peak temperatures with increasing Na loadings suggest that the binding energy of NH_3 at surface acid sites decreases with sodium loading. In other words, sodium not only replaces protons, but it reduces the acid strength of those that remain.

At 0.5 Na/POM (Figure 2-30a), the addition of less than 1 Na/POM shifts the entire high temperature peak to lower temperature by ~25°C. This shift indicates that the counter-cation addition may influence neighboring protons and POMs, and that the POM secondary structure is very sensitive to cation addition. FTIR (Figure 2-11) supports this speculation by showing that

0.5 Na/POM also shifted the Mo-O_b-Mo and Mo-O_c-Mo bands significantly. The addition of 1 Na/POM leads to the elimination of the higher temperature peak. Further Na addition (Figure 2-30b) decreases the intensity of the lower temperature peak, however, the location of the lower temperature peak only shifts slightly over the range of cation substitution.

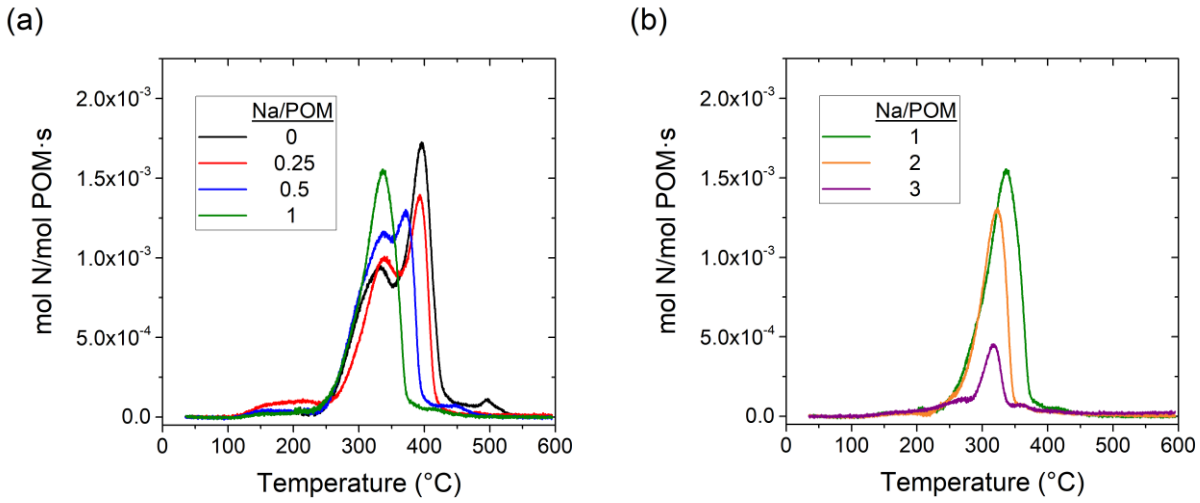

Figure 2-30: NH_4^+ reaction profiles from NH_3 TPD with sodium-exchanged POMs: $Na_xH_{3-x}PMo_{12}O_{40}/SiO_2$, 0.7 POM/nm^2 for a) 0, 0.25, 0.5, and 1 Na/POM and b) 1, 2, and 3 Na/POM.

2.3.5.3.3 Quantification of acid strength

The shifts in peak positions of desorption spectra provide a measure of acid site strength variations. The desorption spectra from NH_3 TPD for NaPMo 0.7 and HPMo 0.04 – 1.35 were fit by assuming first order kinetics and a pre-exponential of 10^{13} s^{-1} as shown in Equation 2-9:

Equation 2-9: Arrhenius-type model for the fitting of first order desorption peaks

$$\frac{\partial \theta}{\partial t} = -A \cdot e^{\frac{E_d}{RT}} \cdot \theta$$

where θ is coverage, $\frac{\partial\theta}{\partial t}$ is the rate of desorption, A is the pre-exponential, E_d is the apparent activation energy, R is the gas constant, and T is absolute temperature.

The resulting apparent activation energies for the release of nitrogen-containing species from NH_4^+, along with the integrated peak areas normalized by POM loading, are shown in Table 2-2. For sodium-exchanged POMs the apparent activation energy decreased with increasing levels of exchange, indicating that the ammonium intermediate is less strongly bound, and thus the sodium exchanged POMs are weaker acids.

Apparent NH_4^+ reaction energy

Na/POM	**kJ/mol** (mol N/mol POM)				POM/nm^2	**kJ/mol** (mol N/mol POM)			
0	**177**	(0.6)	**197**	(1.0)	0.04	**none**			
0.25	**179**	(0.5)	**195**	(0.8)	0.2	**177**	(0.3)	**190**	(0.2)
0.5	**177**	(0.4)	**189**	(0.7)	0.4	**175**	(0.5)	**196**	(0.5)
1	**179**	(0.8)			0.7	**177**	(0.6)	**197**	(1.0)
2	**175**	(0.7)			1.35	**180**	(0.6)	**202**	(1.0)
3	**173**	(0.2)							

Table 2-2: Apparent NH_4^+ reaction energy (and corresponding quantity of N desorbed/POM) for each NH_4^+ peak during NH_3 TPD over $Na_{3-x}H_xPMo_{12}O_{40}/SiO_2$ 0.7 POM/nm^2 and $H_3PMo_{12}O_{40}/SiO_2$ 0.04 to 1.35 POM/nm^2.

Previous studies by Kozhevnikov concluded that POM acidity increases with increasing POM loading on silica, approaching that of the bulk POM for very high coverages. This correlation of acidity to POM loading is in good agreement with our results for various HPMo loadings on silica in Table 2-2. The apparent activation energy for NH_4^+ desorption increases with increasing coverage, indicating POMs increase in acidity with increasing loading. However, these results should be interpreted with caution. Only near or above monolayer coverages (0.7 and 1.35

POM/nm^2) do NH_4^+ and DTBP results agree quantitively (Figure 2-28). Neither NH_3 or N_2 were observed in the desorption spectra for very low loadings (HPMo 0.04), likely due to the deprotonation of the POMs to form $\equiv SiOH_2^+$ groups and the condensation of protons with silanols (see Equation 2-4).

2.3.5.4 Summary and Comparison of Methods for Quantifying Acid Sites

The limitation of NH_3 TPD at measuring acid sites at low loadings and of 1-butene chemisorption of capturing acid site trends with increasing loading highlights the strength of determining acid sites using DTBP titration. With DTBP titration, the importance of carrying out experiments under reaction conditions was to allow the titrant molecules to interact with the sites relevant for catalytic conversion of methanol.

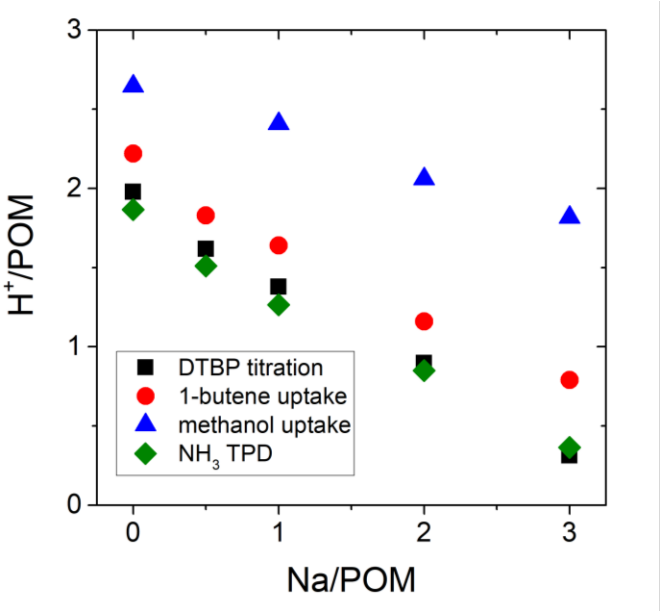

Figure 2-31: Comparison of acid site quantification results using various techniques for $Na_xH_{3-x}PMo_{12}O_{40}/SiO_2$ at 0.2 POM/nm^2 for DTBP titration, methanol uptake, and 1-butene uptake. A POM loading of 0.7 POM/nm^2 was used for the NH_3 TPD experiments.

Figure 2-31 provides strong evidence that the quantity of acid sites indeed decreases linearly with cation addition; the acid site populations obtained by all four techniques used in this work following this general trend. Most methods proved to be sensitive to POM dispersion, with the exception of the titrations under reaction conditions. For example, NaPMo 0.2 and NaPMo 0.7 were observed to have nearly identical quantities of acid sites at all levels of cation-exchange. While DTBP cannot titrate large crystallites of POMs, it has been shown to titrate the catalytically relevant acid sites for conversion of methanol to dimethoxymethane over POM crystallites.[48] Thus, we might expect DTBP to titrate inter-POM acid sites, relevant for conversion of methanol, when other probe molecules such as 1-butene cannot. The disagreement between the trends observed for uptake of methanol and 1-butene with varying loading, as compared to catalytic behavior, suggested that these characterization techniques were not optimal for this study due to the probe molecules not necessarily adsorbing on the catalytically relevant sites. High confidence was put in the technique of DTBP titration as the methanol conversion rate decreased linearly with the quantity of DTBP/POM, fully suppressing the product formation as DTBP fully titrated the catalyst (presumably in a plug flow fashion) and broke through the catalyst bed, as observed by an online mass spectrometer.

The results for NH_3 TPD should be interpreted with caution, as only at near-monolayer coverages do the results agree quantitatively with the DTBP titration results. The inability of this technique to probe POM acid sites interacting with silanols means that we may primarily be probing inter-POM protons, which could form inter-POM NH_4^+ cations after NH_3 exposure. While it is useful to probe the effect of cation addition on these acid sites, in terms of both their

quantity and strength, caution should be used in extending this analysis, as the catalyst under these conditions may not reflect the nature of the active catalyst under reaction conditions.

2.4 Discussion

The synthesis procedures used in this work were chosen from select literature works[25,30,72] to provide supported POM catalysts with dispersed, well-defined active sites. An important aspect of the choice of synthesis procedures is ensuring that the POMs are intact and stable over time. Therefore other syntheses that perhaps yielded even higher dispersion[63,64] were not used, as the harsh conditions in the syntheses were not amenable to keeping POMs in a hydrated state which is essential for keeping POMs intact.

An essential part of the catalyst synthesis was constantly evaluating that the catalysts were in fact dispersed and intact after synthesis and post-reaction. In addition, evaluating the impact of the synthesis procedures on the quantity of acid sites was insightful, as decomposed or highly dehydroxylated POMs are undesirable for this study as both result in a decreased quantity of acid sites.

Several traits were desired for as-synthesized supported POM catalysts. These traits were measured after synthesis and used to evaluate and optimize synthesis procedures. The desirable traits for as-synthesized catalysts include: no bulk-POM diffractions in XRD, strong POM bands in FTIR, high acid site content, reasonable shelf-life, and the ease of synthesis.

The dispersion of POMs was one of the first characteristics of supported POMs that was measured after synthesis, since good POM dispersion was deemed a fundamental property of the model catalyst system envisioned. The XRD results confirmed that POMs are dispersed at a loading a 0.2 POM/nm^2. By increasing the POM loadings, XRD was able to give a qualitative understanding of how the POM dispersion correlated inversely with loading. Comparison with TEM results from the literature[25] was insightful and suggested that even with the formation of small clusters, which were approximately 2-3 nm in diameter at a loading of 0.7 POM/nm^2, methanol could likely access all POMs at loadings of 0.4 - 1.35 POM/nm^2, especially considering the literature precedents regarding the ability of polar molecules to rapidly diffuse throughout POM crystallites.[12]

The addition of cations generally did not impact POM dispersion with the exception of Al. For catalysts with high cation contents (typically around three cations per POM) slightly larger POM clusters may have formed as is evident by the appearance of a weak diffraction at ~ 26˚. The low angle peak tended to shift with cation addition, although not always monotonically. The shift of the low angle peak was attributed to the change in inter-POM spacing as cations replaced hydrated protons. Thus, the incremental shift in peak position with cation addition suggests that cations are interacting intimately with POMs. The appearance of crystallites with the addition of excess Al suggests that the interaction of POMs with cations possessing a high valency is different than the interaction of POMs with mono- or di-valent cations. This speculation is supported by the higher quantity of acid sites observed with Al-exchanged POMs compared to other cations investigated, per a given level of cation-exchange.

The intensity of the four characteristic POM bands in the FTIR spectra of the as-synthesized catalysts was also a very useful tool in evaluating catalyst synthesis techniques. The characteristic POM bands were observed for all levels of cation-exchange, confirming POMs were intact. The shift in POM band locations with cation-exchange at the higher POM loading of 0.7 POM/nm^2 suggests that cations are intimately interacting with POMs, although it is curious that shifts were not observed with cation-exchange at loadings of 0.2 POM/nm^2.

Completing the initial characterization of catalyst, the POM acid sites were quantified in order to properly normalized DME TOF per acid site. Additionally, the acid site quantity was found to be essential to describe the reactivity trends for methanol oxidation and dehydration. The titration of POM acid sites under reaction conditions proved to be the most reliable technique to assess POM acid sites quantities due to the applicability of the technique at a wide range of POM coverages and cation contents. Analysis of NH_3 TPD curves yielded similar results for the acid site content of NaPMo 0.7, providing valuable insight into the decrease in POM acidity with cation-exchange, as has been previously observed by others,[15,20,29] using a variety of techniques. While being potentially interesting techniques to investigate POM dispersion, the chemisorption of 1-butene and methanol were not deemed to be reliable probes of acid sites under the conditions used in this study, at least not in comparison to titrations under reaction conditions. Methanol results did not quantitively agree with titration results, and 1-butene is only applicable for highly dispersed POMs.

The quantity of POM acid sites, as measured by DTBP titration, was found to decrease linearly at a rate of 0.5 H^+/cation for Na^+, Mg^{2+}, and Cu^{2+}. Clearly, stoichiometric exchanged was not

observed (e.g. Mg^{2+} is not observed to exchange with 2 H^+), suggesting that either the exchanged cations have significant interactions with silanol groups on the silica surface and/or not all cations added to the system are located in the vicinity of POMs. The quantity of acid sites was fairly constant over a wide range of loadings (~ 2 H^+/POM), signifying that under reaction conditions the POM – POM and POM – silica interactions are not significantly different, with the exception of the lowest loading (0.04 POM/nm^2), which has significant interactions with silica.

Finally, a goal of this work was to correlate changes in POM reducibility with cation-exchange to the methanol oxidation behavior, as POM reduction is a crucial step in the oxidation reaction pathway.[25,26,61] The UV-Vis edge energy trends with cation exchange were consistent with trend outlined previously in the literature.[16–18] For example, copper- and sodium-exchange render supported POMs more and less reducible, respectively.

Characterization of the catalyst post-reaction was also necessary to confirm that the POM structure and dispersion were retained. No significant differences were observed in POM dispersion post-reaction and the POMs were verified to be intact post-reaction by FTIR. Additionally, XRD showed that POM dispersion did not change significantly after exposure to NH3. Peak shifts with NH3 exposure were observed to be consistent with the formation of NH_4^+ cations.

2.5 Conclusions

This chapter reflects on the procedure and techniques used to prepare supported POM catalysts with well-defined and tunable active sites. The synthesis, treatment, and handling procedures adopted generally ensure that POMs are at least partially hydrated at all stages, including storage. The presence of dispersed, intact POMs was confirmed by FTIR and XRD for both the as-synthesize and post-reaction catalysts. The quantity of acid sites, which was essential to the interpretation of reactivity data, was measured by titration with DTBP under reaction conditions. The strength of acid sites was shown to decrease with cation-exchange using NH_3 TPD. The techniques of 1-butene and methanol chemisorption were explored and shown to be sensitive probes of the POM dispersion and cation content. POM catalysts dispersed on silica at varying coverages and levels of cation-exchange constitute a model catalyst with well-defined and dispersed active sites, with independently controlled quantities of POM, protons, and other cations.

Chapter 3: Dehydration and Oxidation of Alcohols with Supported Polyoxometalates: Effect of Cation-Exchange and Acidity

3.1 Introduction

Methanol has been frequently utilized as a probe reaction for both acid and oxidation catalysis by POMs[25,26]. Figure 3-1 illustrates the basic reaction network for methanol conversion by these catalysts.[25] Acid sites catalyze methanol dehydration to dimethyl ether, while reducible POMs catalyze oxidative dehydrogenation of methanol (CH_3OH) to formaldehyde (HCHO), a portion of which reacts further with methanol to form the secondary products methyl formate (MF, $HCOOCH_3$) and dimethoxy methane (DMM, $CH_2(OCH_3)_2$).

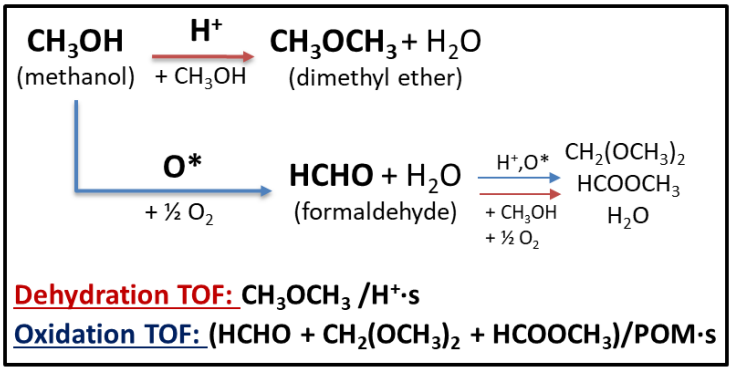

Figure 3-1: Methanol reaction scheme and turnover frequency (TOF) definitions.

Turnover frequencies (TOF) for these two reaction channels are typically reported in terms of the relevant catalyst function[25] (acid or oxidation site) as shown in Figure 3-1.

The depiction of parallel reaction pathways for methanol dehydration and oxidation in Figure 3-1 implies that the catalyst sites responsible for them function independently of each other. However, recent studies of supported $H_3PMo_{12}O_{40}$ catalysts by Iglesia and co-workers have suggested that this is not the case.[25,61] These researchers have proposed that the intermediate involved in formaldehyde production is actually a protonated methanol species or a methoxy species whose formation involves protons from the catalyst. Density functional theory (DFT) calculations have demonstrated that the proton-assisted oxidative dehydrogenation pathway is more energetically favorable than a pathway involving simple methanol dissociation.[61] Others have previously demonstrated a dependence of catalyst oxidation activity on catalyst acid sites.[26]

This chapter explores the impact of Na^+ exchange on supported POM acid and redox properties and its influence on catalysis. The introduction of sodium as a counter-cation may be expected to remove protons, decrease POM acid strength,[14,15] and decrease POM reducibility,[13,17] but otherwise leave the POM intact and readily dispersible on high surface area supports. Variations in POM loading were also investigated, as the effects of exchanged cations may also depend on surface coverage. Preparation methods and reaction conditions were chosen to facilitate comparison with previous studies by Iglesia and co-workers[25,61] which examined methanol reactions over silica-supported $H_3PMo_{12}O_{40}$ at different loadings. We have also observed POMs to be rather unstable and have adapted suitable reactions conditions[25] to prevent POM degradation. As demonstrated in this chapter, turnover frequencies for both methanol dehydration and oxidative dehydrogenation vary with the extent of sodium exchange, indicating that the effects of cation exchange extend beyond simple proton replacement. The effect of sodium-exchange on ethanol dehydration and oxidation was probed as well to determine if the

dependence of methanol oxidation on POM acid properties is unique to methanol or extends to other alcohols.

3.2 Experimental

Catalyst activity was tested using methanol and ethanol as probe reactions. Catalyst samples were loaded in a ¼" quartz tube with a quartz wool plug and placed in a resistively heated vertical split tube furnace (Mellen Microtherm). He (99.99%, Purity Plus) and O_2 (99.99%, Purity Plus) were supplied using mass flow controllers (GF80/GF40, Brooks) while methanol (99.99%, Fisher), ethanol (99.5%, Acros Organics), and water (Ultrapure, Millipore Milli-Q) were supplied using syringe pumps (NE-300, New Era Pump Systems) and vaporized in a home-built manifold in flowing He. Catalysts were pretreated in 2.7 kPa H_2O, 20 kPa O_2, balance He, at reaction temperature (200°C for methanol, 160°C for ethanol) for 30 min. The feed was then switched to a reactant mixture containing 2.7 kPa H_2O, 4kPa of either CH_3OH or C_2H_5OH, and 20 kPa O_2, balance He. The catalyst loading (20 – 200 mg) and total flow rate (10 – 100 sccm) were adjusted to maintain alcohol conversions below 10%. Products were analyzed using an online gas chromatograph (Agilent 7890B) equipped with a DB-1 capillary column connected to a flame ionization detector (FID) and packed Hayesep Q and ShinCarbon ST columns connected to a thermal conductivity detector (TCD). All reaction rates reported here were measured 4 hours after the start of the reaction, in order to give the catalyst ample time to reach steady state.

The dehydration and oxidation TOFs are defined for methanol in Equation 3-1 and for ethanol in Equation 3-2. Methanol (CH_3OH) may undergo dehydration to dimethyl ether (DME) over acid sites or oxidative hydrogenation to formaldehyde (HCHO) over redox sites. Formaldehyde may

react further to form dimethoxymethane (DMM) and methyl formate (MF). The methanol dehydration TOF is defined as the molar production rate of DME per acid site. The oxidation TOF is defined as the sum of the molar production rates of HCHO, DMM, and MF normalized per POM, as each requires the formation of one HCHO, the relevant oxidation product.[25]

Equation 3-1: Methanol TOFs

$$\text{Oxidation TOF } (s^{-1}) = \frac{\text{mol HCHO+mol DMM+mol MF}}{\text{POM}\cdot s}$$

$$\text{Dehydration TOF } (s^{-1}) = \frac{\text{mol DME}}{H^{+}\cdot s}$$

Ethanol (CH_3CH_2OH) may undergo dehydration to either ethylene (C_2H_4) or diethyl ether (DEE) over Brønsted acid sites, or oxidative dehydrogenation to acetaldehyde (AcH). Only trace quantities of secondary products were observed. The ethanol dehydration TOF is defined as the sum of the production rate of the dehydration products, ethylene and diethyl ether, normalized per H^+. The ethanol oxidation TOF is defined as the molar production rate of the sole oxidation product, AcH, normalized per POM.

Equation 3-2: Ethanol TOFs

$$\text{Oxidation TOF } (s^{-1}) = \frac{\text{mol AcH}}{\text{POM}\cdot s}$$

$$\text{Dehydration TOF } (s^{-1}) = \frac{\text{mol } C_2H_4 + \text{mol DEE}}{H^{+}\cdot s}$$

3.3 Results

3.3.1 Methanol oxidation and dehydration

Methanol dehydration and oxidation were used to determine the impact of POM loading and the extent of cation exchange on POM reactivity. The overall selectivity to the primary dehydration product, dimethyl ether (DME), was typically around 80% on a molar basis for all catalysts examined. The oxidation product distribution typically consisted of ~90% formaldehyde on a molar basis with approximately equal amounts of methyl formate and dimethoxymethane making up the remainder. No CO or CO_2 was observed during reactions under differential conversion conditions (<10% methanol conversion). Reactions were run at 200˚C with a feed containing 2.7% water to ensure that the Keggin structure was maintained under reaction conditions. At higher temperatures and/or without water in the reaction feed, POMs may decompose to form MoO_3 species that were observed to migrate out of the catalyst bed as volatile Mo compounds.[45,84] An extreme example of POM decomposition and migration is included in Figure 3-2, for a POM/SiO_2 catalyst after reaction with methanol at 340˚C without co-fed water. As shown in Chapter 2, ATR-FTIR and XRD spectra were obtained for catalysts after reaction (Figure 2-5 and Figure 2-14) at 200˚C with water in the feed. It was confirmed that after reaction, the POMs remained intact and their dispersion was not significantly altered, as has been concluded by others[25] from TEM and NMR for similar reaction conditions.

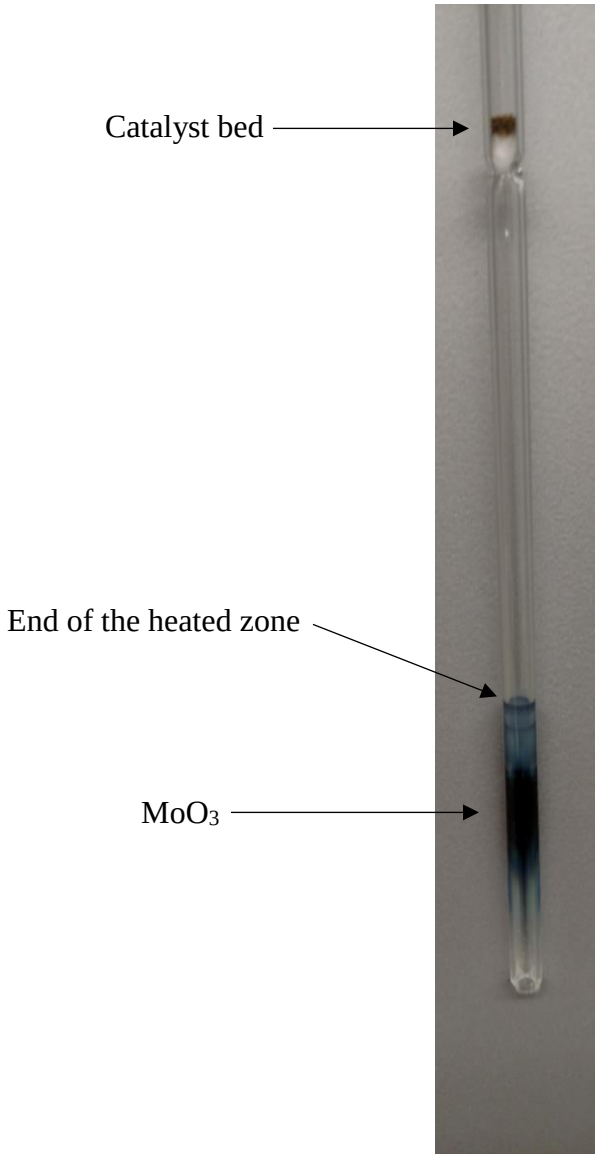

Figure 3-2: A POM/SiO_2 catalyst after reaction with methanol at 340˚C without co-fed water. The harsh conditions resulted in molybdenum migrating out the of catalyst bed and depositing on the first cold spot (~ 100˚C) after exiting the heated zone of the tube furnace.

3.3.2 HPMo 0.04 to 1.35

The dehydration TOF (DME/H^+·s) and oxidation TOF ((HCHO + DMM + MF)/POM·s) for HPMo at various loadings are shown in Figure 3-3. The turnover frequencies for both dehydration and oxidation varied by about a factor of two over the entire range of POM

coverages examined. Trends within this coverage range can be explained by the catalyst characterization results presented in Chapter 2. POMs with a similar proton/POM ratio from DTBP titration experiments (for HPMo 0.2-1.35 POM/nm^2: 1.9 ± 0.1 H^+/POM; see Figure 2-18) have similar turnover frequencies for DME production. At the lowest catalyst loading (0.04 POM/nm^2) the H^+/POM ratio for isolated POMs is lower (0.8 H^+/POM); however, taking this ratio into account, the turnover frequency for dehydration (normalized *per proton*) is still lower. This observation suggests that isolated POMs, perhaps interacting strongly with silica, are less active than the POM clusters observed at higher loadings.

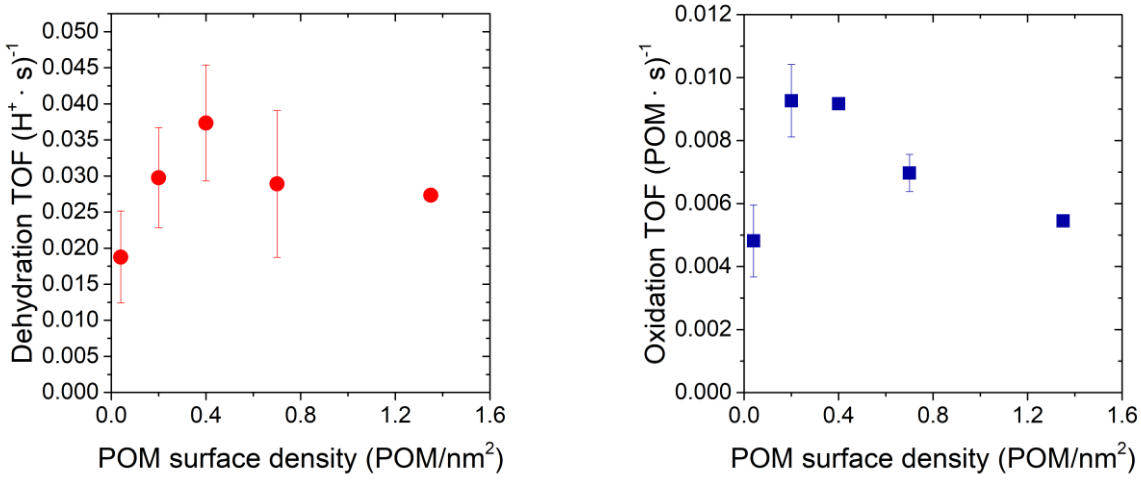

Figure 3-3: Turnover frequencies for $H_3PMo_{12}O_{40}/SiO_2$ at various loadings: 0.04, 0.2, 0.4, 0.7, or 1.35 POM/nm^2. Error bars reflect standard deviations from multiple runs. Reactions were carried out at 200°C in 2.7 kPa H_2O,4 kPa MeOH, 20kPa O_2, balance He.

The trend for oxidation turnover frequencies (normalized per POM) with increasing coverage mirrors that for dehydration. Oxidation TOFs also varied by roughly a factor of two over the entire coverage range examined. The maximum TOFs for both oxidation and dehydration reactions were observed at fractional monolayer POM coverages, with decreasing activity at high POM coverages, where there is evidence of crystallite formation. For catalysts at loadings of

0.04 POM/nm^2 oxidation activity was also reduced, in parallel with the dehydration activity. These results are in good agreement with those reported by Iglesia and co-workers.[25] They observed that the turnover frequencies for both methanol dehydration and oxidation were relatively constant (+/- 10%) for HPMo coverages between 0.04 and 0.7 POM/nm^2.

Interestingly, the oxidation activity appears to track the dehydration activity, as is evident from the parallel trends in TOFs with coverage illustrated in Figure 3-3. The sodium exchange studies, described below, provide additional support for this relationship.

3.3.3 NaPMo 0.2 and 0.7

Reactions of methanol and oxygen were also carried out over the silica-supported, sodium-exchanged POMs ($Na_xH_{3-x}PMo_{12}O_{40}/SiO_2$; x= 0-3; 0.2 or 0.7 POM/nm^2) in order to investigate reactivity trends when proton and POM coverages were varied independently. Shown in Figure 3-4 are the turnover frequencies for both dehydration and oxidation for sodium-exchanged POMs at two loadings, 0.2 and 0.7 POM/nm^2. Both the dehydration TOF and oxidation TOF decrease with sodium addition, indicating that not only does sodium remove Brønsted acid sites (Figure 2-19), it also renders acid and redox sites less active. Consistent with the results for HPMo samples, TOFs for both dehydration and oxidation were essentially independent of POM loading for these two coverages.

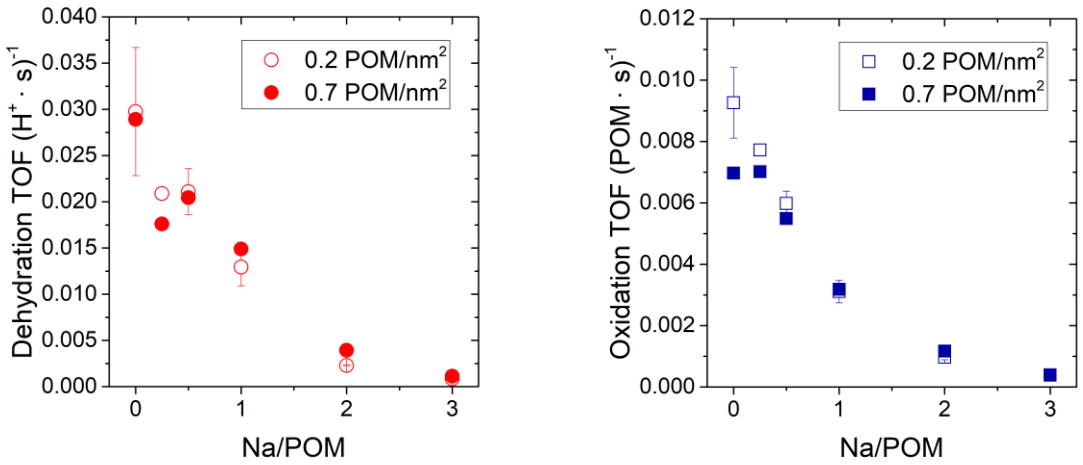

Figure 3-4: Turnover frequencies two series of sodium-exchanged POMs: $Na_xH_{3-x}PMo_{12}O_{40}/SiO_2$, 0.2 or 0.7 POM/nm^2. Error bars are included for the open symbols and reflect standard deviations from multiple runs. Reactions were carried out at 200°C in 2.7 kPa H_2O,4 kPa MeOH, 20kPa O_2, balance He.

While it is expected that the *rates* of reactions involving acid sites would decrease as protons are replaced with Na^+, the results in Figure 3-4 show that the *turnover frequencies* also decrease with increasing sodium content. This trend suggests that sodium exchange not only reduces the number of protons but also decreases the reactivity of the protons that remain. Additionally, it is evident from Figure 3-4 that the trends in dehydration and oxidation TOFs mirror each other, as the increase in Na content produces a TOF decrease of more than an order of magnitude relative to those for HPMo catalysts. The strong correlation of dehydration and oxidation TOFs over the entire range of POM loadings and sodium contents examined is illustrated in Figure 3-5. This linear correlation provides additional evidence to support the involvement of protons in methanol oxidation by POM catalysts.

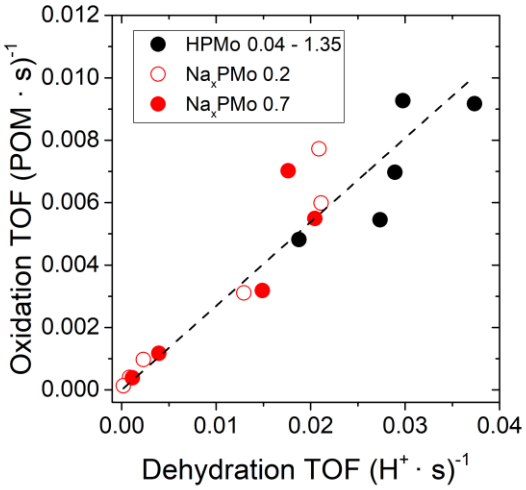

Figure 3-5: Correlation of dehydration and oxidation TOFs for sodium exchanged POMs ($Na_xH_{3-x}PMo_{12}O_{40}/SiO_2$, 0.2 or 0.7 POM/nm^2) and POMs at various loadings ($H_3PMo_{12}O_{40}/SiO_2$ 0.04-1.35 POM/nm^2). Dashed line indicates least squares fit of all data points.

Previous work by Iglesia et al.[25] for POMs at various coverages, with or without co-fed water, suggested that DME rates could be reasonably normalized by the number of accessible protons.[25] This is in good agreement with the results in Figure 3-3 for HPMo at various coverages. However, when protons are exchanged with sodium, the DME TOF decreases sharply. The rate for a dehydration reaction can often be tied to the acid strength of a catalyst.[20,29,30] Literature results utilizing Hammett indicators[15] and NH_3 TPD[14] to characterize acid site strength indicate that sodium decreases POM acid strength, which is consistent with this hypothesis.

3.3.3.1 Apparent Activation Energy

In order to quantify the effect of sodium on the energetics of POM-catalyzed reactions, and the possible correlation with catalyst acidity, both apparent activation energy determinations and ammonia TPD experiments were carried out. If the reduction in DME and oxidation TOFs with sodium exchange can be accounted for entirely by increases in the activation energies of these

reactions, the magnitude of the increase necessary to account for the full range of TOF variations in Figure 3-4 is only 15 kJ/mol. Because this change is rather small, it presents a challenge to determine directly by either experiment or theory. For example, because of POM stability issues, the temperature variation experiments to construct an Arrhenius plot must be carried out at lower temperatures, where the catalyst is less active. In addition, POM proton concentrations may vary with temperature. Iglesia reported ~ 25% higher proton concentrations[25] at 160°C as compared to the proton concentrations reported in Chapter 2 that were measured at 200°C, under otherwise identical reaction conditions. Nevertheless, temperature variation experiments at 180-200°C do produce activation energies (shown in Table 3-1) that generally increase with cation addition, consistent with the decrease in TOF observed with cation addition.

Apparent activation energy (kJ/mol)

	0.2 POM/nm^2		0.7 POM/nm^2	
Na/POM	Oxidation	Dehydration	Oxidation	Dehydration
0	81	64	76	74
0.5	71	68	89	78
1	75	68	72	81
2	89	73	100	79
3	90	79	115	79

Table 3-1: Apparent activation energies for methanol conversion by $Na_xH_{3-x}PMo_{12}O_{40}/SiO_2$, 0.2 or 0.7 POM/nm^2.

3.3.3.2 Correlation with NH_3 TPD

As noted above, the turnover frequencies for both dehydration and oxidation decrease as an increasing number of protons are replaced with sodium. The range of turnover frequencies can be explained by an increase in the apparent activation energies for dehydration and oxidation reactions of about 15 kJ/mol over the range of sodium contents examined. This range is of

comparable magnitude to the decrease in the apparent activation energies (Table 2-2) corresponding to the shift in N_2 peaks in ammonia TPD in Figure 2-30.

Figure 3-6 illustrates the correlation of the methanol dehydration and oxidation TOFs with the apparent activation energies for NH_4^+ reaction, determined by fitting NH_3-TPD curves, as a function of the sodium content for the $Na_xH_{3-x}PMo_{12}O_{40}$ series of catalysts at 0.7 POM/nm^2 loading. In Figure 3-6, ΔE_a NH_4^+ represents the decrease in activation energy, relative to HPMo 0.7, obtained from a first order fit to the total NH_4^+ peaks in the 300-450°C range in Figure 2-30, again assuming a pre-exponential of 10^{13} s^{-1}.

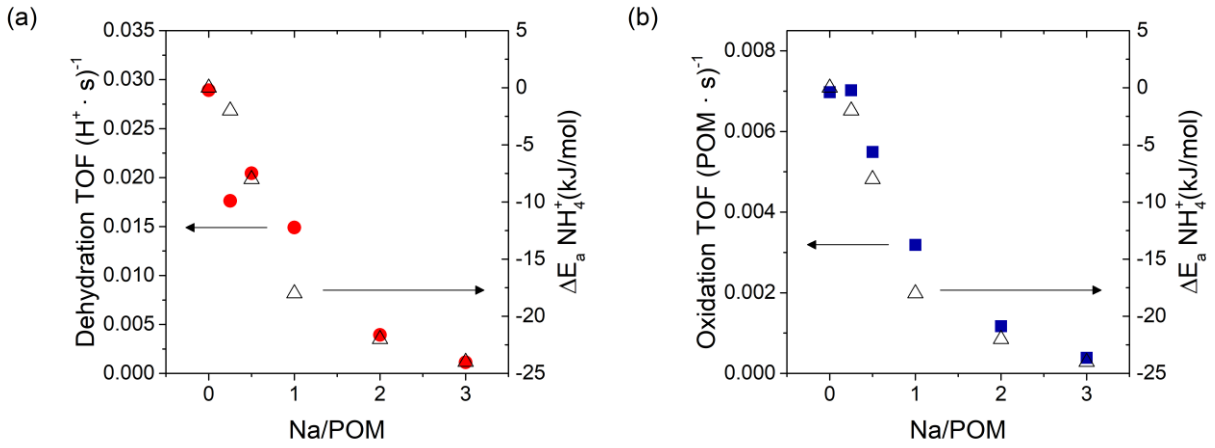

Figure 3-6: Correlation of the calculated activation energy for NH_4^+ reaction during NH_3 TPD with the **a)** Dehydration TOF and **b)** Oxidation TOF for $Na_xH_{3-x}PMo_{12}O_{40}/SiO_2$ at 0.7 POM/nm^2. All energies are relative to $H_3PMo_{12}O_{40}/SiO_2$ 0.7 POM/nm^2.

The correlation between the apparent activation barrier for NH_4^+ reaction and the dehydration TOF is consistent with sodium addition causing a decrease in acid site strength and the acid site population. A similar correlation is observed between ΔE_a NH_4^+ and the oxidation TOF, again suggesting an essential role of protons in the reaction pathway for oxidation as well as dehydration.

3.3.4 Ethanol oxidation and dehydration with NaPMo 0.2

The dehydration and oxidation of ethanol over sodium-exchanged POMs was investigated to determine if the dependence of methanol reactivity on acid site population was unique to methanol or may be extended to other alcohols. The reaction conditions for ethanol were similar to that used for methanol previously, other than the reaction temperature. Since POMs are significantly more active for ethanol conversion than for methanol, the ethanol reactions were carried out at 160°C, rather than at 200°C as was used for methanol, in order to maintain conversion under 10%. The only oxidation product observed was acetaldehyde, and two dehydration products, diethyl ether and ethylene, were observed, typically occurring in an approximate ratio of 4:1 on a molar basis, for all catalysts investigated. Dehydration rates are normalized per proton and oxidation rates are normalized per POM; proton populations were determined by DTBP titration during reaction with ethanol at 160°C.

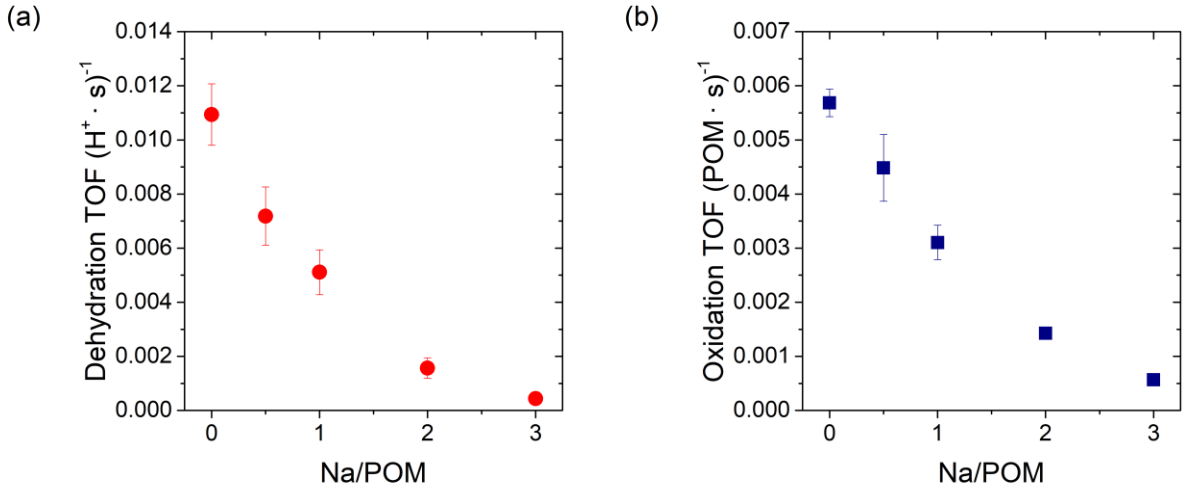

Figure 3-7: Ethanol **a)** dehydration TOF and **b)** oxidation TOF for sodium exchanged POMs: $Na_xH_{3-x}PMo_{12}O_{40}/SiO_2$ 0.2 POM/nm^2. Reactions were carried out at 160°C in 2.7 kPa H_2O, 4 kPa C_2H_5OH, 20 kPa O_2, balance He. Error bars reflect standard deviations from multiple runs.

When the ethanol dehydration and oxidation TOFs are plotted as a function of the quantity of sodium per POM, as shown in Figure 3-7, the rates decrease rapidly with cation addition, mirroring the results for methanol presented in Figure 3-4. The dependence of alcohol dehydration and oxidation TOFs on POM acid properties clearly is not limited to methanol, although alcohols larger than ethanol have not been investigated.

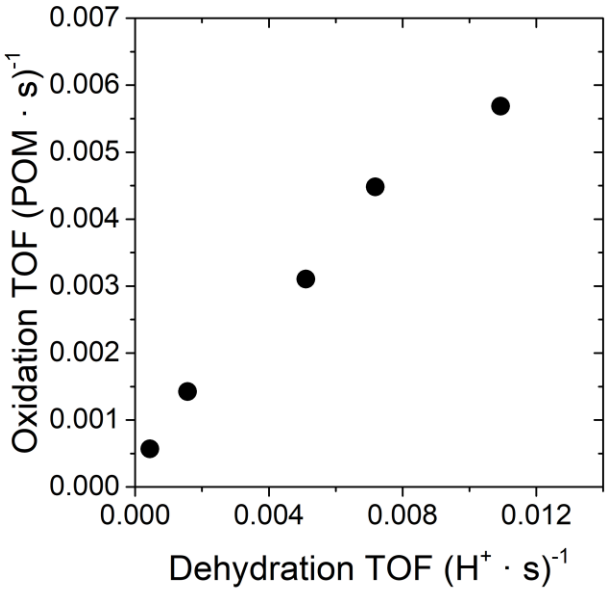

Figure 3-8: Ethanol oxidation TOF as a function of the ethanol dehydration TOF. Reactions were carried out at 160°C in 2.7 kPa H_2O, 4 kPa C_2H_5OH, 20 kPa O_2, balance He.

Figure 3-8 contains the ethanol oxidation TOF plotted as a function of the ethanol dehydration TOF. The linear correlation between ethanol oxidation and dehydration TOF for sodium-exchanged POMs is in good agreement with the behavior found for methanol conversion over these materials, as was shown in Figure 3-5 .

3.4 Discussion

The strong correlation between the oxidation and dehydration pathways (Figure 3-5) is in good agreement with previous observations in the literature, which establish correlations between the overall methanol consumption rate with proton concentration[26] and demonstrate a plausible role of protons in methanol oxidation through theoretical and kinetics investigations.[61]

In addition to providing further evidence for the involvement of POM acid sites in oxidation, we have shown, by varying proton and POM concentrations independently, that cation exchange not only decreases proton population but also decreases reactivity *per proton*. Two possible intermediates have been proposed for formaldehyde formation from methanol, proceeding either through a protonated methanol or through a methoxy whose formation involves interaction with POM protons.[61] For the protonated methanol route, an interaction with a POM proton was demonstrated through DFT calculations, leading us to believe that POM acidity may serve to stabilize intermediates during methanol oxidation. Tatibouet summarized the case for a possible methoxy mediated route,[26] where acidity mediates the formation of a methoxy, and the balance between acid strength and redox properties determines selectivity. In either case substantial alterations to the POM secondary structure and/or acid site properties may adversely affect both the formation and energetics of adsorbed methanol or methoxy species, and their subsequent conversion to formaldehyde and dimethyl ether.

The near constant selectivity with cation exchange makes it unlikely that substantial alterations in the mechanism or energetics of the reaction pathways take place with sodium addition, as any changes would have to impact both pathways similarly. It is much more likely that both reactions

involve protons, and their rates change in parallel with acid site concentration and strength. Although sodium addition has been shown to make POMs less reducible,[13,17] it is difficult to distinguish such an effect from the dependence on acid sites based on the results contained in Chapter 3. The effect of reducibility is discussed in Chapter 4.

The perturbation of POM active sites is much more pronounced in the case of cation addition than with other alterations to the POM secondary structure as is evident by comparing the sodium-exchanged catalyst series at 0.2 POM/nm^2 (NaPMo 0.2) to the other catalyst series contained in this work. For example, altering the POM secondary structure (POM-POM and POM-silica interactions) by varying POM loading for the HPMo 0.04-1.35 series resulted in activity variations of ± 30%, while the TOF of Na_3PMo 0.2 is less than 5% of that of HPMo 0.2. Comparing catalysts with similar levels of acidity further demonstrates this point. For example, HPMo 0.04 (0.9 H^+/POM) and Na_2PMo 0.2 (0.8H^+/POM) have similar acid site populations; however, the sodium-containing catalyst is an order of magnitude less active (5x for oxidation and 8x for DME) than the POM that has been dehydroxylated via interactions with silanols rather than cations. Finally, NaPMo 0.2 and NaPMo 0.7 have noticeably different characteristics in FTIR, XRD, and NH_3 TPD (see Chapter 2 for details), all attributed to the differences in their secondary structure. Yet, they have nearly identical reactivities and proton concentrations at all levels of cation exchange, indicating that the quantity of sodium is the primary factor in perturbing active sites for these catalysts. NH_3 TPD provides some insight into the effect of sodium addition on POM reactivity. As sodium is added to the catalysts, the ammonium cation reaction energy shifts lower in energy by nearly 25 kJ/mol and the acid site quantity is decreased.

Likewise, we expect that the quantity and stability of positively charged intermediates in methanol oxidation and dehydration may be decreased in a similar manner.[85]

In addition to the possible alteration in the energetics of the formation of protonated methanol and methoxy species, changes in POM acid site properties by sodium addition could result in a decrease in POM TOF by several other means. For example, if methanol oxidation and/or dehydration proceed via proton transfer reactions, a decrease in proton mobility may lead to lower TOF. This decrease in TOF could be a result of changes in acid site strength or the loss of an inter-POM hydrogen-bonding network with the substitution of Na^+ for hydrated protons, $(H_2O)_2H^+$. Regardless of the specific mechanism, we believe that sodium disrupts the POM secondary structure, in particular the acid sites, in a manner that strongly perturbs and inhibits the dehydration and oxidation of methanol.

To eliminate the possibility that the dependence of oxidation activity on POM acid sites is unique to methanol, ethanol oxidation and dehydration was investigated at comparable conditions and with identical catalysts. Parallel behavior was observed for ethanol dehydration and oxidation, with decreasing TOFs with cation addition, and a direct correlation between the TOFs of the two pathways. This similar behavior suggests that over POMs both methanol and ethanol oxidation proceed via molecularly adsorbed intermediates involving protons, as described by Iglesia for methanol.[25,61]

It is clear that based on these results, the acidic properties of POMs must be considered when investigating oxidation capabilities of these materials, as the pathways are intimately linked for

alcohol oxidative dehydrogenation. The use of counter-cations to tune POM properties (such as modifying the oxidation potential of POMs[13,16–18]) and to limit acid-catalyzed side reactions to produce a more active and selective catalyst is limited by the adverse effect of cation addition on POM acid properties which are essential for the efficient partial oxidation of methanol for these catalysts.

3.5 Conclusion

The decrease in alcohol oxidation and dehydration turnover frequencies with sodium exchange over these catalysts indicates that acidity is necessary to activate methanol and ethanol over these materials, as TOFs for both the oxidation and dehydration pathways were highly correlated over a range of more than one order of magnitude. The TOF variations of both the oxidation and dehydration pathways can be explained by increases in activation energies of about 15 kJ/mol over the range of sodium exchange examined. These variations agree well with changes in acid site strength, as measured by ammonia temperature programmed desorption/reaction. Because of the dependence of both methanol dehydration and oxidation channels on acid site population and strength, the usefulness of cation exchange to shift the selectivity of the catalyst between these reaction channels is limited.

Chapter 4: Dehydration and Oxidation of Methanol with Supported Polyoxometalates: Effect of Cation Identity and Reducibility

4.1 Introduction

POMs are active both for acid and selective oxidation catalysis, and relationships have been developed between POM composition and the POM acid and redox properties.[10–12] The effect of varying the POM heteroatom and framework metal atoms on POM properties and catalytic behavior is well documented.[10,16,20] As for the counter-cations, we have previously demonstrated a relationship between counter-cation identity and POM reducibility.[16] Ideally, cation-exchange can be used to carefully tune the POM reducibility.[16] Cations that improve POM reducibility might be expected to enhance oxidation activity, while their exchange for protons would decrease POM acidity, thereby increasing oxidation selectivity further. However, it has yet to be demonstrated that such a relationship between counter-cations, POM reducibility, and selective oxidation catalysis exists.

In this chapter, cation-exchanged POMs dispersed on a high surface area support were used to investigate the relationship between POM acid and redox properties and methanol reactivity. POMs in their acid form (i.e., heteropolyacids) were exchanged with Na^+, Mg^{2+}, Al^{3+}, and Cu^{2+} cations chosen to yield a range of effects on POM acid and redox properties. As described in Chapter 2, POM reducibility was probed using UV-Vis of cation-exchanged POMs, where the UV-Vis adsorption edge energy may be correlated with reducibility, as demonstrated previously.[17] In Chapter 3 we used NH_3 TPD to quantify the decrease in POM acidity with sodium addition, however in this chapter, the acid strength was inferred from the methanol

dehydration TOF, a well-known acid site probe reaction known to be sensitive to acid site strength.[30]

Ultimately, the goal of this study was to elucidate the role of acidity and reducibility in the selective oxidation of methanol over POMs, and to determine the potential benefit of cation addition for these catalysts.

4.2 Experimental

Methanol was used as a probe for both oxidation and dehydration activity. Reaction mixtures containing 4 kPa methanol (99.99%, Fisher), 2.7 kPa water (Ultrapure, Millipore Milli-Q), 20 kPa O_2 (99.99%, Purity Plus) and balance He (99.99%, Purity Plus) were delivered using syringe pumps (New Era Pump Systems NE-300) for methanol and water, and mass flow controllers (GF80/GF40, Brooks) for permanent gases. Catalyst samples were loaded into a ¼" quartz tube in a resistively heated furnace (Mellen Microtherm) with a thermocouple placed at the top of the catalyst bed. Catalyst loading (10-200 mg) and flow rate (10-100 sccm) were adjusted to maintain methanol conversions below 10%. Catalysts were pretreated in a flowing stream consisting of 2.7 kPa H_2O, 20 kPa O_2, balance He by ramping from ambient to 200˚C at 10 ˚C/min and holding for 0.5 hours before switching flow to reactant mixtures. Products were analyzed using an online gas chromatograph equipped with a DB-1 capillary column connected to a FID and packed Hayesep Q and ShinCarbon ST columns in series connected to a TCD. All reaction rates reported here were measured after the catalyst was allowed to reach steady state (4 hours). Turnover frequencies were defined as described in Chapter 3 in Equation 3-1.

4.3 Results

4.3.1 [Na, Mg, Al, Cu]PMo 0.2

Both methanol dehydration rates and turnover frequencies decrease with the substitution of Mg, Al, and Cu for protons, as demonstrated in Chapter 3 for silica-supported $Na_xH_{3-x}PMo_{12}O_{40}$ catalysts. Figure 4-1 and Figure 4-2 illustrate the effects of higher-valent cations, compared to that of sodium. Dehydration rates are normalized per proton; proton populations were determined by the DTBP titration method described in Chapter 2.

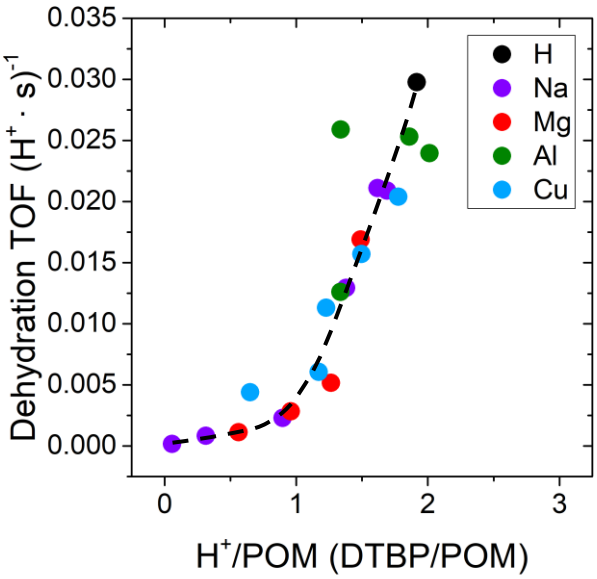

Figure 4-1: Methanol dehydration turnover frequencies for cation-exchanged POMs as a function of the quantity of acid sites per POM as determined by DTBP titration. The catalysts used were $[Na,Mg,Al,Cu]_xH_{3-x}PMo_{12}O_{40}$ 0.2 POM/nm^2 where x is: 0 for H; 0.25, 0.5, 1, 2, 3, or 6 for Na; 0.5, 1, 1.5, or 3 for Mg; 0.5, 1, 2, or 3 for Al; 0.1, 0.5, 1, 1.5, or 3 for Cu. Reactions were carried out at 200°C in 2.7 kPa H_2O, 4 kPa MeOH, 20 kPa O_2, balance He. Dashed line is a smooth curve though the Na_xPMo points, included to guide the eye.

When dehydration rates are plotted vs. proton population per POM, the results essentially fall on a common curve. For sodium-exchanged POMs, we suggested that the reduction in TOFs with increasing extents of cation exchange is due to a reduction of acid site strength with increasing

exchange. Figure 4-1 shows that this effect is similar, whether monovalent (Na^{+}) or divalent cations (Mg^{2+}, Cu^{2+}) are substituted for protons. This observation suggests that the identity of the cations is relatively unimportant compared to their influence on acid site strength.

The results for exchange of the trivalent cation (Al^{3+}) are less definitive. The difference between Al^{3+} and the lower-valent cations is even clearer when dehydration TOFs are plotted against the nominal extent of cation addition, as shown in Figure 4-2. Unlike the other cases, TOFs for methanol dehydration are much less strongly affected by Al^{3+} substitution. It should be noted that if stoichiometric exchange occurred, all protons in $H_3PMo_{12}O_{40}$ should be removed by the exchange of a single Al^{3+} cation per POM. Thus, most of the results for Al^{3+} exchange in Figure 4-2 represent cases where excess aluminum has been added to the catalyst.

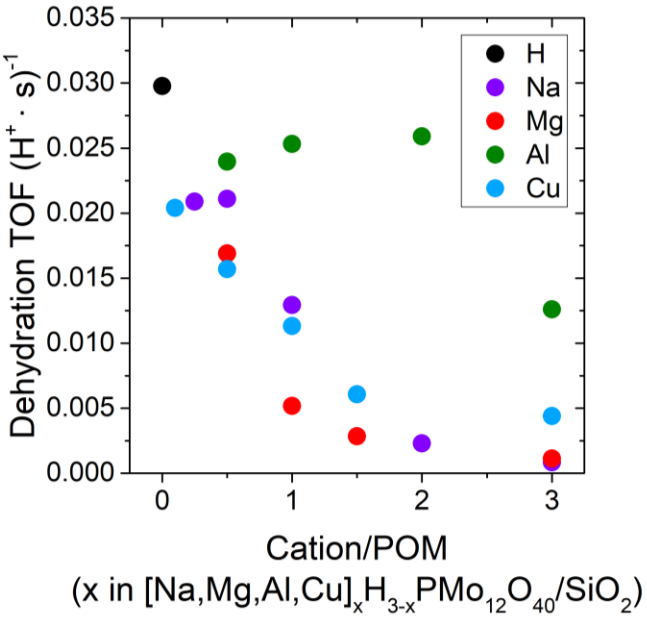

Figure 4-2: Methanol dehydration turnover frequencies for several series of cation-exchanged POMs: $[Na,Mg,Al,Cu]_xH_{3-x}PMo_{12}O_{40}$ 0.2 POM/nm^2 where x is: 0 for H; 0.25, 0.5, 1, 2, or 3 for Na; 0.5, 1, 1.5, or 3 for Mg; 0.5, 1, 2, or 3 for Al; 0.1, 0.5, 1, 1.5, or 3 for Cu. The x-axis represents the nominal quantity of cations added per POM. Reactions were carried out at 200°C in 2.7 kPa H_2O, 4 kPa MeOH, 20 kPa O_2, balance He.

In contrast to the other cation-exchanged catalysts, Al-exchanged POMs, which retain higher levels of acid sites with increasing cation addition, also retain higher TOF with cation exchange as well. In fact, the dehydration TOF for Al-exchanged POMs barely decreases until 3 Al/POM, where we observe a significant quantity of bulk POMs (Figure 2-4). The near constant TOF for Al quantities of 0.5 to 2 suggests that these catalysts have similar acid site strengths, even though the quantity of acid sites decreases by over 0.5 H^+/POM over this range. The maintenance of acid site strength for these catalysts may be a result of Al cations generating Brønsted acidity (Equation 2-5), or the Al cations may exchange poorly with the POM and therefore the Al cations do not perturb the POM acid sites already present.

Similar to the results for methanol dehydration, the oxidation rates decrease rapidly with the addition of Na^+, Mg^{2+}, Al^{3+}, or Cu^{2+} cations to the POMs, with little dependence on cation identity, as shown in Figure 4-3 and Figure 4-4. Oxidation rates are normalized per POM; proton populations were determined by DTBP titration under reaction conditions.

Figure 4-3 contains the oxidation TOF as a function of the quantity of acid sites per POM, as determined by DTBP titrations. The oxidation TOF results all fall on the same curve when plotted as a function of H^+/POM, indicating that the quantity of acid sites is the primary reactivity descriptor for methanol oxidation over cation-exchanged polyoxometalates. Additionally, as proposed previously,[25,26,61] the oxidation of methanol over polyoxometalates may involve protons and may be sensitive to the acid strength of POM protons. Moving left across Figure 4-3, the oxidation TOF decreases, regardless of the cation used. The acid site

strength also decreases as one moves left across Figure 4-3, as the decreasing acid site quantity is indicative of increasing cation interaction with the POMs, which in turn decreases acid strength.[15,20,28]

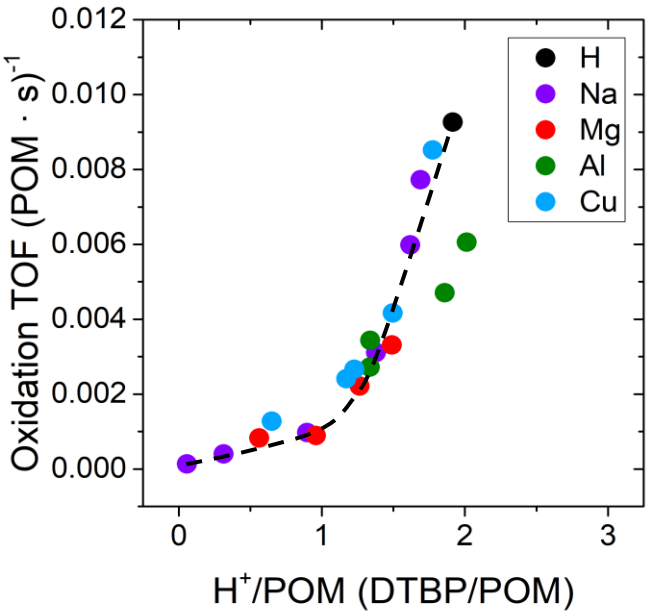

Figure 4-3: Methanol oxidation turnover frequencies for cation-exchanged POMs as a function of the quantity of acid sites per POM as determined by DTBP titration. The catalysts used were $[Na,Mg,Al,Cu]_xH_{3-x}PMo_{12}O_{40}$ 0.2 POM/nm^2 where x is: 0 for H; 0.25, 0.5, 1, 2, or 3 for Na; 0.5, 1, 1.5, or 3 for Mg; 0.5, 1, 2, or 3 for Al; 0.1, 0.5, 1, 1.5, or 3 for Cu. Reactions were carried out at 200°C in 2.7 kPa H_2O, 4 kPa MeOH, 20 kPa O_2, balance He. Dashed line is a smooth curve though the Na_xPMo points, included to guide the eye.

Significantly, these results are in contrast to the trends demonstrated for the UV-Vis adsorption edge energy for POMs cation-exchanged with Na, Mg, Al, and Cu (Table 2-1). Based on those trends, POMs exchanged with Cu are expected to be more active for selective oxidation catalysis, as Cu rendered the POM more reducible, and POM reduction is a crucial part of the rate-limiting step for methanol oxidation.[25] Similarly, Na and Mg exchange rendered POMs less reducible and therefore less capable of carrying out the redox cycles necessary for an active

oxidation catalysts. In contrast to these trends, very few differences in the TOFs of POMs exchanged with Cu, Na, and Mg were observed.

The differences that were observed are mostly easily visualized by plotting the oxidation TOF as a function of the nominal quantity of cation per POM, as shown in Figure 4-4. The Al-exchanged POMs likely retain a higher oxidation TOF due the increased quantity of acid sites observed with Al exchange (see Figure 2-20). However, the extent to which Al retains higher activities with cation exchange is much smaller with the oxidation TOF than that observed for dehydration TOF in Figure 4-2.

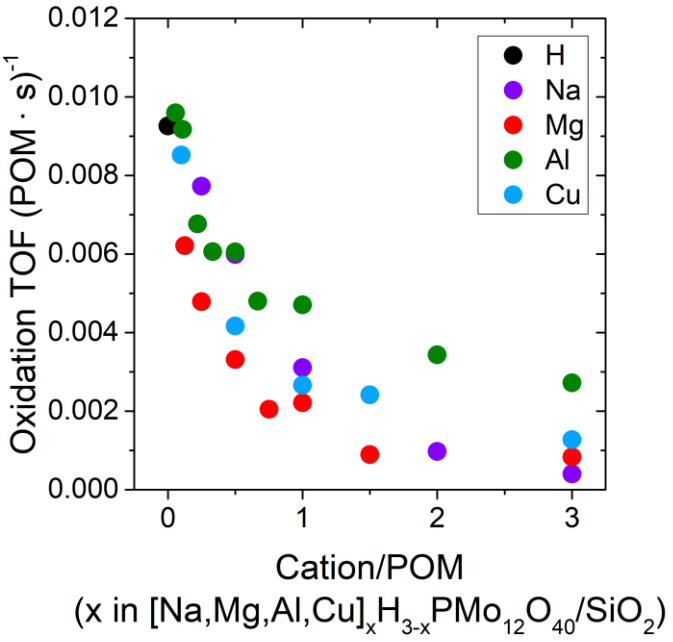

Figure 4-4: Methanol oxidation turnover frequencies for several series of cation-exchanged POMs: $[Na,Mg,Al,Cu]_xH_{3-x}PMo_{12}O_{40}$ 0.2 POM/nm^2 where x is: 0 for H; 0.25, 0.5, 1, 2, or 3 for Na; 0.125, 0.25, 0.5, 0.75, 1, 1.5, or 3 for Mg; 0.057, 0.11, 0.22, 0.33, 0.5, 0.66, 1, 2, or 3 for Al; 0.1, 0.5, 1, 1.5, or 3 for Cu. The x-axis represents the nominal quantity of cations added per POM during synthesis. Reactions were carried out at 200°C in 2.7 kPa H_2O, 4 kPa MeOH, 20 kPa O_2, balance He.

Finally, it is worth emphasizing that the shifts in UV-Vis edge energy, and therefore the changes in POM redox properties induced by cation exchange, do not appear to play a role in the observed changes in oxidation TOF with cation exchange. Rather, any effect of the alterations to the POM redox properties are far outweighed by the effect of cation addition on the POM acid properties.

4.4 Discussion

By investigating supported POMs exchanged with sodium, Chapter 3 established that acid sites are of paramount importance for a high TOF for both methanol dehydration and oxidation. Theoretical and kinetics studies by Iglesia and coworkers[25,61] for methanol reaction over HPMo confirmed that DME formation proceeds through protonated methanol monomers and dimers. More controversially,[25,26] they suggested that methanol oxidation to formaldehyde is more favorable via molecularly-bound methanol intermediate, interacting with POM protons and oxygen groups, than via a dissociative route involving a methoxy group. It seems probable that methanol protonation must be a crucial step for both methanol dehydration and oxidation with these catalysts, explaining the dependence of methanol reactivity on POM acid site quantity and strength observed for sodium exchanged POMs in Chapter 3 and in this chapter.

The current work expands upon Chapter 3 by examining cation exchange with cations other than sodium. Very few differences were observed between the behavior of supported POMs when exchanged with Na^+, Mg^{2+}, or Cu^{2+}. As discussed in Chapter 2, well-dispersed POMs were observed for the [Na,Mg,Cu]PMo series of catalysts, with acid site quantities decreasing linearly with cation addition at a rate of 0.5±0.1 H^+/POM per cation added, which is rather surprising

considering the different charges of the cations. In addition to behaving similarly with respect to acid site quantity, the catalytic activity for acid-catalyzed reactions was also similar for Na, Mg, and Cu. With the addition of these cations, the DME TOF rapidly decreased, presumably due to decreasing acid site strength with cation addition. Furthermore, the oxidation activity of these catalysts was very similar, mirroring the trends observed for dehydration, indicating that the alteration of POM acid sites with the addition of Na, Mg, or Cu results in a general decrease in reactivity for methanol over these materials. This trend is demonstrated by plotting the TOF as a function of H^+/POM (Figure 4-1 and Figure 4-3).

Variations in the reducibility of the cation-exchanged catalysts seems to play no distinguishable role in determining the oxidation activity, which is surprising considering the proposed transition state involves reduction of POM framework metal atoms (Mo^{VI} to Mo^{V}).[25] As suggested by the strong correlation of acid and oxidation activities above, the interaction of methanol with protons, rather than oxidation of the protonated complex, appears to be rate-determining under the conditions of our experiments.

The presence of acid sites is important for methanol oxidation, as protonated methanol monomers, dimers, or hydrogen-bonded methanol-proton species appear to provide the lowest energy path for the formation of dimethyl ether and formaldehyde.[25,61] In addition to the acid site population, the acid site strength is important, as parallels can be drawn between acid site strength and the adsorption energy of relevant charged intermediates.[85] Therefore, any decreases in acid site strength with cation addition may have detrimental effects on the adsorption energy for the above-mentioned intermediates, as well as transition states.

The behavior of Al-exchanged POMs was different than that of the other cations used in this work. These catalysts retained a higher quantity of acid sites with cation addition (~0.2 H^+ were removed on average per 1 Al^{3+}). Bulk POM diffraction lines were observed in XRD for high levels of cation exchange, and this catalyst series exhibited a higher, yet still generally decreasing, dehydration and oxidation TOF with Al addition compared to other cation-exchanged catalysts. As depicted in Equation 2-5, reactions of aluminum cations with water may produce additional acid sites on the catalyst.

Altogether, the correlations between TOF and acid site density support the notion that the differences in TOF result from the acid properties of the catalyst, not from the identity of the cation or its influence on POM reducibility. Therefore, although cations may interact differently with the POMs, what is relevant for our systems is the degree of cation interaction, which in turn determines the POM acid site concentration and acid strength.

Based upon this analysis, the feasibility of using POM cations to improve POM oxidation activity is quite limited. Kozhevnikov characterized the acid strength of supported and cation exchanged POMs via ammonia adsorption microcalorimetry.[28] Those workers found that both supporting POMs on a high surface area supports (SiO_2, TiO_2, ZrO_2, Nb_2O_5, $Cs_3PW_{12}O_{40}$) and cation-exchanging POMs with Cs led to a significant decrease in acid strength, and ultimately that the initial heat of ammonia adsorption, a measure of acid site strength, correlated very well with the rate of ethanol dehydration. Janik also investigated cation-exchanged and supported POMs via DFT calculations, reaching similar conclusions.[20] Similarly, Moffat investigated the acid strength of cation-exchanged POMs using Hammett indicators,[15] determining that cation

addition decreases acid strength; for cation-exchanged POMs, increasing the polarizing power of the cation increased the acid strength, (i.e., $H^+ >> Al^{3+} > Mg^{2+} > Na^+$).

In contrast, other studies have found beneficial effects associated with POM cation exchange at industrially relevant conditions,[11,13,14,21] including in the patent literature.[11,16] However, POMs may not be intact at these harsh conditions.[45,50–53] At mild conditions where POMs are confirmed to be intact (in our hands $T \leq 200°C$ with co-fed H_2O) there is little *catalytic* benefit of cation-exchange (although cation exchange with cations like Cs may improve stability, surface area, and solubility for some applications[11,23]), as the activation and coordination of reactants and reaction intermediates via interactions with acid sites control the kinetics of both dehydration and oxidation pathways.

4.5 Conclusions

The dehydration and oxidation of methanol over cation-exchanged POMs were investigated, and few differences in activity were found for different cations at comparable levels of cation exchange, especially with respect to varying POM redox properties, as measured by UV-Vis adsorption edge energy. Rather, the acidic properties of the cation-exchanged POMs were the primary descriptor for both dehydration, a well-known Brønsted acid catalyzed reaction, and oxidative dehydrogenation, which evidently involves both redox sites as well as Brønsted acid sites over POMs. This conclusion is strengthened by the fact that the only cation that exhibited starkly different behavior when exchanged with POMs, AlPMo, fell into line when the TOFs were plotted as a function of H^+/POM. This critical role of protons in the oxidative dehydrogenation route suggests that small alkanols may undergo oxidation via a molecular route

over POMs that evidently involves significant interaction of reactive intermediates with POM protons. Additionally, although it has been proposed that the rate-limiting step in methanol oxidation over POMs involves POM reduction, evidently this electron transfer is facile enough to not impact oxidation rates in light of other changes to POM properties, in particular the nature of the acid sites, and in general the binding of reaction intermediates. Together these results suggest that, at mild conditions where POMs are intact, the opportunity to use counter-cation exchange to tailor POM properties to improve selectivity and activity is quite limited, as cations have an adverse impact on POM protons which are crucial to activating reactants, and the effects of varying POM reducibility are small and not catalytically relevant at these conditions.

Chapter 5: Activity Coefficients for Solid Acid Catalysts

5.1 Introduction

The decrease in the methanol dehydration and oxidation TOFs with cation addition reported in Chapters 3 and 4 was attributed to an alteration in POM acid properties. In this chapter, these trends with cation addition are discussed in terms of the 'non-ideal' behavior of POM acid sites with cation addition. As a point of comparison, consider a heterogeneous acid catalyst that exhibits 'ideal' behavior with compositional changes: ZSM-5. The acid site concentration of zeolites such as ZSM-5 may be varied systematically by controlling the Si/Al ratio during synthesis. A set of ZSM-5 catalysts with Si/Al ratios from 12 to over 10,000 (Si/Al ratio is inversely proportional to acid site concentration) exhibited a constant TOF for the acid catalyzed reaction of hexane cracking[86] over the entire concentration range reported. The behavior observed for this zeolite catalyst is analogous to the behavior expected for an ideal solution; the properties of the system are independent of concentration. This is in stark contrast to the catalyst system investigated in this work, where the TOFs for acid-catalyzed reactions were very sensitive to the replacement of protons with counter-cations.

Due to the non-ideal behavior of POMs with cation addition, it may be more appropriate to describe acid catalysis by supported POMs as occurring in concentrated acid solution (waters of hydration plus anions and cations). The non-ideal and concentration-dependent nature of POM acid sites is explored in this chapter through the lens of solution chemistry. Namely, aqueous electrolytes demonstrate non-ideal behavior with concentration, even at dilute concentrations.

The theory of Debye and Hückel, and extensions thereof, are well suited to describe the non-idealities of electrolytes in solution and is adapted in this work to describe the non-ideal behavior of cation-exchanged POMs.

As discussed in detail below, a case is made for the presence of hydrated clusters of POMs under reaction conditions to justify the use of models based on aqueous solutions of electrolytes to described cation-exchanged POMs. The highly solvated nature of such a cluster may be rather analogous to solution chemistry.

5.1.1 Hydrated POMs and POM clusters

As noted previously, bulk POMs such as $H_3PMo_{12}O_{40}$ may possess over 30 waters of crystallization (10 per proton). While the dispersed POMs and POM clusters demonstrated in Chapter 2 represent 2-dimensional rather than 3-dimensional structures and might therefore be expected to present a different environment for waters of crystallization than bulk crystallites, these also likely exhibit some extent of hydration under both ambient conditions and reaction conditions in which water is present.

The majority of the 30 waters of hydration in bulk POMs are weakly bound and approximately 6 waters of hydration remain after heating to 30˚C in vacuo (determined gravimetrically as described in Chapter 2). The water molecules present in $H_3PMo_{12}O_{40}\cdot 6H_2O$ form inter-POM hydrogen bonding networks with POM protons, in the form of $(H_2O)_2H^+$ cations.[10] Both $H_3PMo_{12}O_{40}$ and $Cu_{1.5}PMo_{12}O_{40}$ retain waters of hydration up to ~200˚C for the bulk POM salts, as determined by TGA,[9] demonstrating the strength of interactions between POMs and waters of

hydration. Further evidence for the presence of hydrated POM clusters on silica exists. For example, the low angle peak in XRD observed for silica supported POMs (as discussed in Chapter 2) has been attributed to hydrated POM clusters.[46] Additionally, XRD of POMs immediately after a methacrolein oxidation reaction (300˚C, co-fed water) detected a crystal structure consistent with the presence of 6 waters of hydration in the post-reaction catalyst.[9,87]

In addition to being able to hold onto a large quantity of waters of hydration, POMs may also exhibit pseudo-liquid behavior under reaction conditions if they are sufficiently hydrated.[9] The pseudo-liquid behavior of hydrated POMs is characterized by the ability of polar molecules to rapidly diffuse and react throughout the catalyst bulk, as polar molecules such as alcohols can replace waters of hydration. There are several examples that provide evidence for the presence of pseudo-liquid behavior for the supported POMs in this work. First, at loadings above a monolayer (e.g., HPMo 1.35), the formation of bulk POMs only results in a slight decrease in rates, as observed in XRD. This result is expected for catalysts that could exhibit pseudo-liquid[9] behavior under reaction conditions, as most POMs may still be accessible to polar reactants. Thus, when the POM coverage is varied from ca. 0.25 monolayers, where no crystallites are present, to greater than monolayer coverage, all acid sites remain accessible and exhibit similar activity, as shown in this work and previously by Iglesia and co-workers.[25] Further, for sodium-exchanged catalysts, the different dispersion characteristics of NaPMo 0.2 and NaPMo 0.7 had little impact on the reactivity of these catalysts for methanol conversion. This again suggests that the local environment of the protons differs little, whether the POMs are well dispersed or present in clusters and crystallites.

Finally, in the experiments presented in previous chapters, water was co-fed during reactions with methanol at a pressure of 2.7 kPa H_2O. Co-feeding water was essential to keep the POMs from decomposing and migrating down the reactor tube as volatile MoO_3 (see discussion in Chapter 3). Given the relatively mild reaction conditions utilized, co-fed water (and the water generated as a product of methanol dehydration and oxidative dehydrogenation) would also be expected to promote hydration of the ions present on the catalyst. Thus, although these reaction studies represent classical gas-solid contact catalysis, it may be worthwhile to consider the surface environment as a concentrated aqueous solution. This approach is considered below, along with the insights it provides into the observed effects of cation exchange on POM reactivity.

5.1.2 Non-ideal solutions and activity coefficients

In a concentrated aqueous acid system, the effect of concentration and salt addition is described by activity coefficients. Activity coefficients, first defined in Equation 1-3 and again in Equation 5-1 for convenience, describe the deviation of a component from ideal behavior. Activity coefficients may be calculated using simple expressions such as the Debye-Huckel limiting law and Harned's rule,[58,88,89] which is discussed in further detail in the following sections.

Equation 5-1: Relation between thermodynamic activity, activity coefficients, and concentration

$$a_i = \gamma_i \cdot \frac{c_i}{c^o}$$

where, for component *i*, a_i is the thermodynamic activity, γ_i is the activity coefficient, c_i is the concentration of *i*, and c^o is the standard state concentration. By convention a_i and γ_i are unitless and typically the standard state is chosen to set both quantities equal to 1 for a pure substance.

5.2 Background: Activity coefficients for electrolyte solutions

Debye-Hückel theory was introduced in the Chapter 1 as a simple model of the electrostatic interactions of electrolyte solutions. However, the Debye-Hückel limiting law, introduced in Equation 1-4 and included below in Equation 5-2 for convenience, is only applicable for very dilute solutions. The extension of this theory to solutions at higher concentrations by Hückel[90] and others[91] introduced terms to consider effective ion size[91] and the effects of increasing ions concentration on the dielectric constant of the solution.[90,91] The effective ion size describes the radius of the ion and its closely bound water molecules. The microscopic dielectric constant may vary due to displacement of solvent.[91] In addition to the simple improvements described here many advancements have been made by building upon the simple model proposed by Debye and Hückel.[59]

Equation 5-2: Debye-Hückel limiting law

$$\ln(\gamma) = -A|z_+ z_-|\frac{\sqrt{I}}{1 + B\text{å}\sqrt{I}}$$

where A and B are constants that depend on the temperature and dielectric constant (ε) of the solvent, z_+ and z_- are the ion charges, å is the effective ion size, and I is the ionic strength of the solution, first defined in Equation 1-5 and repeated in Equation 5-3 below for convenience:

Equation 5-3: Ionic Strength

$$I = \frac{1}{2}\sum_{i}^{n} m_i z_i^2$$

where I is the ionic strength of the system, m_i is the concentration of component *i* in molality (mol/kg), and z_i is the ion charge. The summation is over all electrolyte components, both anions and cations.

Of relevance to this work is Harned's rule, described in detail in the following section. Briefly, Harned's rule relates the activity coefficient of one electrolyte component in a binary aqueous mixture (e.g., HCl) to the concentration of the other component (e.g., NaCl), given that the system is at a constant ionic strength. Harned's rule was first developed as an empirical relationship[92] to describe the activity coefficients of electrolyte mixtures. However, the general form of Harned's rule may be directly derived from Debye-Hückel theory[92] using the work of Hückel[90] on the variation of the dielectric constant with concentration as a guide and assuming constant total molality and effective ion size.[92]

5.2.1 Harned's rule

Harned's rule states that the logarithm of the activity coefficient of one strong electrolyte (B) in a two-component mixture at constant ionic strength (Equation 5-3) varies in direct proportion to the concentration of the other electrolyte (C),[88,89] as shown in Equation 5-4.

Equation 5-4: Harned's rule

$$\log_{10}(\gamma_B) = \log_{10}\left(\gamma_B^{\text{pure}}\right) - \alpha \cdot m_C$$

In Equation 5-4, γ_B is the activity coefficient for species B in the mixture, γ_B^{pure} is the activity coefficient of B in pure solvent, α is the Harned coefficient, and m_C is the concentration of species C, typically in units of molality or molarity (mol/kg or mol/L, respectively). Harned's rule has been use to characterize over 70 aqueous electrolyte systems,[89] such as aqueous mixtures of {KOH + KCl}(aq) or {HCl + $AlCl_3$}(aq).[89,93]

5.2.1.1 Harned's rule example: HCl and NaCl

A brief example is included here for the application of Harned's rule to describe the activity coefficients of an aqueous mixture of electrolytes: {HCl + NaCl}(aq). HCl is component B in Equation 5-4 and NaCl component C; the ionic strength is held constant at 1 mol/kg for this example.

Rowland and May[89] have tabulated Harned coefficients for a great number of aqueous electrolyte mixtures, and report a Harned coefficient of α=0.753 for an aqueous solution of HCl and NaCl at an ionic strength of 1 mol/kg (Harned coefficients are available at ionic strengths from 0.1 to 3 mol/kg). Note that for a 1:1 electrolyte such as HCl the ionic strength is equivalent in value to the concentration (see Equation 5-3).

Pure HCl at a concentration of 1 mol/kg was set as the standard state and the activity coefficient of pure HCl, γ_B^{pure}, was set equal to 1. The activity coefficients calculated using Harned's rule were used to calculate the thermodynamic activity (defined in Equation 5-1) of HCl in the mixture. The thermodynamic activity (which may be thought of as 'effective concentration') of

HCl is presented in Figure 5-1 as a function of the HCl an NaCl concentrations. Note that the total concentration of HCl + NaCl is maintained at 1 mol/kg.

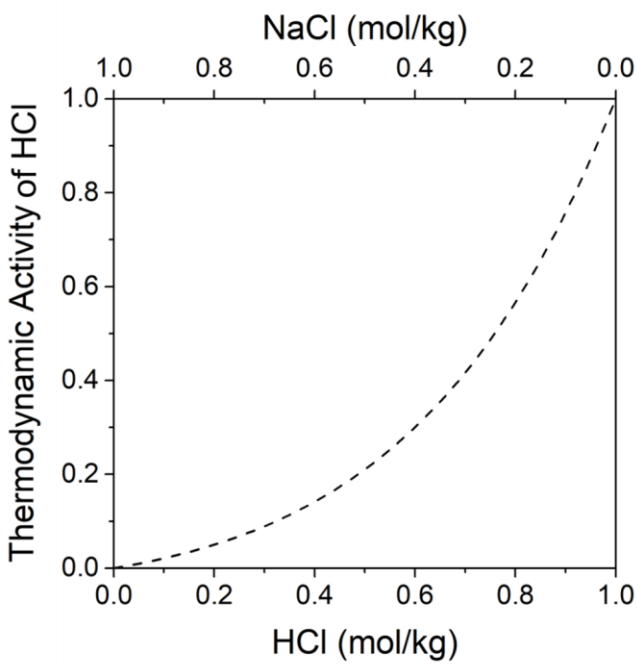

Figure 5-1: Example of using activity coefficients calculated using Harned's rule to define the thermodynamic activity of HCl in a solution with NaCl. Plot depicts the thermodynamic activity of HCl as a function of the HCl and NaCl concentration at a total concentration of 1 mol/kg. The Harned coefficient for the {HCl + NaCl}(aq) system, $\alpha = 0.753$, was obtained from tabulated values.[89]

One can clearly see that the thermodynamic activity of HCl decreases at a faster rate than the concentration of HCl with the addition of NaCl. For example, for a 50:50 mixture of HCl and NaCl, the concentration of HCl is 0.5 mol/kg, but the *thermodynamic activity* of HCl is 0.21. Therefore a 50:50 mixture of HCl and NaCl is much less acidic than HCl at 0.5 mol/kg without NaCl in the system. This may be analogous the behavior of cation-exchanged POMs, whose activity decrease much more rapidly with cation-exchange than with POM concentration.

5.2.2 Developing activity coefficients for supported POMs

While the activity coefficients for aqueous electrolytes have been well described, defining activity coefficients for solid acids has previously not been realized.[94] The deviation of POM acid sites from 'ideal' catalytic behavior for methanol to dehydration could, in principle, be described by an activity coefficient. In this case the 'ideal' behavior is defined as the POM without cation addition, HPMo 0.2. The activity coefficients are a function of the concentration of the charged species on the catalyst surface, POM^{3+}, H^+, Na^+, Mg^{2+}, etc., in a hydrated environment perhaps analogous to an aqueous solution of electrolytes. Treating hydrated POM clusters as an electrolyte solution may serve to extend the well-understood thermodynamics of aqueous systems to solid acids.

5.2.2.1 Debye-Hückel theory and HPMo 0.04 – 1.35

The Debye-Hückel limiting law (Equation 5-2) relates the activity of a species to the ionic strength and ion charges. This simple relation could in principal describe non-idealities of a single electrolyte varying in concentration, for example the catalyst series of HPMo 0.04 – 1.35. Note that the Debye-Hückel limiting law has three parameters, A, B, and å, compared to the single parameter, α, in Harned's rule.

Unfortunately, the catalyst series of HPMo 0.04 – 1.35 does not seem to be useful for analysis using a relation derived from Debye-Hückel theory. For example, the catalysts at 0.2 – 1.35 POM/nm^2 have very similar *local* structure including acid site concentration, dehydration and oxidation TOFs, and size of POM clusters.[25] While the density of POM clusters varies with

loading, the local nature of the POMs, such as hydration and ionic strength, which are described by the Debye-Hückel model, remain fairly constant.

Perhaps with more data for POMs at low loadings (< 0.2 POM/nm^2), where POMs begin to interact strongly with silica, a suitable treatment could be attempted using the Debye-Hückel limiting law. It should be noted in such a case the activity coefficients would decrease with decreasing POM concentration, the inverse of the relation typically observed for electrolyte solutions.

5.2.2.2 Harned's rule and cation-exchanged POMs

Harned's rule is uniquely suited to describe the activity coefficients of cation-exchanged POMs using a single parameter model grounded in the thermodynamics of Debye-Hückel theory. In contrast to the case for HPMo 0.04 – 1.35, cation-exchanged POMs exhibit significant decreases in catalytic activity and acid site concentration with increasing levels of cation exchange, paralleling the behavior observed for solutions of aqueous acid-salt mixtures. The applicability of this single parameter model to describe the variation of activity coefficients with cation-addition for supported is described below.

The applicability of Harned's rule to cation-exchanged POMs is demonstrated using NaPMo 0.2 as the example. First, it is assumed that the POMs on the silica surface undergo stoichiometric exchange with sodium addition to form $Na_xH_{3-x}PMo_{12}O_{40}$ supported on SiO_2 at a loading of 0.2 POM/nm^2. Then, as Na^+ is exchanged for H^+, neither the total charge nor the concentration of ionic species (including the POMs) are changing, leading to a constant ionic strength (Equation

5-3) with cation-exchange. A constant ionic strength with varying ion concentration is an essential component of Harned's rule. In addition, a given Harned coefficient is only applicable at a single ionic strength. The second consideration is that Harned's rule is used to relate the activity coefficient of one component, B, to the concentration of the other component, C. This relation is clearly exhibited in the system of the NaPMo 0.2 catalysts, as the catalytic activity of POM acid sites ('B') for acid-catalyzed reactions decrease sharply with the addition of sodium ('C'). The following sections detail the methods used to apply Harned's rule to cation-exchanged POMs to relate the cation content and catalytic activity of these catalysts to the activity coefficients for the POM acid sites.

5.3 Methods

The methods used for the application of Harned's rule to cation-exchanged POMs are briefly discussed here. For simplicity NaPMo 0.2 is used as an example, however the methods described in this section are applicable to all the cation-exchanged POM catalysts used in this work.

5.3.1 Re-define Harned's rule for cation-exchanged POMs

Harned's rule is re-defined in this section specifically for cation-exchanged POMs. First, however, the choice of concentration units is discussed in detail. When Harned's rule was defined in Equation 5-4, m_C (concentration of C in mol/kg or mol/L) was used as the concentration-dependent variable. Several other concentration variables commonly used[89] are I_C, the ionic strength contribution of electrolyte C only, and y_C, the ionic strength fraction of component C: $y_C = I_C/I$ (ionic strength, I, was defined in Equation 5-3). The choice of the concentration variable and/or units does not impact the application of Harned's rule, only the

magnitude of the Harned coefficient.[89] Additionally, Harned coefficients may readily be transformed to the preferred form to coincide with the form of the concentration variable.[89]

Na_xPMo 0.2 contains POMs dispersed on silica at coverage of 0.2 POM/nm^2, corresponding to a POM content of 10.3 wt%, or in terms of molality, 0.063 mol POM/kg SiO_2. Clearly defining concentration using molality (mol/kg) and molarity (mol/L) is insufficient for supported POMs, as the mass and volume of the support are irrelevant to the system under consideration.

POM coverage, perhaps in units of POM/nm^2 or μmol POM/m^2, might seem to be more appropriate to describe the concentration of a species on a 2D surface. However, assuming POMs or POM clusters are isolated from each other, the POM loading becomes an extensive parameter and is irrelevant to the thermodynamic properties of cation-exchanged POMs. As a case in point, the NaPMo 0.2 and NaPMo 0.7 catalysts exhibit nearly identical TOFs in spite of their different coverages. As concentration and loading appear to be unsuitable metrics for these supported POMs, variables based on ionic strength, I_C and y_C, may appear to be more appropriate choices. However, POMs reactivities were observed to be insensitive to the ionic strength contribution of the cation, as Na^+, Mg^{2+}, and Cu^{2+} were observed to give rise to nearly identical catalytic behavior with cation addition. The addition of Al^{3+} should have had the most significant impact on POM acidity because of its greater charge if ionic strength of the cation played an essential role in proton thermodynamic activity, but this also appeared not to be the case.

It should again be noted that the choice of units is rather arbitrary and does not impact the ability of the model to describe POM behavior. As neither the concentration, coverage, or ionic strength

was found to be suitable, but all of these variables ultimately depend on the concentration of Na^+ (or $Na_3PMo_{12}O_{40}$), the simplest but most intuitive variable may be the quantity of cation exchanged per POM. The quantity of cation/POM is an apt descriptor of POM catalytic activity, as demonstrated in Chapters 3 and 4, and is not sensitive to loading or support properties.

Harned's rule, redefined for cation-exchanged POMs supported on silica, using the quantity of cations exchanged per POM as the dependent variable is shown in Equation 5-5. For NaPMo 0.2, the activity coefficient of component B, $H_3PMo_{12}O_{40}$, is related to the concentration of component C, $Na_3PMo_{12}O_{40}$, using Harned's rule.

Equation 5-5: Harned's rule defined for Na_xPMo.

$$\log_{10}(\gamma_H)=\log_{10}\left(\gamma_{\mathrm{H}}^{\mathrm{pure}}\right)\text{-}\alpha N_{Na^+}$$

where γ_H is the activity coefficient for $H_3PMo_{12}O_{40}$, α is the Harned coefficient, and N_{Na^+} is the quantity of sodium per POM, γ_H^{pure} is the activity coefficient for pure $H_3PMo_{12}O_{40}$ on a two-dimensional support (i.e., taking HPMo 0.2 as the standard state). Traditionally, the activity of the pure substance that serves as the standard state is set equal to one, thus $\gamma_H^{\mathrm{pure}} = 1$ throughout this chapter. Therefore, the activity coefficient for the POM protons varies from $\gamma_H = 1$ for HPMo 0.2 ($N_{Na^+} = 0$) and tends to decrease toward $\gamma_H = 0$ as N_{Na^+} increases.

It is recognized that $H_3PMo_{12}O_{40}$ and $Na_3PMo_{12}O_{40}$ are not expected to be phase pure species on the silica support, but rather a mixture ($Na_xH_{3-x}PMo_{12}O_{40}$) whose average concentration varies with Na content. It may be desirable to define an activity coefficient for the POM protons,

however it is not possible to rigorously define single ion activity coefficients based on experimental measurements[95] (a solution containing only H^+ ions cannot be prepared). However, activities may still be described in terms of single ions for simplicity. For example, in the definition of pH, where pH = $-\log_{10}[a_{H^+}]$, a_{H^+} is the activity of protons in solution and is purely notational in nature. Likewise, to avoid confusion, γ_H, γ_H^{pure}, and related expressions are hereafter referred to as relating to the activity of POM protons, while it is recognized that more rigorously they represent the activity of $H_3PMo_{12}O_{40}$.

5.3.2 Applying Harned's rule to cation-exchanged supported POM catalysts

Thermodynamic activity may be used to define equilibrium constants and reaction rates of systems that exhibit deviations from ideal behavior. The relationship between thermodynamic activity, activity coefficients, and concentration was defined in Equation 5-1. The thermodynamic activity is re-defined specifically for POM protons in Equation 5-6 below.

Equation 5-6: Thermodynamic activity of POM protons

$$a_H = \gamma_H \cdot \frac{[H^+]}{c^o}$$

where a_H is the thermodynamic activity of POM protons, $[H^+]$ is the concentration of POM protons in units of mol H^+/mol POM, and c^o is the standard state concentration, defined such that a_H and γ_H are unitless and equal to 1 at the standard state. As the standard state was set as HPMo 0.2, c^o is therefore equal to the quantity of H^+/POM determined experimentally in this work for the HPMo 0.2 catalyst.

The dehydration TOF, defined using the *thermodynamic activity* of POM protons, is given in Equation 5-7. TOF_γ is used to denote turnover frequencies defined using thermodynamic activity, in order to avoid confusion with the TOFs used in Chapters 3 and 4.

Equation 5-7: Dehydration TOF defined using proton thermodynamic activity, a_{H^+}, rather than proton concentration.

$$Dehydration\ TOF_\gamma\ (s^{-1}) = \frac{Dehydration\ TOF}{\gamma_H} = \frac{mol\ DME}{mol\ H^+ \cdot \gamma_H \cdot s} = \frac{mol\ DME}{a_H \cdot c^o \cdot s}$$

where TOF_γ is the turnover frequency defined using activity coefficients.

The relation $\frac{mol\ DME}{mol\ H^+ \cdot \gamma_H \cdot s}$ is used in the y-axis label of plots containing TOF_γ, in order to make it clear that both the concentration of protons and the activity coefficients of protons were used to normalize rates.

5.3.3 Criteria for calculating the Harned coefficient, α

Typically, the Harned coefficients may be determined experimentally, such as through electrochemical[88,89] measurements of an aqueous solution with various ratios of two electrolytes, or with calculations from data for the individual electrolytes.[96] In our case, experimental data for aqueous POMs is not readily available, and likely would not be directly applicable to a system of solid hydrated POM clusters. Instead, the Harned coefficient is treated as an adjustable parameter to demonstrate that the functional form of Harned's rule may accurately describe the behavior of the POM acid sites with cation exchange.

In order to define values for the activity coefficients of POM protons, the dehydration TOF, known to be sensitive to POM acid strength,[30] is used as a proxy of the deviation of the POM acid sites from ideal behavior, relative to the standard state behavior of the supported POMs without cation-exchange (HPMo 0.2). The methods and assumptions necessary to use the catalytic activity of cation-exchanged POMs to derive Harned coefficients are discussed in detail here.

First, consider that TOF_{γ}, rigorously defined with the thermodynamic activity of POM protons, should be invariant with the extent of cation-exchange. Activity coefficients, by definition, account for deviations of a system from ideal behavior. In other words, the disruption of POM protons via cation addition is already accounted for the in TOF_{γ} and we may consider the dehydration rates appropriately normalized per the *effective* concentration of POM protons.

Therefore, the Harned coefficients were optimized using the Solver tool in Excel in order to obtain a series of TOF_{γ} values that are invariant with cation content. Specifically, the optimal Harned coefficient minimized the least square difference between the TOF_{γ} of HPMo and the TOF_{γ} of the cation-exchanged POMs. A unique Harned coefficient was used for each series of cation-exchanged POMs.

The methods used to fit the activity coefficients to the dehydration TOF data are easily visualized. With the optimal Harned coefficient, a double y-axis plot of TOF and γ vs N_{Na^+} should result in a perfect overlay of the two curves. Additionally, a plot of TOF_{γ} vs. N_{Na^+} should be constant and show no observable deviations with the extent of cation exchange.

5.3.1 Key Assumptions and Limitations

Prior to applying this analysis to the catalysts exchanged with higher-valent cations, it should be noted that a key assumption in Harned's rule is that the system is at a constant ionic strength as the concentrations of individual species are varied. Using the nominal stoichiometries for cation-exchange, this assumption is trivial for systems such as {KCl + KOH}(aq) or {$H_3PMo_{12}O_{40}$ + $Na_3PMo_{12}O_{40}$}(s), as the cations and anions of each electrolyte are of identical charge. However, in the system of {$H_3PMo_{12}O_{40}$ + $Mg_{1.5}PMo_{12}O_{40}$}(s), in which Mg^{2+} is exchanged for H^+, the ionic strength contribution of the cation increases proportional to z^2 (see Equation 5-3). Relative to $H_3PMo_{12}O_{40}$ (the standard state), exchanging a nominally stoichiometric quantity of cations for protons results in the increase of the total ionic strength by 0% for $Na_3PMo_{12}O_{40}$, 25% for $Mg_{1.5}PMo_{12}O_{40}$, and 50% for $Al_1PMo_{12}O_{40}$.

While this increase in ionic strength with cation addition is known, it is neglected for the purpose of this work, as the true nature of the local environment of the POM is unknown. For example, as shown in Chapter 2, cation addition resulted in the removal of protons at a non-stoichiometric rate, regardless of cation identity or charge. To account for the non-stoichiometric exchange, there must be significant interaction of silanols with both POMs and cations, since the charge is expected to be locally conserved in the vicinity of the POM clusters. Therefore, it would be inappropriate to assume that the entirety of the charge added to the system as cations would be directly interacting with the POM, making it difficult to determine the local ionic strength of the POM clusters. Without a sufficient physical model of the local charge structure to define the true ionic strength in the vicinity of the POMs, a simplified model was adopted that neglected the effect of cation addition on ionic strength and considered only the concentration of the

electrolyte species. To provide some justification of this treatment, the quantity of acid sites and TOFs do decrease in proportion to the total quantity of cations and do not saturate with the addition of a stoichiometric quantity of cations.

5.4 Results

The optimized Harned coefficients determined for each catalyst series used in this work are presented in Table 5-1. The Harned coefficients for [Na,Mg,Cu]PMo 0.2 and NaPMo 0.7 are similar, as these catalysts series exhibited similar dehydration TOFs with cation addition (see Figure 3-4 and Figure 4-2). The Harned coefficient for AlPMo 0.2 is significantly lower than the other coefficients, as POMs rates decreased only slightly with Al addition. The results are next gone over in detail, first for NaPMo 0.2 for the sake of simplicity.

NaPMo	NaPMo 0.7	MgPMo	AlPMo	CuPMo
0.52	0.43	0.68	0.07	0.46

Table 5-1: Harned coefficients (α) for cation exchanged POMs supported on silica. The Harned coefficients presented minimized the deviation in TOF_γ with cation exchange. Each catalyst series was optimized individually.

5.4.1 NaPMo 0.2

The activity coefficients for the series of sodium-exchanged POMs at a loading of 0.2 POM/nm^2 are presented in Figure 5-2 as a function of the quantity of sodium per POM (open symbols). The activity coefficient values were calculated using Harned's rule and $\alpha = 0.52$. The dehydration TOF (closed symbols) are also included in Figure 5-2 to give a visual indication of goodness of fit between the activity coefficients of the POM protons and the non-ideal behavior observed in

the acid-catalyzed reaction. The y-axes were scaled to match the TOF of the standard state, HPMo 0.2, with the standard state activity coefficient, $\gamma_H = 1$. This way, it is relatively easy to visualize that when the rates per proton and activity coefficients overlap, the TOF normalized using thermodynamic activity (TOF_γ) is invariant with the extent of cation-exchange.

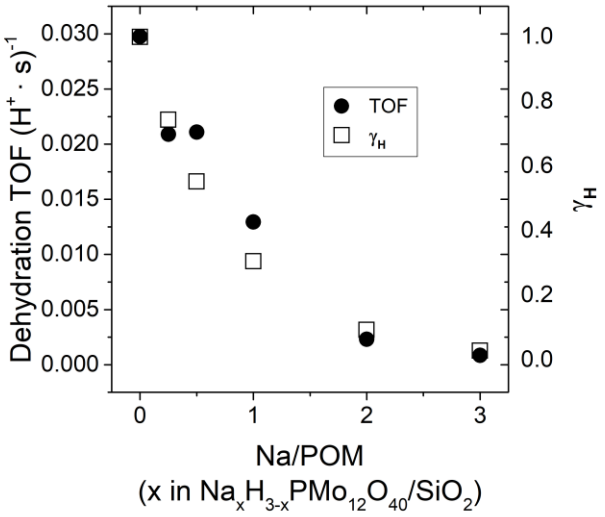

Figure 5-2: Closed symbols: Methanol dehydration turnover frequencies for Na_xPMo 0.2 as a function of the quantity of sodium per POM. Open symbols: Activity coefficients for Na_xPMo calculated using a Harned coefficient of $\alpha = 0.52$ and the quantity of sodium per POM at a given level of cation-exchange. The standard state was set as the catalyst without cation-exchange, HPMo 0.2 and corresponds to $\gamma_H = 1$. Axes are scaled to match the TOF of the standard state, HPMo 0.2, with an activity coefficient of 1.

The dehydration TOF_γ values, defined using the thermodynamic activity of POM protons rather than acid site concentration, are presented in Figure 5-3 for the NaPMo 0.2 catalyst series. The Harned coefficient of $\alpha = 0.52$ was optimized using least squares regression to obtain the minimal variation of TOF_γ with cation addition. The variation in TOF is of comparable magnitude to the variations observed with varying POM loading on silica, as was presented in Figure 3-3.

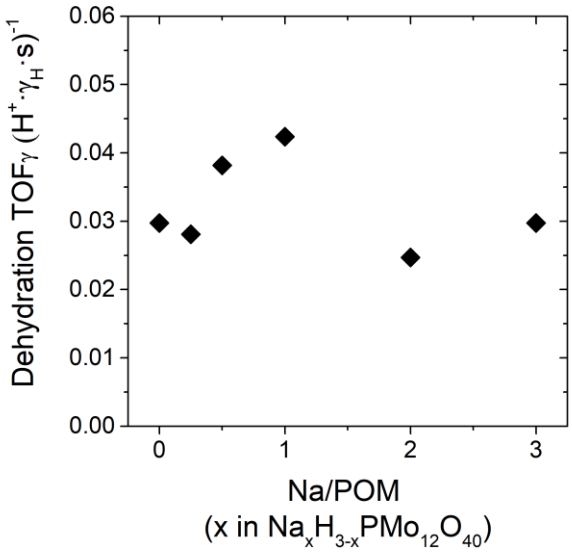

Figure 5-3: Dehydration TOF_γ for the NaPMo 0.2 catalyst series, calculated by normalizing dehydration rates per proton activity, a_H, rather than per proton.

The ability of activity coefficients, defined in this chapter to reasonably normalize to dehydration rates to obtain near-constant TOF_γ over a range of cation contents, is in stark contrast to the large variations in TOF reported in Chapters 3 and 4. The excellent fit supports the model of POMs as hydrated clusters under reaction conditions and the treatment of hydrated POM clusters as two-dimensional electrolyte solutions.

5.4.2 NaPMo 0.7 and [Mg,Al,Cu]PMo 0.2

The activity coefficients for NaPMo 0.7 and [Mg,Al,Cu]PMo 0.2 are presented in Figure 5-4 as a function of the quantity of cation per POM, along with the corresponding dehydration TOF.

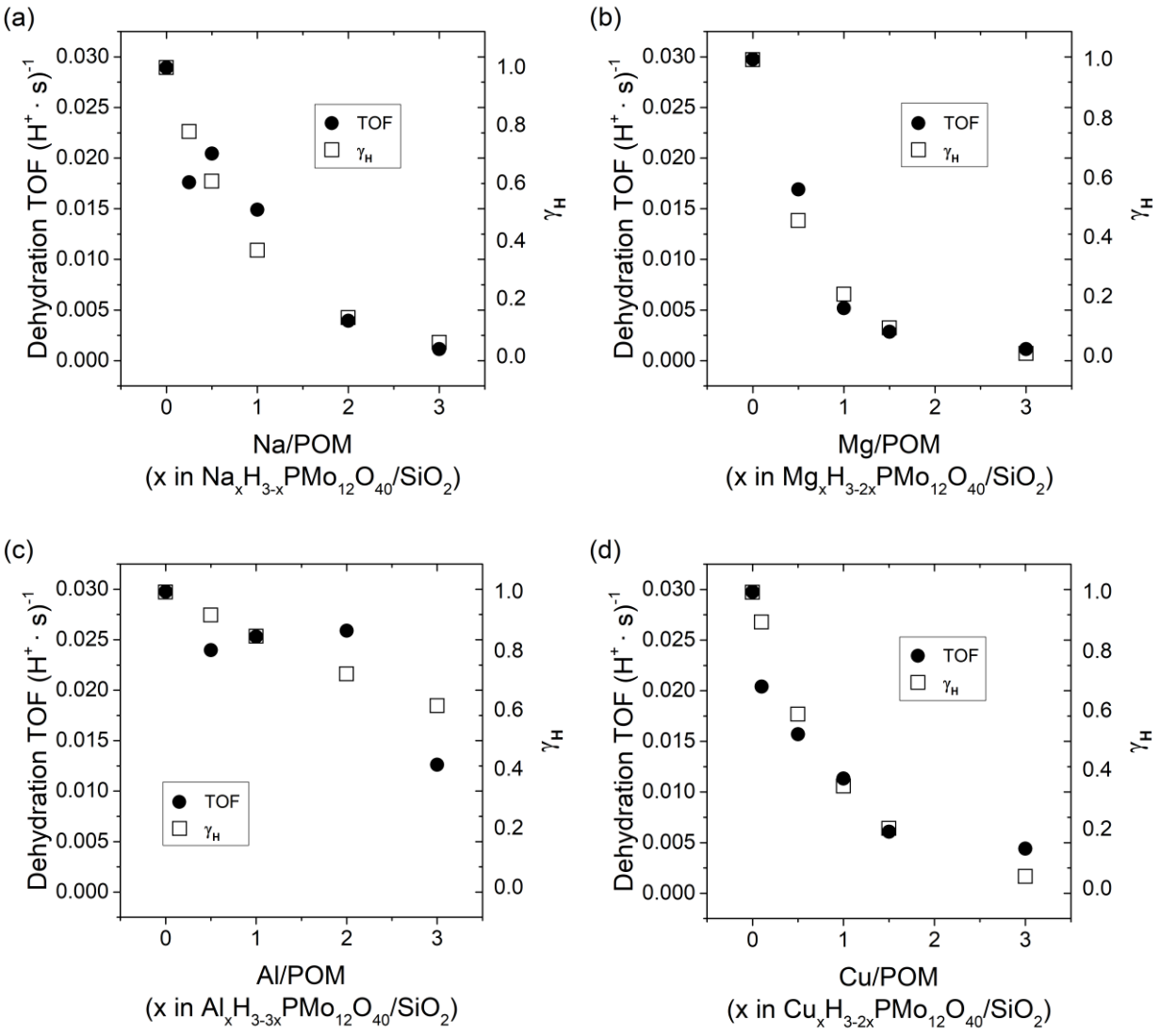

Figure 5-4: Closed symbols: Methanol dehydration turnover frequencies for **a)** NaPMo 0.7, **b)** MgPMo 0.2, **c)** AlPMo 0.2, and **d)** CuPMo 0.2. TOFs are normalized per proton as determined by DTBP titration. Open symbols: Activity coefficients calculated using Harned coefficients listed in Table 5-1 and the respective coverage of each cation at a given level of cation-exchange. The standard state was set as the catalyst without cation-exchange, either HPMo 0.2 or HPMo 0.7, and corresponds to $\gamma_H^{pure} = 1$. Axes are scaled to match the TOF of the standard state with an activity of 1.

Reasonable agreement was seen between the activity coefficients and the dehydration TOFs, even for cations such as Al that exhibited significantly different behavior than the other cations. As noted previously, [Na,Mg,Cu]PMo 0.2 and NaPMo 0.7 have similar Harned coefficients as

they exhibit similar TOF and acid site concentration trends with cation exchange. The physical meaning behind the values of Harned coefficients may be visualized using Figure 5-4. MgPMo 0.2 possesses the largest Harned coefficient of $\alpha = 0.68$. By examining Figure 5-4 it is apparent that the activity coefficient decreases more rapidly for MgPMo 0.2 than for NaPMo 0.7 or CuPMo 0.2 ($\alpha = 0.46$ and 0.43, respectively). Finally, for AlPMo 0.2, with $\alpha = 0.07$, the activity coefficient only decreases by approximately 40% over the entire range of cation-exchange. Clearly the larger the value of the Harned coefficient, the more that the cation is perturbing the POM acid sites.

The dehydration rates normalized per proton thermodynamic activity (TOF_γ) are presented in Figure 5-5 for all cation-exchanged POMs discussed in this work. The dehydration TOF_γ does not monotonically decrease with cation addition as was observed when acid site concentration was used to normalize TOFs. The dehydration TOF_γ is generally within ± 50% for all cations used and all levels of cation-exchange; there do not seem to be any clear trends in the TOF data as was observed with the rates normalized per proton. The ability of activity coefficients to describe the activity of various cations, extents of cation-exchange, and POM loadings is quite remarkable.

It should be noted that the model described in Equation 5-5 did not capture the behavior of POMs exchanged with excess cation very well. In particular Mg_3PMo, Cu_3PMo, and Na_6PMo were not included in Figure 5-5 as they were significantly off scale ($TOF_\gamma > 0.1$). Likely the model does not capture the behavior of POMs with excess cation well as the model has no information on the diminishing returns of cation-exchange, with respect to both POM catalytic

activity and acid site concentration, with the addition of large quantities of cations. Nor does the model account for the necessity of balancing the excess charges in the system. Excess charge may perhaps be balanced via interactions of cations with the silica surface for cases with a quantity of cation in excess of the stoichiometric requirement.

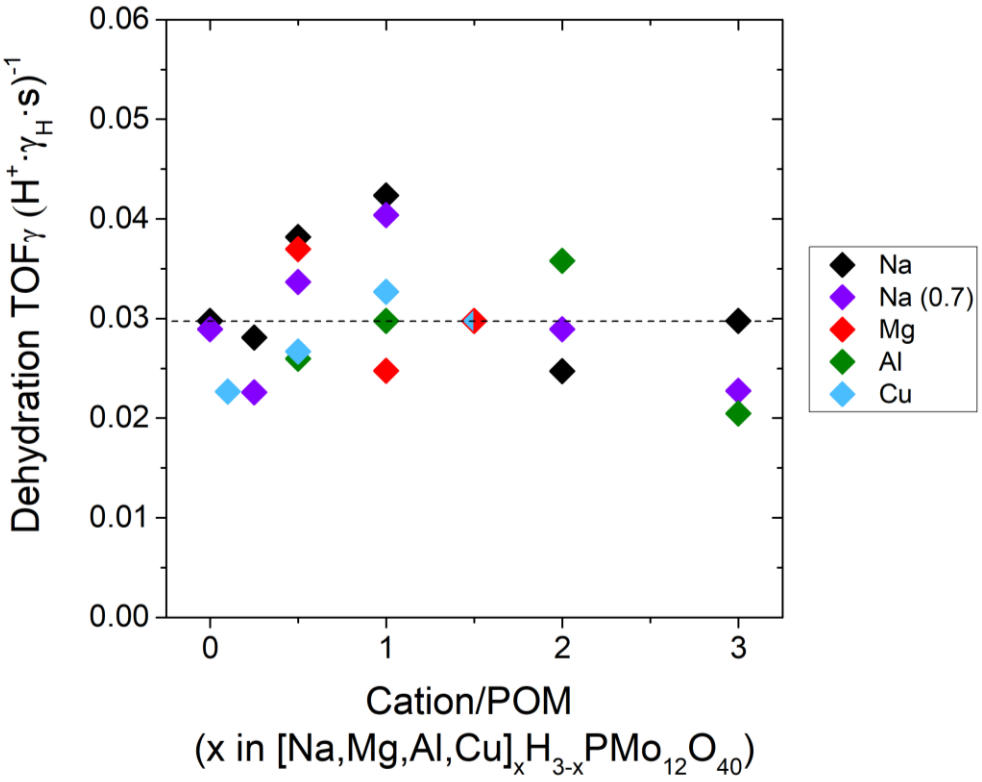

Figure 5-5: Dehydration TOF_γ for the $[Na,Mg,Al,Cu]_xPMo$ 0.2 and Na_xPMo 0.7 catalyst series, calculated by normalizing dehydration rates per proton activity, a_{H^+}, rather than per proton. Horizontal dashed line indicates a constant TOF_γ with respect to the catalyst without cation-exchange, HPMo 0.2.

5.4.3 Extent of proton removal and Harned's rule

The methods section of this chapter discussed in detail the choice of dependent variable used in Harned's rule. The choice of variable had no impact on the goodness of fit of the model, as all of the options discussed ultimately depended on a single quantity, the number of cations per POM.

However, the fraction of protons removed with cation addition may also reflect the nature of POM acid sites. This fraction is defined as the extent of proton removal (χ) by counter-cation addition and is discussed here as an alternative method for the determination of activity coefficients for POM acid sites. The extent of proton removal (χ) is defined in Equation 5-8 below, using the NaPMo 0.2 catalyst series as an example.

Equation 5-8: The fractional extent of proton removal, χ, as a function of the quantity of acid sites per POM, N_{H^+}.

$$\chi = \frac{N_{H^+,HPMo} - N_{H^+,Na_xPMo}}{N_{H^+,HPMo}}$$

where χ is the extent of proton removal, $N_{H^+,HPMo}$ is the quantity of protons per POM for HPMo 0.2, and N_{H^+,Na_xPMo} is the quantity of protons per POM for a catalyst with cation-exchange, in this case for sodium-exchanged POMs.

The motivation for using the extent of proton removal is three-fold. Firstly, stoichiometric exchange was not observed between counter-cations and POM acid sites and POMs behaved nearly identically with the addition of either mono- or di-valent cations. Additionally, with stoichiometric exchange, only one Al^{3+} is required to exchange with all POM protons, however AlPMo 0.2 retained the highest quantity of acid sites per POM, as determined by DTBP titration. Clearly not all of the cations added to the system are intimately interacting with the POMs, due to constraints on local charge conservation (however, many POM properties do decrease monotonically with cation addition). The second driver behind the use of χ, the extent of proton removal, is that it is an experimentally measured quantity, obtained under reaction conditions. χ

may represent the degree to which cations are interacting with POMs. Finally, treating the extent of cation interaction in this manner may avoid the issue outlined previously for the variation of ionic strength with cation-exchange. By assuming that POMs only 'feel' enough charge to remove a proportional quantity of protons, the local charge structure of HPMo 0.2 would be maintained and the ionic strength of the POM cluster would remain constant.

Table 5-2 contains the values of N_{H^+} (H^+/POM) and χ for all catalysts used in this work. χ varies between a value of zero for HPMo 0.2 (by definition) to 0.97 for Na_6PMo 0.2. With the addition of 3 cations per POM the extent of proton removal is within the range of $\chi = 0.65 - 0.85$, with the exception of Al-exchanged POMs.

Na	**H^+**	**χ**	**Mg**	**H^+**	**χ**	**Al**	**H^+**	**χ**	**Cu**	**H^+**	**χ**	**Na (0.7)**	**H^+**	**χ**
0	1.92	0	0	1.92	0	0	1.92	0	0	1.92	0	0	2.08	0
0.25	1.69	0.12	0.5	1.49	0.22	0.5	2.01	-0.05	0.1	1.78	0.07	0.25	1.90	0.08
0.5	1.62	0.16	1	1.27	0.34	1	1.86	0.03	0.5	1.50	0.22	0.5	1.72	0.17
1	1.38	0.28	1.5	0.96	0.50	2	1.34	0.30	1	1.23	0.36	1	1.45	0.30
2	0.90	0.53	3	0.56	0.71	3	1.34	0.30	1.5	1.17	0.39	2	1.00	0.52
3	0.31	0.84							3	0.65	0.66	3	0.40	0.81
6	0.06	0.97												

Table 5-2: The quantity of cation per POM, the quantity of H^+ per POM (N_{H^+}), and the extent of proton removal (χ) for all the catalysts used in this work.

Harned's rule defined using χ as the dependent variable is defined in Equation 5-9:

Equation 5-9: Harned's rule defined using the extent of proton removal, χ.

$$\log_{10}(\gamma_H)=\log_{10}\left(\gamma_{\mathrm{H}}^{\mathrm{pure}}\right)-\alpha'\chi$$

where α' is the Harned coefficient defined for the extent of proton removal.

The novelty of using the extent of proton removal as the dependent variable in Harned's rule is readily apparent by inspecting Figure 5-6, which contains the dehydration TOF and γ_H plotted as a function of the acid sites per POM.

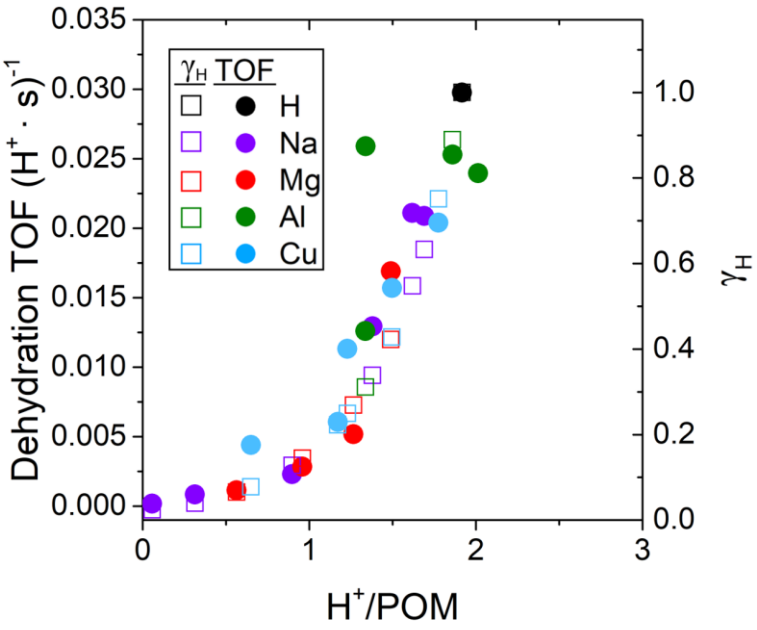

Figure 5-6: Dehydration TOF and proton activity coefficient (γ_H) for [Na,Mg,Al,Cu]PMo 0.2. Activity coefficients were calculated using the extent of proton removal, χ, and Equation 5-9. A single Harned coefficient of $\alpha' = 1.68$ was used for all the catalyst series.

In contrast to activity coefficients calculated using N_{cation} as the dependent variable, when χ was used in Harned's rule a single value of α' could describe all of the catalyst series reasonably well. All of the activity coefficients in Figure 5-6 fall on the same curve as both Equation 5-9 (Harned's rule) and the x-axis are only a function of the quantity of H^+/POM.

The dehydration rates normalized using proton thermodynamic activities, TOF_γ, determined using the extent of proton removal, χ, are presented in Figure 5-7.

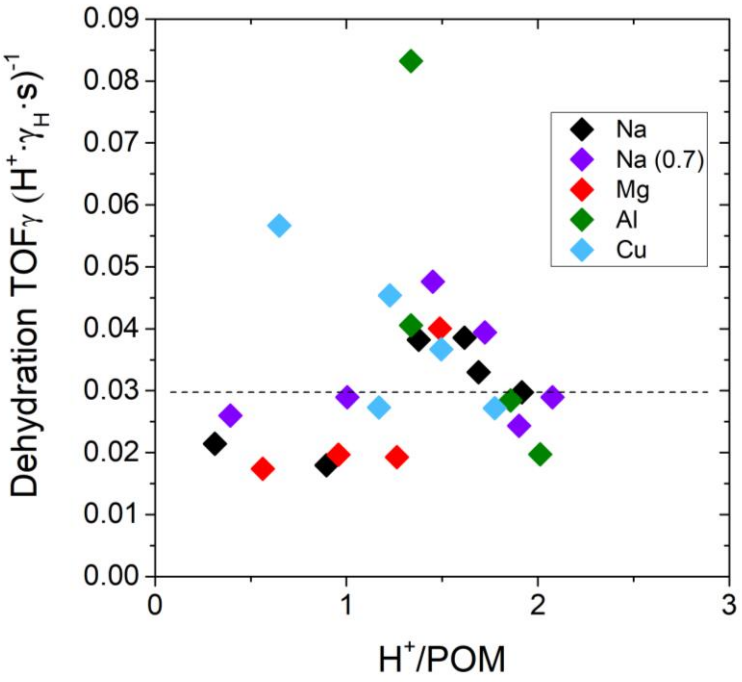

Figure 5-7: Dehydration TOF_γ for the [Na,Mg,Al,Cu]PMo 0.2 and NaPMo 0.7 catalyst series, calculated by normalizing dehydration rates per proton activity, α_{H^+}, rather than per proton. Activity coefficients were calculated using the extent of proton removal, χ. Horizontal dashed line indicates a constant TOF_γ with respect to the catalyst without cation exchange, HPMo 0.2.

The dehydration TOF_γ values calculated using χ are reasonably constant over the range of cation-exchange, especially considering that a single parameter, α', could describe all of the catalysts contained in this work. The systematic over- or under-estimation of the dehydration TOF_γ for specific catalyst series in Figure 5-7 is a consequence of using a single Harned coefficient. An equivalent goodness of fit, as compared to activity coefficients calculated using N_{cation}, is achievable if individual Harned coefficients are used for each catalyst series.

5.4.4 Application of activity coefficients to oxidation

The analysis in this chapter up to this point was focused on the development and application of activity coefficients for POM acid sites to describe the decrease in dehydration TOF with cation addition. Similar decreases in TOF were also observed for the oxidation pathway. It follows that the decrease in oxidation TOF may also be described and appropriately normalized using activity coefficients to define the oxidation TOF_{γ}.

This treatment may perhaps be justified by examining how changes in γ_H may impact the kinetics of methanol oxidation over cation-exchanged POMs. The decrease in γ_H, and therefore the POM acid strength, could lead to a destabilization of key intermediates which involve POM protons. By inspecting the kinetic model described by Iglesia,[25,61] likely intermediates that could be impacted by changes to POM acid strength and γ_H include a molecularly adsorbed methanol species strongly interacting with a proton and the transition state. The transition involves a methanol molecule, weakly interacting with a POM proton, undergoing C-H activation and the transfer of the H to a POM oxygen.[25] A decrease in the equilibrium constant for the adsorbed methanol or a decrease in the rate constant for the transition state in proportion to the changes calculated for γ_H with cation exchange would decrease the methanol oxidation rate similarly to the changes in TOF observed in this work.

Consideration must be given to the fact that oxidation TOFs in the previous chapters were normalized per POM, as they have been normalized in other works involving methanol oxidation over POMs,[25] even though in this work we observed strong correlation between the acid properties and the oxidation TOF. The oxidation TOF_{γ}, defined using the activity coefficients of

the POM protons (calculated using N_{cation}), is defined in Equation 5-10 below. Note this equation uses the POM concentration, not the acid site concentration, and thus does not formally include the thermodynamic activity of the protons, a_{H^+}, as defined in Equation 5-6. Nor does Equation 5-10 rigorously correspond to or integrate with the kinetics described by Iglesia.[25] However it is still insightful to estimate how the proton thermodynamic activity may impact oxidation pathways.

Equation 5-10: Oxidation TOF defined using the proton activity coefficient and POM concentration.

$$\text{Oxidation TOF}_{\gamma}\ (s^{-1}) = \frac{\text{mol (HCHO + DMM + MF)}}{\text{mol POM} \cdot \gamma_H \cdot \text{s}}$$

As can be seen in Figure 5-8 below, the oxidation TOF_{γ}, normalized using the proton activity coefficient, is reasonably constant over a range of cation-exchange. There are some consistent under- and over-estimation depending on the cation type, as well as some erratic behavior for POMs with 3 cations per POM; the latter may be attributed to the magnification of small differences by the extremely low rates with the presence of a large quantity of cation. It should be noted that these normalizations were produced using the same activity coefficients that were used for the dehydration TOF fits earlier, using N_{cation} as the dependent variable as in Equation 5-5. In other words, the Harned coefficients were not re-calculated for oxidation. Therefore, the activity coefficients used to produce Figure 5-8 are not necessarily optimal for obtaining the flattest possible TOF_{γ} with cation exchange but, perhaps, are more theoretically sound as they are based on a solely acid catalyzed reaction, which in principle primarily involves the POM protons of interest.

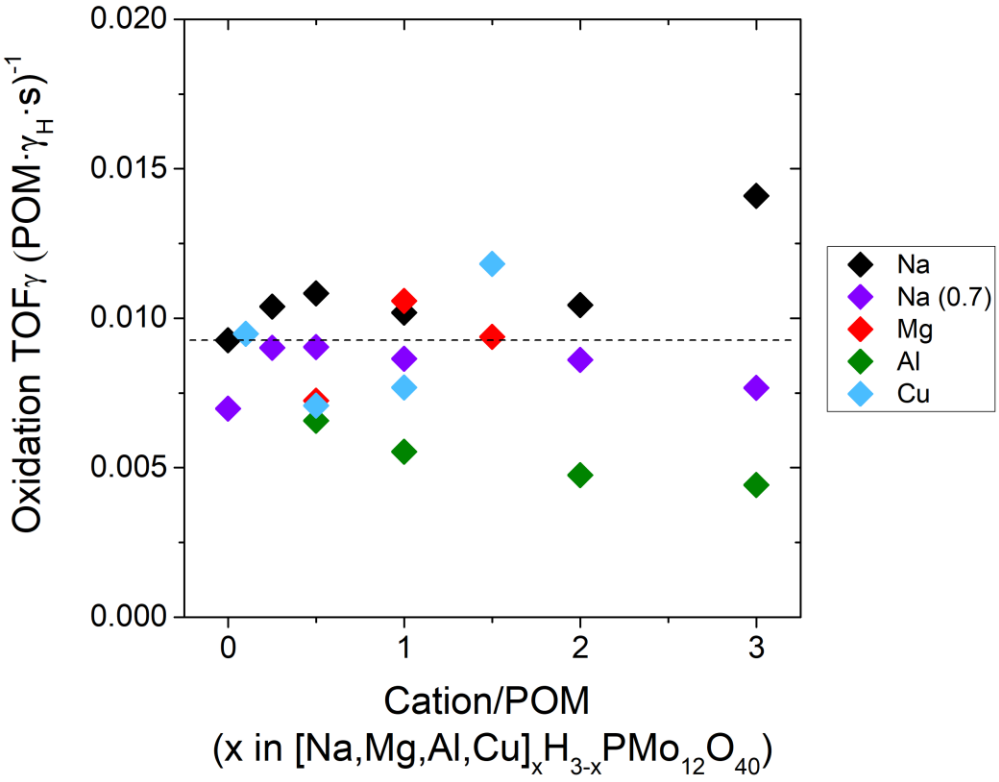

Figure 5-8: Oxidation TOF for the $[Na,Mg,Al,Cu]_xPMo$ 0.2 and Na_xPMo 0.7 catalyst series, calculated by normalizing oxidation rates per POM, as typically done in this work, as well as per activity coefficient of the protons, γ_{H^+}. Horizontal dashed line indicates a constant TOF with respect to the catalyst without cation-exchange, HPMo 0.2.

The ability of the proton activity coefficients to reasonably normalize the oxidation TOF is analogous to the analysis in Chapter 3 regarding the changes in POM acid site strength, as measured by NH_3 TPD. In both cases, the properties of the POM acid sites can be used to describe the destabilization of intermediates and transition states in the oxidation pathway, even though ultimately it may be appropriate to normalize rates using POM quantity rather than proton quantity, since many reaction steps occur utilizing the POM Mo and oxygen sites, as well as POM protons.

5.5 Discussion

Cation-exchanged supported POM catalysts exhibit variations in acid site strength and in dehydration rates that are in stark contrast to the ideal solution-like behavior that may be expected for a solid acid catalyst with reasonably dispersed acid sites. Similar non-ideality is observed in concentrated acid-salt mixtures. In this chapter, the well-accepted formalisms for solutions of mixed electrolytes were applied to solid acids for first time. The excellent ability of Harned's rule, adapted for a hydrated solid electrolyte, to capture the trends observed in TOF with cation addition is quite remarkable.

For the case of cation-exchanged POMs supported on silica it was argued that POMs are hydrated under reaction conditions, creating a solution-like local chemical environment. This system is clearly analogous to aqueous electrolyte solutions and Debye-Hückel theory and extensions thereof, such as Harned's rule, may be readily applied. However, it is worth pointing out that regardless of the degree of hydration of the POMs, the same theoretical treatments may still be applicable. For example, as the 'solvent' of the system changes (for supported POMs the 'solvent' is the interaction of ions with waters of hydration, ≡SiOH groups, neighboring POMs, etc.) the constants in A, B and å in Equation 5-2 and in α in Equation 5-4 change, reflecting variations in parameters such as dielectric constant and effective ion size. However, Debye-Hückel theory would still describe the electrostatic interactions of protons with their environment, regardless of the 'solvent' of the system changing. Experimental evidence for this conclusion exists. For example, POMs were observed to behaved nearly identically with sodium addition with or without co-feeding water; the addition of sodium results in a rapid decrease in

TOF regardless of water content. Co-feeding water serves to increase POM stability, as observed in this work, as well as slightly inhibiting methanol oxidation, as water competes for relevant sites.[25] While not explored in further detail in this work, Harned's rule may be able to capture non-ideal behavior of cation-exchanged POMs for reactions without water co-feed as well. It is noted, however, that water may still be present as it is generated as a reaction product for both oxidation and dehydration.

Formally, rate laws and turnover frequencies should be defined based on the thermodynamic activity of each species rather than the concentration. However, this is rarely the case. In this chapter, the thermodynamic activity was used to properly normalize dehydration rates to obtain TOFs that are roughly invariant with cation exchange. The activity coefficients of protons were also used to normalize the oxidation rates, however, in this case the thermodynamic activity was not rigorously used. Rather, the activity coefficients of the protons were multiplied by the concentration of POMs (not the protons as would be required to calculate the thermodynamic activity). This hybrid activity reflects the effect of cation addition on POM protons, which are essential in the mechanism of methanol oxidation, while respecting the appropriateness of normalizing oxidation rates by the true active site, which is considered to be an entire POM in this work.

The fact that both N_{cation} and χ can describe activity well is not surprising because they are linearly related (see Figure 2-20). It also is encouraging because while little is known of the nature of cations and protons in the vicinity of the POMs, we can relate the linear change in

POM properties in multiple ways and get the same results: the interaction of counter-cations decreases the thermodynamic activity of POM protons.

The ability of a single parameter model, with significant physical meaning and wide-spread use in aqueous electrolyte systems, to produce activity coefficients that directly align with the TOF results presented here is quite remarkable. These results affirm the treatment of POMs as hydrated electrolyte clusters and hydrated POM protons as the active sites for methanol dehydration and oxidation. This work also suggests a framework for treatment of activity coefficients of other solid acid catalysts that exhibit non-ideal behavior with changes in the quantity or identity of ionic species.

5.6 Conclusions

A framework for applying activity coefficients to describe solid acid catalysts was developed and applied to cation-exchanged POMs to demonstrate that a decrease in the thermodynamic activity of acid sites may be responsible for TOF decreases with cation addition. Dehydration rates could be appropriately normalized using the thermodynamic activity of protons rather than the proton concentration. Activity coefficients could also provide insight into the oxidation pathway as well. Harned's rule could be used to calculate activity coefficients for POMs using either the quantity of cation per POM or the quantity of acid sites as the dependent variable. Valuable insight into the possible role of cations in perturbing POM acid sites was gleaned via the application of Harned's rule and considering the thermodynamics of Debye-Hückel theory as they apply to the system of cation-exchanged POMs supported on silica. This methodology may be adapted to

other systems of hydrated solid acid catalysts to describe non-ideal behavior with changes in the ionic environment of the material.

Chapter 6: Conclusions and Recommended Future Directions

6.1 Conclusions

The vision of a model transition metal-oxide catalysts with well-defined, isolated, and tunable active sites was realized in this work. The model catalyst system was comprised of POMs dispersed on fumed silica with various cations exchanged for POM protons. The presence of dispersed and intact POMs was confirmed using FTIR and XRD, respectively, as it was essential to demonstrate that the desired system had indeed been synthesized. The ability of cation exchange to alter POM reducibility was evaluated using UV-Vis. Various techniques, including DTBP titration, NH_3 TPD, and methanol dehydration were used to quantify the effect of cations on POM acid properties.

Many methods for the synthesis of supported POM catalysts were investigated. The treatment of the fumed silica prior to POM loading and the procedures used for incipient wetness impregnation, drying, calcination, and storage were of paramount importance for the shelf-life, dispersion, and stability of supported POM catalysts. Admittedly some characteristics such as dispersion and shelf-life had little if any effect on the catalytic behavior of the catalysts. However, in order to have confidence in the experimental results and to be able to claim that this work involved the use of the model catalysts that were envisioned, characteristics such as dispersion and shelf-life are still important.

Essential to an investigation of cation-exchanged POMs is to demonstrate that the cations are in fact interacting intimately with the POMs. Evidence is in abundance that various POM characteristics change incrementally with cation addition. This includes monotonic changes in the vibrational frequencies, acid site concentrations, acid strengths, reducibility, and catalytic acidity of POMs with cation-exchange. However, the exact nature of the interaction of POMs, cations, and the silica support is not clear. An example that exemplifies this point is the non-stoichiometric exchange of cations and protons and the nearly identical behavior of POMs exchanged with mono- or divalent cations.

The perturbation of POM acid sites, either by varying the POM loading or by the introduction of sodium as the counter-cation, served to decrease the rates for both dehydration and oxidation of methanol and ethanol. The direct relationship between the pathways suggests an intimate role of the POM protons in the activation and conversion of methanol and ethanol over these catalysts. The decrease in the TOFs with sodium addition was attributed to a decrease in the acid strength of the catalysts which may lead to changes in the energy of relevant proton-mediated intermediates. Apparent activation energy trends were consistent with an increase in the energy of the rate limiting intermediates and/or transition states with cation addition. Although acidity has been proposed to have an important role in the oxidation of methanol by other authors previously,[25,26] the non-linear dependence of TOF on acid sites is quite unique and to our knowledge unprecedented. As clearly demonstrated with cation-exchange, the need to consider acid properties is crucial for future investigations of alcohol reactivity over POMs.

The exchange of POMs with cations other than sodium provided valuable insight into the nature of this model catalyst. Remarkably similar reactivity trends were observed for POMs exchanged with mono-, di-, or trivalent cations when the TOF were plotted as a function of the quantity of acid sites per POM. Thus, the rapid decrease in TOF with cation exchange is directly associated with the catalyst acid properties which perhaps are determined by the degree of cation interaction with the POMs. Although cations were demonstrated to alter the POM reducibility, this had no observable effect of the oxidation activity of the cation-exchanged catalysts. Rather the observed trends tracked the acid properties of the catalysts.

The possibilities of using the model catalyst system described and synthesized in this work to create a tunable and selective oxidation catalyst are quite limited. Both loading POMs on a high surface area support and cation-exchanging POMs leads to a decrease in the POM acid site quantity and strength,[15,20,28] which in turn leads to a less active catalyst. In addition, the dependency of the alcohol oxidation pathway on the acid properties of the POMs limits potential selectivity benefits of cation addition, especially considering that no effect of POM reducibility on methanol oxidation was observed in this work. Many authors have reported that cation-exchange may be beneficial for POM catalytic properties.[11,13,14,16,21] Cations may increase surface area, stability, and have various other synergies as a promoter. However, for the model system and mild conditions employed in this work, a route for cations to improve POM activity is not feasible based on the current analysis.

The inability of cations to improve POM activity or selectivity in the current model system does not prevent these catalysts from being used in other useful and insightful investigations of

fundamental catalytic properties using a model catalyst, even though they may be rather inactive at high levels of cation exchange. An example is the development of activity coefficients for solid acid catalysts that was developed in this work. The thermodynamic activity of POM protons was described by drawing analogies between hydrated POM clusters and concentrated solutions of electrolytes. Harned's rule, which is applicable to mixtures of aqueous electrolytes, was adapted to the POM system and was able to qualitatively track the observed catalytic activity trends. The ability of activity coefficients to describe the non-ideal behavior of cation-exchanged POMs is promising and may provide a basis for the development and extension of activity coefficients for other solid acid systems that exhibit non-ideal behavior.

6.2 Recommended Future Directions

Although the cation-exchanged supported POM catalysts studied in this work did not produce a more selective oxidation catalyst, these materials still represent a very well-defined oxide system that presents a unique opportunity to further develop our understanding of metal oxide catalysts. Further investigations of this cation-exchanged POM system may reveal further insights into the role of protons in alcohol oxidation, the underlying mechanisms behind the effect of cations on POM acid strength, or perhaps reveal exciting and unexpected new directions, such as the importance of acidity in methanol oxidation over POMs that was demonstrated in this work.

6.2.1 In-situ XRD

In this work it was confirmed that POMs were dispersed and intact before and after reactions with methanol. However, it is also desirable to confirm these properties hold under reaction conditions, perhaps by using in-situ characterization of the catalysts under reaction conditions.

In-situ FTIR was not required to confirm POMs were intact under reaction conditions in this work, as there are characteristic behaviors of POMs that indicate the POMs have decomposed. The most obvious marker of POM decomposition involves the migration of molybdenum species out of the catalyst bed. Another strong indicator of POM decomposition is a decrease in the solely acid-catalyzed products with time on stream, as the POM decomposition product, MoO_3, does not possess the strong Brønsted acid sites necessary for alcohol dehydration.

In contrast, in-situ XRD is required to confirm that POMs remain well-dispersed under reaction conditions. As was described previously in Chapter 5, POMs are expected to be hydrated under reaction conditions and this may cause a redistribution of the POMs. Additional information may be gleaned from XRD on the hydration level of POMs under reaction conditions.[11] These results together may provide further evidence for the model of POMs as hydrated clusters under reaction conditions as proposed in Chapter 5, as well as confirmation that POMs are reasonably well-dispersed before, during, and after reaction. It should be noted that the small POM clusters on the order of several nanometers in diameter, as observed by Iglesia,[25] are considered dispersed for the purposes of this study, as the relevant catalytic sites in these POM clusters are still accessible to reactants.

6.2.2 DFT

Density Functional Theory (DFT) is a promising computational technique that has been used previously to calculate the energy of adsorbed intermediates on POMs,[67,68] the interaction of POMs and water,[97] the mechanisms of POM decomposition,[50] proton mobility,[98,99] acid properties,[20,27,67,99] and to elucidated the mechanisms and energetics of alcohol dehydration and

oxidation over POMs.[20,25,27,61,77] Of particular relevance Janik has investigated alcohol dehydration over POMs and found that both supporting POMs and cation-exchanging POMs increases the deprotonation energy (DPE, inversely proportion to acid strength) and the activation barrier for the dehydration of the alcohol.[20] Additionally DFT and kinetic (discussed in the next section) investigations of methanol oxidation and dehydration over supported POMs, performed by Iglesia and coworkers,[25,61] were used extensively in this work to evaluate the role of acidity and reducibility in the methanol reaction pathways. The Iglesia group used DFT calculations to determine that H-abstraction from an undissociated methanol, rather than from a methoxy, was the relevant intermediate for methanol oxidation over POMs.[61] In addition the H-addition energy (HAE) was demonstrated to be a suitable reactivity descriptor for calculating the oxidation activity for POMs of different compositions.[25,61] An opportunity exists to calculate the HAE for POMs with cation exchange to determine if this quantity explains the results found in the current work. The HAE and DPE were calculated for POMs titrated with a N-donating molecules such as DTBP[20,25] and the results agreed well with the decrease in the oxidation and dehydration rates of methanol during DTBP titration. Similar results may be expected for cation-exchanged POMs. However, the results of this work demonstrate that it is essential to include hydration effects in such calculations.

6.2.3 Kinetics

Similar considerations as discussed in the previous section with DFT motivate the investigation of the kinetics of alcohol oxidation and dehydration over cation-exchanged polyoxometalates. Measuring the rate and equilibrium constants for methanol oxidation and dehydration for several catalysts, each with a different level of cation exchange, may be insightful into determining the

mechanisms behind the deactivation of POMs via cation addition. The apparent activation barriers (Table 3-1) were measured in this work; however, the results merit further investigation using more detailed kinetic experiments to elucidate the underlying phenomena.

Previously detailed kinetics for methanol dehydration and oxidation over silica supported POMs without cation-exchange have been used to elucidate the elementary steps of methanol conversion over POMs of various compositions.[25,61] Similar procedures have been used for the investigation of propanol dehydration over zeolites to elucidate the role of water in the dehydration pathway.[100] The proposed procedure for cation-exchanged POMs closely follow those used by Lercher and coworkers[100] and would involve varying the methanol and water partial pressures (0.1 – 4 kPa CH_3OH, 0-4 kPa H_2O) at various temperatures (160 – 200˚C). A kinetic model similar to the one used by Iglesia and coworkers[25] could then be used to obtain the values of the rate and equilibrium constants at each temperature, which in turn could be used to regress the how the energetics of the transition state varies with cation exchange. Complementary experiments include the measurement of the methanol adsorption energy via calorimetry (discussed in the next section) or modelling of the reaction pathway of methanol conversion over POMs via DFT (discussed in the previous section). These experiments would help determine if the destabilization of an adsorbed intermediate or the transition state is responsible for the decreases in activity with cation addition.

There are several challenges associated with kinetics measurements of methanol dehydration and oxidation over cation-exchanged POMs. These include the low activity of cation-exchanged POMs and the low sensitivity of the FID detector of the GC for formaldehyde. The several order

of magnitude difference in activity between POMs with and without cation exchange requires widely different space velocities for the different catalysts in order to maintain differential conversion while still being able to produce measurable quantities of products. This issue is exacerbated by the low sensitivity of the FID detector for formaldehyde. Suitable sensitivity may be obtained by maintaining conversion at rates (2-10% conversion) where enough formaldehyde is produced to reliably detect, using ethanol oxidation and dehydration for the kinetic studies rather than methanol, or the installation of a Polyarc reactor upstream of the FID. The Polyarc reactor combines an oxidation catalyst with the function of a typical methanizer, which converts CO_x into methane. Thus, the Polyarc converts all carbon containing compounds into methane for facile quantification and excellent sensitivity. The use of a Polyarc attachment is recommended for all future catalytic studies involving formaldehyde as a product.

6.2.4 Calorimetry

Measurements of the differential heat of adsorption of methanol and ammonia, using a calorimeter, would very beneficial for several reasons. The first is the differential heat of adsorption of methanol would provide an accurate adsorption enthalpy values for use in interpreting the measured equilibrium constants for catalysts with varying cation contents. In addition as stand-alone values without doing kinetic experiments in parallel, the change in the heat of adsorption with cation addition would elucidate if cations inhibit the formation of adsorbed methanol on the catalyst, an important intermediate.[25]

The second used of calorimetry would be to measure the initial heat of ammonia adsorption, a rigorous and appropriate measure of acid sites strength[85] which has been demonstrated to be

effective for describing POM acidity.[28,29] Ammonia adsorption calorimetry is the preferred method for acid sites measurements over NH_3 TPD which was used in this work. Several issues persist with NH_3 TPD using POMs, as it is only applicable at near monolayer coverages for POMs supported on silica and the ammonia is mostly oxidized upon desorption. Ammonia adsorption calorimetry would eliminate several issues associate with NH_3 TPD. The oxidation of NH_3 would be a non-issue as it is not necessary to heat the catalyst or desorb the ammonia. Additionally as only the initial heat of adsorption of ammonia is required to describe the acid site strength for POMs,[28] the troublesome interaction of ammonia and silica observed during NH_3 TPD may be avoided at the low coverage of ammonia required to measure the initial heat of adsorption.

The measurements of the heat of adsorption may be performed using a variety of apparatuses and experimental setups. A simple apparatus for the measurement of heats of adsorption was described by Kozhevnikov and required two mass flow controllers, a 10 port Valco valve, a microcalorimeter. Ammonia was pulsed into a flow of nitrogen and passed over the catalyst. The heat of adsorption was measured by the calorimeter and the quantity of ammonia that was not adsorbed onto the catalyst was measured using a titrator. An on-line mass spectrometer (such as the Hiden HPR-20 used in this work) would be a suitable substitute for the titrator and could be used to quantify the adsorption amounts for other probe molecules such as methanol.

6.2.5 Activity coefficients

Activity coefficients could potentially be used to describe the behavior of other solid acid catalyst systems that exhibit non-ideal behavior. These systems could exhibit non-idealities with

cation addition, in varying acid site concentration, or in varying water partial pressures. The concepts presented in this work may apply to other systems, in ways not previously recognized, bu using the formalisms for aqueous solutions of electrolytes.

POMs are an ideal system for the extension of activity coefficients from aqueous electrolytes to solid catalysts containing hydrated species. Activity coefficients of aqueous POM-cation solutions could be measured using the established techniques for aqueous electrolytes.[89] Likewise, the activity coefficient of bulk POMs could be measured using a combination of techniques. Some techniques typically used for aqueous systems still may apply to bulk POMs, due to the pseudo-liquid behavior of hydrated bulk POMs. Thus, a single material could be used to bridge the gap between aqueous and solid electrolytes and enable the development of rigorous thermodynamic treatments of solid catalysts containing hydrated electrolyte species.

6.2.6 Supported POMs as model transition-metal oxide catalysts

The outlook for supported cation-exchanged POMs presented in this work was significantly dampened by the dominant role of acidity in the reactivity of alcohols over these catalysts. Multiple authors have reported that both supporting POMs and cation-exchanging POMs lead to a decrease in POM acidity,[10,11,20,29] and no exceptions to these trends were found in this work. Other potential probe molecules were explored, such as ethylene and acetaldehyde, however POMs can only activate these molecules at harsh conditions (~ 300˚C)[56,57] where POMs are unlikely to retain the Keggin structure.[45,50–53]

The trade-off between activating reactants and catalyst stability is a foundational issue in the study of model catalysts in general. Fortunately for POMs, dehydration and oxidative dehydrogenation of alcohol proceeds at mild temperatures over these catalysts. Unfortunately, it seems that the interaction of alcohols with POM protons is responsible for the formation of the relevant intermediates and transition states that allow for such facile conversion of alcohols to ethers and aldehydes at these mild conditions. Thus, the tunable and selective model catalysts based on cation-exchanged POMs that were envisioned in this work are not feasible due to the importance of acidity in activating reactants. However, POMs may still find applications as model catalysts as the relationship between POM properties and reactivities for the conversion of alcohols is establish for changes in the POM heteroatom, framework metal atom, and, with the addition of this work, the counter-cation. In summary, cation-exchanged supported POMs are an interesting model catalyst system to study dehydration and selective oxidation catalysis.

Bibliography

1. Nørskov, J. K., Abild-Pedersen, F., Studt, F. & Bligaard, T. Density functional theory in surface chemistry and catalysis. *Proc. Natl. Acad. Sci.* **108,** 937–943 (2011).
2. Bond, G. C. The Use of Kinetics in Evaluating Mechanisms in Heterogeneous Catalysis. *Catal. Rev.* **50,** 532–567 (2008).
3. Jones, C. W., Tao, F. & Garland, M. V. Introduction to Special Issue on Operando and In Situ Studies of Catalysis. *ACS Catal.* **2,** 2444–2445 (2012).
4. Dou, J., Sun, Z., Opalade, A. A., Wang, N., Fu, W. & Tao, F. Operando chemistry of catalyst surfaces during catalysis. *Chem. Soc. Rev.* **46,** 2001–2027 (2017).
5. Wu, Z., Overbury, S. H. *Catalysis by Materials with Well-Defined Structures* (Elsevier, 2015).
6. Cargnello, M., Doan-Nguyen, V. V. T., Gordon, T. R., Diaz, R. E., Stach, E. A., Gorte, R. J., Fornasiero, P. & Murray, C. B. Control of Metal Nanocrystal Size Reveals Metal-Support Interface Role for Ceria Catalysts. *Science* **341,** 771–773 (2013).
7. Jones, J., Xiong, H., DeLaRiva, A. T., Peterson, E. J., Pham, H., Challa, S. R., Qi, G., Oh, S., Wiebenga, M. H., Pereira Hernandez, X. I., Wang, Y. & Datye, A. K. Thermally stable single-atom platinum-on-ceria catalysts via atom trapping. *Science* **353,** 150–154 (2016).
8. Dal Santo, V., Guidotti, M., Psaro, R., Marchese, L., Carniato, F. & Bisio, C. Rational design of single-site heterogeneous catalysts: towards high chemo-, regio- and stereoselectivity. *Proc. R. Soc. Math. Phys. Eng. Sci.* **468,** 1904–1926 (2012).

9. Misono, M. Heterogeneous Catalysis by Heteropoly Compounds of Molybdenum and Tungsten. *Catal. Rev.* **29,** 269–321 (1987).

10. Kozhevnikov, I. V. Heteropoly Acids and Related Compounds as Catalysts for Fine Chemical Synthesis. *Catal. Rev.* **37,** 311–352 (1995).

11. Mizuno, N. & Misono, M. Heterogeneous Catalysis. *Chem. Rev.* **98,** 199–218 (1998).

12. Mizuno, N. & Misono, M. Heteropolyanions in catalysis. *J. Mol. Catal.* **86,** 319–342 (1994).

13. AI, M. Effects of cations introduced into 12-molybdophosphoric acid on the catalyst properties. *Appl. Catal.* **4,** 245–256 (1982).

14. Ai, M. Characteristics of heteropoly compounds as catalysts for selective oxidation. *J. Catal.* **71,** 88–98 (1981).

15. Ghosh, A. K. & Moffat, J. B. Acidity of heteropoly compounds. *J. Catal.* **101,** 238–245 (1986).

16. Barteau, M. A., Lyons, J. E. & Song, I. K. Surface chemistry and catalysis on well-defined oxide surfaces: nanoscale design bases for single-site heterogeneous catalysts. *J. Catal.* **216,** 236–245 (2003).

17. Barteau, K. P., Lyons, J. E., Song, I. K. & Barteau, M. A. UV-visible spectroscopy as a probe of heteropolyacid redox properties: Application to liquid phase oxidations. *Top. Catal.* **41,** 55–62 (2006).

18. Song, I. K. & Barteau, M. A. Redox properties of Keggin-type heteropolyacid (HPA) catalysts: effect of counter-cation, heteroatom, and polyatom substitution. *J. Mol. Catal. Chem.* **212,** 229–236 (2004).

19. Song, I. K., Kim, H. S. & Chun, M.-S. On the reduction potential of cation-exchanged heteropolyacids (HPAs). *Korean J. Chem. Eng.* **20,** 844–849 (2003).

20. Janik, M. J., Macht, J., Iglesia, E. & Neurock, M. Correlating Acid Properties and Catalytic Function: A First-Principles Analysis of Alcohol Dehydration Pathways on Polyoxometalates. *J. Phys. Chem. C* **113,** 1872–1885 (2009).

21. Okuhara, T., Mizuno, N. & Misono, M. Catalytic Chemistry of Heteropoly Compounds. in *Advances in Catalysis* (ed. D.D. Eley, W. O. H. and B. G.) **41,** 113–252 (Academic Press, 1996).

22. Xu, S., Wang, L., Chu, W. & Yang, W. Catalytic oxidation of ethylene to acetic acid on Pd–HPA/SiO_2 catalysts with different heteropoly acids. *React. Kinet. Catal. Lett.* **98,** 107–115 (2009).

23. Okuhara, T., Mizuno, N. & Misono, M. Catalysis by heteropoly compounds—recent developments. *Appl. Catal. Gen.* **222,** 63–77 (2001).

24. Moro-oka, Y. The role of acidic properties of metal oxide catalysts in the catalytic oxidation. *Appl. Catal. Gen.* **181,** 323–329 (1999).

25. Deshlahra, P., Carr, R. T., Chai, S.-H. & Iglesia, E. Mechanistic Details and Reactivity Descriptors in Oxidation and Acid Catalysis of Methanol. *ACS Catal.* **5,** 666–682 (2015).

26. Tatibouët, J. M. Methanol oxidation as a catalytic surface probe. *Appl. Catal. Gen.* **148,** 213–252 (1997).

27. Macht, J., Janik, M. J., Neurock, M. & Iglesia, E. Catalytic Consequences of Composition in Polyoxometalate Clusters with Keggin Structure. *Angew. Chem. Int. Ed.* **46,** 7864–7868 (2007).

28. Alharbi, W., Brown, E., Kozhevnikova, E. F. & Kozhevnikov, I. V. Dehydration of ethanol over heteropoly acid catalysts in the gas phase. *J. Catal.* **319,** 174–181 (2014).

29. Alharbi, W., Kozhevnikova, E. F. & Kozhevnikov, I. V. Dehydration of Methanol to Dimethyl Ether over Heteropoly Acid Catalysts: The Relationship between Reaction Rate and Catalyst Acid Strength. *ACS Catal.* **5,** 7186–7193 (2015).

30. Carr, R. T., Neurock, M. & Iglesia, E. Catalytic consequences of acid strength in the conversion of methanol to dimethyl ether. *J. Catal.* **278,** 78–93 (2011).

31. Kasztelan, S. & Moffat, J. B. The oxidation of methane on heteropolyoxometalates III. Effect of the addition of cesium on silica-supported 12-molybdophosphoric acid, molybdena, vanadia, and iron oxide. *J. Catal.* **112,** 54–65 (1988).

32. Liu, Y., Murata, K., Inaba, M. & Mimura, N. Selective oxidation of propylene to acetone by molecular oxygen over $M_{x/2}H_{5-x}[PMo_{10}V_2O_{40}]$/HMS ($M=Cu^{2+}$, Co^{2+}, Ni^{2+}). *Catal. Commun.* **4,** 281–285 (2003).

33. Min, J.-S. & Mizuno, N. Effects of additives on catalytic performance of heteropoly compounds for selective oxidation of light alkanes. *Catal. Today* **71,** 89–96 (2001).

34. Mokhtar, M., Basahel, S. N. & Ali, T. T. Ethanol to hydrocarbons using silver substituted polyoxometalates: Physicochemical and catalytic study. *J. Ind. Eng. Chem.* **20,** 46–53 (2014).

35. Parent, M. A. & Moffat, J. B. Isomerization of 1-butene on silver and thallium 12-tungstophosphate: the effect of the cation on acid strength distributions. *Catal. Lett.* **60,** 191–197 (1999).

36. Aboukaïs, A., Ghoussoub, D., Blouet-Crusson, E., Rigole, M. & Guelton, M. Oxidative dehydrogenation of isobutyric acid on $H_4PVMo_{11}O_{40}$, $Na_xH_{4-x}PVMo_{11}O_{40}$ and Cu_yH_{4-}

$_{2y}PVMo_{11}O_{40}$ heteropolyacid catalysts supported on silica. *Appl. Catal. Gen.* **111,** 109–118 (1994).

37. Liu-Cai, F. X., Pham, C., Bey, F. & Herve, G. Oxidation of isobutane catalyzed by vanadyl, copper and cesium substituted $H_3PMo_{12}O_{40}$. *React. Kinet. Catal. Lett.* **75,** 305–314 (2002).

38. Mizuno, N., Ishige, H., Seki, Y., Misono, M., Suh, D.-J., Han, W. & Kudo, T. Low-temperature oxygenation of methane into formic acid with molecular oxygen in the presence of hydrogen catalysed by $Pd_{0.08}Cs_{2.5}H_{1.34}PVMo_{11}O_{40}$. *Chem. Commun.* 1295–1296 (1997).

39. Nagaraju, P., Balaraju, M., Reddy, K. M., Prasad, P. S. S. & Lingaiah, N. Selective oxidation of allylic alcohols catalyzed by silver exchanged molybdovanado phosphoric acid catalyst in the presence of molecular oxygen. *Catal. Commun.* **9,** 1389–1393 (2008).

40. Rhule, J. T., Neiwert, W. A., Hardcastle, K. I., Do, B. T. & Hill, C. L. $Ag_5PV_2Mo_{10}O_{40}$, a Heterogeneous Catalyst for Air-Based Selective Oxidation at Ambient Temperature. *J. Am. Chem. Soc.* **123,** 12101–12102 (2001).

41. Rocchiccioli-Deltcheff, C., Aouissi, A., Launay, S. & Fournier, M. Silica-supported 12-molybdophosphoric acid catalysts: Influence of the thermal treatments and of the Mo contents on their behavior, from IR, Raman, X-ray diffraction studies, and catalytic reactivity in the methanol oxidation. *J. Mol. Catal. Chem.* **114,** 331–342 (1996).

42. Tessonnier, J.-P., Goubert-Renaudin, S., Alia, S., Yan, Y. & Barteau, M. A. Structure, Stability, and Electronic Interactions of Polyoxometalates on Functionalized Graphene Sheets. *Langmuir* **29,** 393–402 (2013).

43. Rocchiccioli-Deltcheff, C., Amirouche, M. & Fournier, M. Structure and catalytic properties of silica-supported polyoxomolybdates III. 12-molybdosilicic acid catalysts: vibrational study of the dispersion effect and nature of the mo species in interaction with the silica support. *J. Catal.* **138,** 445–456 (1992).

44. Rocchiccioli-Deltcheff, C., Fournier, M., Franck, R. & Thouvenot, R. Vibrational investigations of polyoxometalates. 2. Evidence for anion-anion interactions in molybdenum(VI) and tungsten(VI) compounds related to the Keggin structure. *Inorg. Chem.* **22,** 207–216 (1983).

45. Molinari, J. E., Nakka, L., Kim, T. & Wachs, I. E. Dynamic Surface Structures and Reactivity of Vanadium-Containing Molybdophosphoric Acid ($H_{3+x}PMo_{12-x}V_xO_{40}$) Keggin Catalysts during Methanol Oxidation and Dehydration. *ACS Catal.* **1,** 1536–1548 (2011).

46. Madhusudhan Rao, P., Wolfson, A., Kababya, S., Vega, S. & Landau, M. V. Immobilization of molecular $H_3PW_{12}O_{40}$ heteropolyacid catalyst in alumina-grafted silica-gel and mesostructured SBA-15 silica matrices. *J. Catal.* **232,** 210–225 (2005).

47. Kim, H., Park, D. R., Park, S., Jung, J. C., Lee, S.-B. & Song, I. K. Preparation, characterization, and catalytic activity of $H_5PMo_{10}V_2O_{40}$ immobilized on nitrogen-containing mesoporous carbon ($PMo_{10}V_2$/N-MC) for selective conversion of methanol to dimethoxymethane. *Korean J. Chem. Eng.* **26,** 660–665 (2009).

48. Liu, H., Bayat, N. & Iglesia, E. Site Titration with Organic Bases During Catalysis: Selectivity Modifier and Structural Probe in Methanol Oxidation on Keggin Clusters. *Angew. Chem. Int. Ed.* **42,** 5072–5075 (2003).

49. Viswanadham, B., Srikanth, A. & Chary, K. V. R. Characterization and reactivity of 11-molybdo-1-vanadophosphoric acid catalyst supported on zirconia for dehydration of glycerol to acrolein. *J. Chem. Sci.* **126,** 445–454 (2014).

50. Janik, M. J., Bardin, B. B., Davis, R. J. & Neurock, M. A Quantum Chemical Study of the Decomposition of Keggin-Structured Heteropolyacids. *J. Phys. Chem. B* **110,** 4170–4178 (2006).

51. Mestl, G., Ilkenhans, T., Spielbauer, D., Dieterle, M., Timpe, O., Kröhnert, J., Jentoft, F., Knözinger, H. & Schlögl, R. Thermally and chemically induced structural transformations of Keggin-type heteropoly acid catalysts. *Appl. Catal. Gen.* **210,** 13–34 (2001).

52. Lee, J. K., Melsheimer, J., Berndt, S., Mestl, G., Schlögl, R. & Köhler, K. Transient responses of the local electronic and geometric structures of vanado-molybdo-phoshate catalysts $H_{3+n}PV_nMo_{12-n}O_{40}$ in selective oxidation. *Appl. Catal. Gen.* **214,** 125–148 (2001).

53. Jentoft, F. C., Klokishner, S., Kröhnert, J., Melsheimer, J., Ressler, T., Timpe, O., Wienold, J. & Schlögl, R. The structure of molybdenum-heteropoly acids under conditions of gas-phase selective oxidation catalysis: a multi-method in situ study. *Appl. Catal. Gen.* **256,** 291–317 (2003).

54. Sorensen, C. & Weber. Oxidative Dehydrogenation of Methanol Catalyzed by Samples Containing Well Defined Ensembles of Vanadium. *J. Catal.* **142,** 1–17 (1993).

55. Song, I. K., Shin, S. K. & Lee, W. Y. Catalytic Activity of $H_3PMo_{12}O_{40}$-Blended Polysulfone Film in the Oxidation of Ethanol to Acetaldehyde. *J. Catal.* **144,** 348–351 (1993).

56. Evnin, A. B., Rabo, J. A. & Kasai, P. H. Heterogeneously catalyzed vapor-phase oxidation of ethylene to acetaldehyde. *J. Catal.* **30,** 109–117 (1973).

57. Mori, H., Mizuno, N. & Misono, M. Factors controlling the selectivity of the oxidation of acetaldehyde over heteropoly compounds. *J. Catal.* **131,** 133–142 (1991).

58. Harned, H. S. & Owen, B. B. *The physical chemistry of electrolytic solutions*. (Reinhold Pub. Corp., 1963).

59. Wright, M. R. *An Introduction to Aqueous Electrolyte Solutions* (Wiley, 2007).

60. Pilling, M. J. & Seakins, P. W. *Reaction kinetics*. (Oxford University Press, 1995).

61. Deshlahra, P. & Iglesia, E. Methanol Oxidative Dehydrogenation on Oxide Catalysts: Molecular and Dissociative Routes and Hydrogen Addition Energies as Descriptors of Reactivity. *J. Phys. Chem. C* **118,** 26115–26129 (2014).

62. Liu, H. & Iglesia, E. Effects of support on bifunctional methanol oxidation pathways catalyzed by polyoxometallate Keggin clusters. *J. Catal.* **223,** 161–169 (2004).

63. Tatibouët, J.-M., Montalescot, C. & Brückman, K. A new method to prepare silica supported heteropolyanion catalysts formation on the silica surface of calcium and magnesium salts of phosphomolybdic acid, $H_3PMo_{12}O_{40}$. *Appl. Catal. Gen.* **138,** L1–L6 (1996).

64. Choi, S., Wang, Y., Nie, Z., Liu, J. & Peden, C. H. F. Cs-substituted tungstophosphoric acid salt supported on mesoporous silica. *Catal. Today* **55,** 117–124 (2000).

65. Farneth, W. E., Staley, R. H., Domaille, P. J. & Farlee, R. D. Comparison of structure and thermal chemistry of stoichiometric and catalytic alkoxy-substituted molybdenum heteropolyanions: carbon-13 CP-MAS NMR spectrum of a chemisorbed reaction intermediate. *J. Am. Chem. Soc.* **109,** 4018–4023 (1987).

66. Kim, W.-G., Kim, M.-W., Kim, J.-H. & Seo, G. Dispersion measurement of heteropoly acid supported on KIT-1 mesoporous material. *Microporous Mesoporous Mater.* **57,** 113–120 (2003).

67. Janik, M. J., Davis, R. J. & Neurock, M. The relationship between adsorption and solid acidity of heteropolyacids. *Catal. Today* **105,** 134–143 (2005).

68. Campbell, K. A., Janik, M. J., Davis, R. J. & Neurock, M. Ab initio and microcalorimetric investigations of alkene adsorption on phosphotungstic acid. *Langmuir ACS J. Surf. Colloids* **21,** 4738–4745 (2005).

69. Liu, C. C. & Maciel, G. E. The Fumed Silica Surface: A Study by NMR. *J. Am. Chem. Soc.* **118,** 5103–5119 (1996).

70. Zhuravlev, L. T. The surface chemistry of amorphous silica. Zhuravlev model. *Colloids Surf. Physicochem. Eng. Asp.* **173,** 1–38 (2000).

71. Grinenval, E., Rozanska, X., Baudouin, A., Berrier, E., Delbecq, F., Sautet, P., Basset, J.-M. & Lefebvre, F. Controlled Interactions between Anhydrous Keggin-Type Heteropolyacids and Silica Support: Preparation and Characterization of Well-Defined Silica-Supported Polyoxometalate Species. *J. Phys. Chem. C* **114,** 19024–19034 (2010).

72. Macht, J., Carr, R. T. & Iglesia, E. Consequences of Acid Strength for Isomerization and Elimination Catalysis on Solid Acids. *J. Am. Chem. Soc.* **131,** 6554–6565 (2009).

73. Brückman, K., Che, M., Haber, J. & Tatibouet, J. M. On the physicochemical and catalytic properties of $H_5PV_2Mo_{10}O_{40}$ supported on silica. *Catal. Lett.* **25,** 225–240

74. Madhusudhan Rao, P., Wolfson, A., Kababya, S., Vega, S. & Landau, M. V. Immobilization of molecular H3PW12O40 heteropolyacid catalyst in alumina-grafted silica-gel and mesostructured SBA-15 silica matrices. *J. Catal.* **232,** 210–225 (2005).

75. Youn, M. H., Kim, H., Jung, J. C., Song, I. K., Barteau, K. P. & Barteau, M. A. UV-vis spectroscopy studies of $H_3PMo_{12-x}W_xO_{40}$ heteropolyacid (HPA) catalysts in the solid state: Effects of water content and polyatom substitution. *J. Mol. Catal. Chem.* **241,** 227–232 (2005).

76. Knaeble, W. & Iglesia, E. Kinetic and Theoretical Insights into the Mechanism of Alkanol Dehydration on Solid Brønsted Acid Catalysts. *J. Phys. Chem. C* **120,** 3371–3389 (2016).

77. Macht, J., Janik, M. J., Neurock, M. & Iglesia, E. Mechanistic Consequences of Composition in Acid Catalysis by Polyoxometalate Keggin Clusters. *J. Am. Chem. Soc.* **130,** 10369–10379 (2008).

78. Kuang, W., Rives, A., Fournier, M. & Hubaut, R. Structure and reactivity of silica-supported 12-tungstophosphoric acid. *Appl. Catal. Gen.* **250,** 221–229 (2003).

79. Zhang, Y., Du, Z. & Min, E. Effect of acidity and structures of supported tungstophosphoric acid on its catalytic activity and selectivity in liquid phase synthesis of ethylbenzene. *Catal. Today* **93–95,** 327–332 (2004).

80. Libby, M. C., Watson, P. C. & Barteau, M. A. Synthesis of Ketenes with Oxide Catalysts. *Ind. Eng. Chem. Res.* **33,** 2904–2912 (1994).

81. Badlani, M. & Wachs, I. E. Methanol: a 'smart' chemical probe molecule. *Catal. Lett.* **75,** 137–149

82. Ilhan, S., Kahruman, C. & Yusufoglu, I. Characterization of the thermal decomposition products of ammonium phosphomolybdate hydrate. *J. Anal. Appl. Pyrolysis* **78,** 363–370 (2007).

83. Damyanova, S., Cubeiro, M. L. & Fierro, J. L. G. Acid-redox properties of titania-supported 12-molybdophosphates for methanol oxidation. *J. Mol. Catal. Chem.* **142,** 85–100 (1999).

84. Soares, A. P. V., Portela, M. F., Kiennemann, A. & Hilaire, L. Mechanism of deactivation of iron-molybdate catalysts prepared by coprecipitation and sol–gel techniques in methanol to formaldehyde oxidation. *Chem. Eng. Sci.* **58,** 1315–1322 (2003).

85. Wang, C.-M., Brogaard, R. Y., Weckhuysen, B. M., Nørskov, J. K. & Studt, F. Reactivity Descriptor in Solid Acid Catalysis: Predicting Turnover Frequencies for Propene Methylation in Zeotypes. *J. Phys. Chem. Lett.* **5,** 1516–1521 (2014).

86. Aris, R., Bell, A. T., Boudart, M., Chen, N. Y., Gates, B. C., & Hagg, W. O. *Catalyst design: progress and perspectives*. (Wiley, 1987).

87. Konishi, Y., Sakata, K., Misono, M. & Yoneda, Y. Catalysis by heteropoly compounds: IV. Oxidation of methacrolein to methacrylic acid over 12-molybdophosphoric acid. *J. Catal.* **77,** 169–179 (1982).

88. Harned, H. S. & Gary, R. The Activity Coefficient of Hydrochloric Acid in Concentrated Aqueous Higher Valence Type Chloride Solutions at 25°. I. The System Hydrochloric Acid-Barium Chloride. *J. Am. Chem. Soc.* **76,** 5924–5927 (1954).

89. Rowland, D. & May, P. M. An Investigation of Harned's Rule for Predicting the Activity Coefficients of Strong Aqueous Electrolyte Solution Mixtures at 25 °C. *J. Chem. Eng. Data* **62,** 310–327 (2017).

90. Huckel, H. The theory of concentrated aqueous solutions of strong electrolytes. *Phys. Z.* **26,** 93–147 (1926).

91. Scatchard, G. Concentrated Solutions of Strong Electrolytes. *Chem. Rev.* **19,** 309–327 (1936).

92. Harned, H. S. The Activity Coefficient of Hydrochloric Acid In Concentrated Solutions of Strong Electrolytes. *J. Am. Chem. Soc.* **48,** 326–342 (1926).

93. Harned, H. S. & Gary, R. The Activity Coefficient of Hydrochloric Acid in Concentrated Aqueous Higher Valence Type Chloride Solutions at 25°. III. The System Hydrochloric Acid-Aluminum Chloride. *J. Am. Chem. Soc.* **77,** 4695–4697 (1955).

94. Tanabe, K., Misono, M., Hattori, H., & Ono, Y. *New Solid Acids and Bases* (Elsevier Science, 1990).

95. Guggenheim, E. A. The Conceptions of Electrical Potential Difference between Two Phases and the Individual Activities of Ions. *J. Phys. Chem.* **33,** 842–849 (1928).

96. Wood, J. R. Thermodynamics of brine-salt equilibria — II. The system NaCl-KCl-H_2O from 0 to 200°C. *Geochim. Cosmochim. Acta* **40,** 1211–1220 (1976).

97. Janik, M. J., Campbell, K. A., Bardin, B. B., Davis, R. J. & Neurock, M. A computational and experimental study of anhydrous phosphotungstic acid and its interaction with water molecules. *Appl. Catal. Gen.* **256,** 51–68 (2003).

98. Janik, M. J., Davis, R. J. & Neurock, M. Anhydrous and Water-Assisted Proton Mobility in Phosphotungstic Acid. *J. Am. Chem. Soc.* **127,** 5238–5245 (2005).

99. Yang, J., Janik, M. J., Ma, D., Zheng, A. M., Zhang, M. J., Neurock, M., Davis, R. J., Ye, C. H. & Deng, F. Location, acid strength, and mobility of the acidic protons in Keggin 12-$H_3PW_{12}O_{40}$: A combined solid-state NMR spectroscopy and DFT quantum chemical calculation study. *J. Am. Chem. Soc.* **127,** 18274–18280 (2005).

100. Zhi, Y., Shi, H., Mu, L., Liu, Y., Mei, D., Camaioni, D. M. & Lercher, J. A. Dehydration Pathways of 1-Propanol on HZSM-5 in the Presence and Absence of Water. *J. Am. Chem. Soc.* **137,** 15781–15794 (2015).